

Locales and Mechanisms of TrkB Activation within Hippocampus

By

Jeffrey Helgager

Department of Neurobiology
Duke University

Date: _____
Approved:

James O. McNamara, Supervisor

Anne West, Chair

J. Victor Nadler

Dennis Thiele

Dissertation submitted in partial fulfillment of
the requirements for the degree of Doctor
of Philosophy in the Department of
Neurobiology in the Graduate School
of Duke University

2013

UMI Number: 3613674

All rights reserved

INFORMATION TO ALL USERS

The quality of this reproduction is dependent upon the quality of the copy submitted.

In the unlikely event that the author did not send a complete manuscript and there are missing pages, these will be noted. Also, if material had to be removed, a note will indicate the deletion.



UMI 3613674

Published by ProQuest LLC (2014). Copyright in the Dissertation held by the Author.

Microform Edition © ProQuest LLC.

All rights reserved. This work is protected against unauthorized copying under Title 17, United States Code



ProQuest LLC.
789 East Eisenhower Parkway
P.O. Box 1346
Ann Arbor, MI 48106 - 1346

ABSTRACT

Locales and Mechanisms of TrkB Activation within Hippocampus

By

Jeffrey Helgager

Department of Neurobiology
Duke University

Date: _____
Approved:

James O. McNamara, Supervisor

Anne West, Chair

J. Victor Nadler

Dennis Thiele

An abstract of a dissertation submitted in partial fulfillment of
the requirements for the degree of Doctor
of Philosophy in the Department of
Neurobiology in the Graduate School
of Duke University

2013

Copyright by
Jeffrey Helgager
2013

Abstract

Understanding the mechanisms of limbic epileptogenesis in cellular and molecular terms may provide novel therapeutic targets for its prevention. The neurotrophin receptor tropomyosin-related kinase B (TrkB) is thought to be critical for limbic epileptogenesis. Enhanced activation of TrkB, revealed by immunodetection of enhanced phosphorylated TrkB (pTrkB), a surrogate measure of its activation, has been identified within the hippocampus in multiple animal models. Knowledge of the cellular locale of activated TrkB is necessary to elucidate its functional consequences. Using an antibody selective to pTrkB in conjunction with confocal microscopy and cellular markers, we determined the cellular and subcellular locale of enhanced pTrkB induced by status epilepticus (SE) evoked by infusion of kainic acid into the amygdala of adult mice. SE induced enhanced pTrkB immunoreactivity in two distinct populations of principal neurons within the hippocampus—the dentate granule cells and CA1 pyramidal cells. Enhanced immunoreactivity within granule cells was found within mossy fiber axons and giant synaptic boutons. By contrast, enhanced immunoreactivity was found within apical dendritic shafts and spines of CA1 pyramidal cells. A common feature of this enhanced pTrkB at these cellular locales is its localization to excitatory synapses between excitatory neurons, presynaptically in the granule cells and postsynaptically in CA1 pyramidal cells. Long-term potentiation (LTP) is one cellular consequence of TrkB activation at these excitatory synapses that may promote epileptogenesis.

The importance of TrkB in diverse neuronal processes, as well as its involvement in various disorders of the nervous system, underscores the importance of understanding how it is activated. The canonical neurotrophin ligand which activates TrkB is brain derived neurotrophic factor (BDNF). Zinc, however, has also been demonstrated to activate this receptor through a mechanism whereby it does not directly interact with it, known as transactivation. Presynaptic vesicles of mossy fiber boutons of stratum lucidum are particularly enriched in zinc, where it is co-released with glutamate in an activity dependent fashion, and incorporated into these vesicles by the zinc transporter, ZnT3. Given the presence of large quantities of zinc within stratum lucidum, we hypothesized that this metal may contribute to TrkB transactivation at this locale. To this end, we examined the contributions of both BDNF and synaptic vesicular zinc to TrkB activation in stratum lucidum of mouse hippocampus under physiological conditions. Utilization of mice which are genetic knockouts for *BDNF* and/or *ZnT3* allowed us to examine TrkB activation in the absence of one or both of these ligands. This was done using an antibody for pTrkB in conjunction with confocal microscopy, assaying immunoreactivity at the cellular and synaptic locales within stratum lucidum where pTrkB was previously found to be enriched. Our results suggest that BDNF contributes to TrkB activation within stratum lucidum. Interestingly, *ZnT3* mice displayed an increase in BDNF protein and TrkB activation, demonstrating that synaptic zinc regulates BDNF and TrkB signaling at this locale.

Contents

| | |
|---|------|
| Abstract | iv |
| List of Tables | x |
| List of Figures | xi |
| Acknowledgements..... | xiii |
| 1. Introduction..... | 1 |
| 1.1 Overview | 1 |
| 1.2 Epilepsy..... | 3 |
| 1.2.1 Clinical Aspects of Epilepsy..... | 5 |
| 1.2.2 Models of Epilepsy for Research Purposes..... | 8 |
| 1.2.2.1 The Pilocarpine Model..... | 9 |
| 1.2.2.2 The Kainic Acid Model and Kainic Acid Microinfusion Models | 10 |
| 1.2.2.3 The Kindling Model..... | 12 |
| 1.3 Overview of Hippocampal Circuitry | 13 |
| 1.4 The Neurotrophin Receptors, TrkB, and Synaptic Plasticity..... | 16 |
| 1.4.1 Overview of the Neurotrophin Receptors and Their Molecular Biology | 16 |
| 1.4.2 Transactivation of Neurotrophin Receptors..... | 21 |
| 1.4.3 The TrkB Receptor and Long Term Potentiation | 25 |
| 1.4.4 The TrkB Receptor and Epilepsy..... | 27 |
| 1.5 Zinc in the CNS | 31 |
| 1.5.1 Vesicular zinc and plasticity at the mf-CA3 synapse | 34 |
| 2. The Cellular and Synaptic Location of Activated TrkB in Mouse Hippocampus during Limbic Epileptogenesis..... | 38 |

| | |
|--|----|
| 2.1 Introduction..... | 38 |
| 2.2 Materials and Methods..... | 40 |
| 2.2.1 Thy1-GFP Expressing Mice..... | 40 |
| 2.2.2 Induction of SE | 41 |
| 2.2.2.1 SE Induced by Microinfusion of KA | 42 |
| 2.2.2.2 SE Induced by Pilocarpine..... | 44 |
| 2.2.3 Preparation of Brain Specimens for Immunohistochemistry..... | 45 |
| 2.2.4 Antibody Characterization | 47 |
| 2.2.5 Immunohistochemistry | 49 |
| 2.2.6 Confocal Microscopy and Data Analysis..... | 49 |
| 2.2.6.1 Imaging Parameters | 49 |
| 2.2.6.2 Quantification of pY816 Immunoreactivity..... | 51 |
| 2.3 Results..... | 54 |
| 2.3.1 Enhanced pY816 Immunoreactivity within Stratum Lucidum Following Kainic Acid Status Epilepticus (KA-SE)..... | 54 |
| 2.3.2 Localization of Stratum Lucidum pY816 Immunoreactivity to Mossy Fiber Axons Following KA-SE | 59 |
| 2.3.3 Quantification of pY816 Immunoreactivity Within Axons of Stratum Lucidum Following KA-SE | 65 |
| 2.3.4 Localization of Stratum Lucidum pY816 Immunoreactivity to Mossy Fiber Axons Following Pilocarpine SE | 66 |
| 2.3.5 Enhanced pY816 Immunoreactivity Within Synaptic Mossy Fiber Boutons Following KA-SE | 68 |
| 2.3.6 Localization of pY816 Immunoreactivity within Apical Dendritic Shafts of CA1 Pyramidal Cells Following KA-SE | 71 |

| | |
|---|-----|
| 2.3.7 Localization of pY816 Immunoreactivity Within Apical Dendritic Shafts of CA1 Pyramidal Cells Following Pilocarpine SE | 75 |
| 2.3.8 Characterization of pY816 Immunoreactivity Within Apical Dendritic Shafts of Pyramidal Cells in CA1 Following KA-SE..... | 77 |
| 2.3.9 Enhanced pY816 Immunoreactivity Within Dendritic Spines of Pyramidal Cells in CA1 Stratum Radiatum Following KA-SE | 80 |
| 2.4 Discussion..... | 85 |
| 3. The Contribution of Vesicular Zinc to Transactivation of TrkB in Stratum Lucidum of Mouse Hippocampus | 94 |
| 3.1 Introduction..... | 94 |
| 3.2 Materials and Methods..... | 97 |
| 3.2.1 Generation of BDNF Mutant, ZnT3 Mutant, and ZnT3/BDNF Double Mutant Mice | 97 |
| 3.2.2 Preparation of Brain Specimens for Immunohistochemistry | 100 |
| 3.2.3 Immunohistochemistry | 101 |
| 3.2.4 Confocal Microscopy and Data Analysis..... | 102 |
| 3.2.4.1 Imaging Parameters | 102 |
| 3.2.4.2 Quantification of pY816 Immunoreactivity within Stratum Lucidum of Hippocampus | 103 |
| 3.2.5 Preparation of Brain Specimens for Western Blot and ELISA..... | 105 |
| 3.2.6 Western Blot | 106 |
| 3.2.7 BDNF ELISA..... | 107 |
| 3.3 Results..... | 108 |
| 3.3.1 Decreased Axonal and Synaptic pY816 Immunoreactivity within Stratum Lucidum in BDNF ^{-/-} Mice..... | 108 |

| | |
|--|-----|
| 3.3.2 Enhanced Axonal and Unchanged Synaptic pY816 TrkB Immunoreactivity within Stratum Lucidum of ZnT3 ^{-/-} Mice | 112 |
| 3.3.3 Total TrkB Levels Are Unchanged in the Hippocampi of ZnT3 ^{-/-} Mice | 115 |
| 3.3.4 BDNF Levels Increase within Hippocampi of ZnT3 ^{-/-} Mice | 115 |
| 3.3.5 Axonal and Synaptic pY816 TrkB Immunoreactivity within Stratum Lucidum Is Reduced in ZnT3 ^{-/-} BDNF ^{-/-} Compared to ZnT3 ^{-/-} BDNF ^{+/+} Mice | 117 |
| 3.3.6 Axonal and Synaptic pY816 TrkB Immunoreactivity in Stratum Lucidum Is Not Further Reduced in ZnT3 ^{-/-} BDNF ^{-/-} Compared to ZnT3 ^{+/+} BDNF ^{-/-} Mice..... | 119 |
| 3.4 Discussion | 121 |
| 4. Concluding Remarks and Future Directions..... | 126 |
| 4.1 Examples of How the Findings of This Dissertation May Guide Epilepsy Research | 127 |
| 4.2 Better Elucidating the Cellular and Synaptic Locales of Activated TrkB within Mouse Hippocampus | 129 |
| 4.3 Further Assessing the Contribution of Vesicular Zinc to Transactivation of TrkB in Stratum Lucidum of Mouse Hippocampus | 133 |
| Works Cited | 137 |
| Biography..... | 159 |

List of Tables

| | |
|---|----|
| Table 1: Primary antibodies employed in study. | 47 |
| Table 2: Secondary Antibodies Employed in Study. | 47 |

List of Figures

| | |
|---|----|
| Figure 1: Confocal micrographs of hippocampus in a Thy1-GFP expressing mouse..... | 14 |
| Figure 2: Schematic of TrkB, its important tyrosine signaling residues, and downstream signaling pathways..... | 20 |
| Figure 3: Zinc activates TrkB signaling by a BDNF-independent mechanism..... | 23 |
| Figure 4: Immunoreactivity labeling phosphorylated tyrosine 816 (pY816) of TrkB is enhanced within stratum lucidum (SL) following kainic acid (KA) induced status epilepticus (SE), observed preferentially in the hippocampus ipsilateral to KA microinfusion..... | 55 |
| Figure 5: High magnification (630x) images reveal discrete patches of pY816 immunoreactivity within SL, enhanced preferentially on the side ipsilateral to KA microinfusion..... | 58 |
| Figure 6: pY816 TrkB immunoreactivity colocalizes with axons of dentate granule cells (DGCs) in SL of hippocampus under both NS conditions and following KA-SE..... | 60 |
| Figure 7: pY816 TrkB immunoreactivity does not prominently colocalize with MAP2 stained dendrites of CA3 pyramids under either NS conditions or following KA-SE..... | 62 |
| Figure 8: Colocalization of pY816 TrkB immunoreactivity with cellular markers within the CA3c region of SL..... | 64 |
| Figure 9: pY816 immunoreactivity increases within SL following pilocarpine SE, and colocalizes with axons of DGCs..... | 67 |
| Figure 10: pY816 TrkB immunoreactivity is enhanced within synaptic mossy fiber boutons in SL following KA-SE, observed preferentially in the hippocampus ipsilateral to infusion..... | 69 |
| Figure 11: pY816 TrkB immunoreactivity is enhanced within apical dendrites of SR of CA1 following KA-SE, observed preferentially in the hippocampus ipsilateral to infusion..... | 72 |
| Figure 12: pY816 TrkB immunoreactivity is intracellular and punctate within the dendritic shaft of proximal apical dendrites of CA1 pyramidal cells..... | 76 |
| Figure 13: pY816 TrkB immunoreactivity is enriched preferentially within the portion of the apical dendritic shaft of CA1 pyramidal cells more proximal to soma..... | 79 |

| | |
|---|-----|
| Figure 14: pY816 TrkB immunoreactivity is enhanced within dendritic spines in CA1 SR following KA-SE, observed preferentially in the hippocampus ipsilateral to infusion.... | 81 |
| Figure 15: Breeding strategies for generating <i>BDNF</i> , <i>ZnT3</i> , and <i>ZnT3/BDNF</i> mutant and double mutant mice..... | 99 |
| Figure 16: pY816 TrkB immunoreactivity is enriched in mossy fiber axons and synapses within stratum lucidum (SL) of mouse hippocampus..... | 109 |
| Figure 17: pY816 TrkB immunoreactivity in mossy fiber axons and synapses within SL is decreased in <i>BDNF</i> ^{-/-} compared to <i>BDNF</i> ^{+/+} mice..... | 111 |
| Figure 18: Axonal pY816 TrkB immunoreactivity increases in axons but remains unchanged at synapses within SL in <i>ZnT3</i> ^{-/-} compared to <i>ZnT3</i> ^{+/+} mice. | 113 |
| Figure 19: Total TrkB and BDNF levels in whole hippocampal homogenates comparing <i>ZnT3</i> ^{-/-} and <i>ZnT3</i> ^{+/+} animals. | 116 |
| Figure 20: pY816 TrkB immunoreactivity in mossy fiber axons and synapses within SL is decreased in <i>ZnT3</i> ^{-/-} <i>BDNF</i> ^{-/-} double knockouts compared to <i>ZnT3</i> ^{-/-} <i>BDNF</i> ^{+/+} single knockout mice..... | 118 |
| Figure 21: Axonal and synaptic pY816 TrkB immunoreactivity is not further reduced within SL in <i>ZnT3</i> ^{-/-} <i>BDNF</i> ^{-/-} double knockouts compared to <i>ZnT3</i> ^{+/+} <i>BDNF</i> ^{-/-} single knockout mice..... | 120 |

Acknowledgements

I would like to thank everybody who has contributed to making this dissertation possible. Above all, I would like to thank my mentor, James O. McNamara, for his support and guidance throughout the time I have spent as a graduate student. He has been an invaluable role model throughout my development as a scientist, and his intelligent insights, logic, and unwavering enthusiasm will be qualities that I will continue to aspire to. I would like to also thank current and past members of my thesis committee: Anne West, Dennis Thiele, J. Victor Nadler, and Guoping Feng. Their time, energy, and critical insights into my work have been integral to the completion of this dissertation. I would like to acknowledge members of the McNamara lab who have helped me with experimental techniques necessary for my work and who may be coauthors on manuscripts included in this dissertation: Gumei Liu, Xiaoping He, and Yang Zhong Huang. Furthermore, the critical readings and analyses by A. Soren Leonard and Yang Zhong Huang of portions of this dissertation and documents relating to it have been infinitely valuable. I would also like to acknowledge Wei-Hua Qian, who spent considerable time on animal husbandry and genotyping relating to projects within this thesis, and Guoping Feng for providing the Thy1-GFP mice used for this dissertation. On a personal level, I would like to thank my parents and friends for their support throughout the time I have been in graduate school. Finally, I would like to thank Ram Puranam, A. Soren Leonard, Yang Zhong Huang, and Josh Lord for providing friendship, support, and guidance during my time here.

1. Introduction

1.1 Overview

Epileptogenesis is defined as the process by which a normal brain becomes epileptic. Understanding the cellular and molecular mechanisms by which epileptogenesis occurs will lead to a better understanding of the pathophysiology of this serious disease, and may reveal novel targets that can be the subjects of pharmacologic therapy. A central concept in the pathogenesis of epilepsy, introduced by the British neurologist Sir William Gowers who described the observation that “seizures beget seizures”, is that seizures themselves actually lead to permanent changes in brain plasticity that facilitate the development of epilepsy (Gowers, 1881). Though the underlying mechanisms by which these changes occur are not fully understood, multiple lines of evidence implicate the neurotrophin receptor, tropomyosin-related kinase B (TrkB), as being central to this phenomenon (Binder et al., 1999b; He et al., 2004; He et al., 2010; Liu, submitted). Such findings underscore the importance of understanding the specific neuroanatomical locales within the brain where TrkB signaling occurs, as well as what ligands mediate activation of this receptor at these locations. This is because elucidating where TrkB signaling occurs during epileptogenesis is likely to implicate specific cell populations, as well as subcellular locations within them, that contribute to neuronal excitability culminating in epilepsy. Understanding the ligands involved in TrkB receptor activation at these locales will further clarify molecules that may be central to this phenomenon. Such insights will better refine specific cellular and molecular

targets for study in epilepsy research, which are likely to be helpful in development of therapies against this disease. The objective of the investigations undertaken within this dissertation, therefore, was to better elucidate both of these aspects of TrkB signaling.

Numerous studies have demonstrated that TrkB is activated within hippocampus in models of temporal lobe epilepsy (TLE), suggesting the importance of its activation within this structure for the process of limbic epileptogenesis (Binder et al., 1999a; Danzer et al., 2004; He et al., 2004; He et al., 2002; He et al., 2010). For this reason, I set out to better define the cellular and synaptic locales where activated TrkB was enriched within hippocampus during epileptogenesis using a mouse model of limbic epilepsy. This was done by employing an antibody specific for a phosphorylated tyrosine residue (pY816) on the receptor, a surrogate marker for activated TrkB (Segal et al., 1996), using immunohistochemistry coupled with confocal microscopy.

Previous work from our laboratory has demonstrated that the transition metal, zinc, can cause activation of TrkB *in vitro* through a mechanism whereby it does not directly interact with the receptor (Huang et al., 2008). Zinc is particularly enriched within synaptic vesicles of dentate granule cells in a region of hippocampus known as stratum lucidum, and released from these vesicles during neuronal activity (Choi and Koh, 1998; Frederickson and Danscher, 1990; Frederickson et al., 2005). Interestingly, activated TrkB has also been found to be particularly enriched at this location during the development of limbic epilepsy (Binder et al., 1999a; Danzer et al., 2004; He et al., 2004; He et al., 2002; He et al., 2010). Because of both the temporal and spatial concordance of

this ligand and its activated receptor within stratum lucidum, I hypothesized that synaptic zinc may contribute to TrkB activation within this region. Therefore, I set out to test the relative contributions of both synaptic zinc and the canonical TrkB ligand, brain derived neurotrophic factor (BDNF), to TrkB activation within stratum lucidum of mouse hippocampus under physiological conditions. This line of investigation employed the same immunohistochemical techniques as for the activated TrkB localization studies, and also utilized mice that were deficient in synaptic zinc and/or BDNF (Cole et al., 1999; He et al., 2004). Completion of these studies yielded valuable information on both the anatomic locales of TrkB activation within hippocampus and the ligands contributing to its activation, and provided new insights into the understanding of TrkB signaling that are likely to be pertinent to the understanding of limbic epileptogenesis.

1.2 Epilepsy

Epilepsy is a serious neurological disease which is also very common, defined most simply by the occurrence of repeated and unprovoked seizures (Engel and Pedley, 2008). The disorder is estimated to have a prevalence of approximately 4-10 per 100,000, and though it may develop at any age, arises more often in young and elderly individuals (Forsgren et al., 2005; Sander, 2003). Lifetime prevalence rates of epilepsy are higher, as most that develop the disease go into remission within five years of diagnosis (Sander, 2003). However, up to one third of those who are initially diagnosed, even in developed countries where antiepileptic drugs are readily available, will eventually go on to develop medically refractory epilepsy (Kwan and Sander, 2004).

Epilepsy has a devastating impact on the life of the afflicted individual. In those with the most severe refractory epilepsy, the only viable treatment option may be surgical resection of significant portions of brain tissue in an attempt to remove the epileptic foci (Engel and Pedley, 2008), the magnitude of such an operation demonstrating the sheer severity of the disease these patients are experiencing. In addition to significant lifestyle impairments, those with symptomatic epilepsy have an increased risk of sudden death, with a shortened life expectancy of as much as 18 years (Gaitatzis et al., 2004; Lhatoo et al., 2001). Even in patients who are able to control their disease with the use of antiepileptic drugs, side effects from these medications can be significant, having a substantial impact on adherence to medication regimes and representing a major source of morbidity, disability, and even mortality related to epilepsy (Perucca and Gilliam, 2012). Furthermore, all antiepileptic drugs in use provide only symptomatic treatment, acting generally to reduce neuronal excitability, such as drugs which block sodium or calcium channels, or augment neuronal inhibition, such as drugs which enhance the activity of GABA receptors. These nonspecific mechanisms of action contribute to the severity of the side effects experienced, and the inability of these drugs to treat the underlying abnormality contributes to a significant risk of relapse in patients who decide to discontinue pharmacologic therapy (Engel and Pedley, 2008). Patients may therefore need to stay on these therapies for life, and also endure their difficult to tolerate side effects. All of these issues exemplify the need for new and effective treatments for this horrible disease. Basic science research into the molecular and cellular mechanisms of

epileptogenesis is a crucial first step in identifying new potential therapeutic targets that may more effectively treat or even cure epilepsy.

1.2.1 Clinical Aspects of Epilepsy

Epilepsy is the occurrence of repeated seizures, which are themselves defined as paroxysmal episodes of aberrant neuronal activity accompanied by stereotypical changes in behavior (Engel and Pedley, 2008). Such behavioral changes can range from momentary losses of consciousness to episodes of generalized myoclonic convulsions involving the entire body, and the accompanying aberrant, synchronous neuronal activity can be recorded with the use of an electroencephalogram (EEG). Epilepsy is not actually one disease, but rather represents a broad constellation of symptoms that arise from a variety of underlying causes, which in many cases may not be known. To this end, the epilepsies can be broadly classified into those arising from structural/metabolic, genetic, and unknown causes (Berg et al., 2010). Structural/metabolic epilepsies are those in which seizures arise as a consequence of specific etiologies such as a brain lesion, for example after traumatic brain injury. Genetic epilepsies, as the name implies, arise from an underlying genetic syndrome. Those with an unknown etiology likely fall into one of the two former categories, but the cause cannot be identified.

Specific types of seizures are classified clinically based on a system devised by the International League Against Epilepsy (2010), with the two major classifications being focal and generalized seizures. Generalized seizures are those where aberrant neuronal activity engages both brain hemispheres, and can involve both cortical and

subcortical structures. These seizures are further classified into tonic-clonic, absence, myoclonic, clonic, tonic, and atonic based on their specific behavioral and EEG features. Focal seizures, as their name suggests, originate from a specific epileptogenic focus within the brain and are limited to only one hemisphere, though they have the potential to secondarily generalize. Note that a previous version of this classification system further categorized seizures into simple, where the sufferer remains conscious during the event, and complex, where a loss of consciousness was involved (1989). A particularly severe form of seizures is known as status epilepticus (SE), defined clinically as uninterrupted seizures lasting more than five minutes or the occurrence of two or more seizures in which the patient does not return to baseline conditions, and it can potentially last for days (Nair et al., 2011). It is one of the most common neurological emergencies, requires immediate treatment to end the episode, and mortality in those with SE may be up to 20% (Trinka et al., 2012).

The most common epilepsies are focal, with the most common source of seizure activity being the temporal lobe (Engel and Pedley, 2008). TLE also represents the largest single class of epilepsy in patients who are refractory to medical treatment (Shukla and Prasad, 2012), making it particularly important to study. At present, those with medically intractable TLE may face surgical resection as the only treatment option, which can make the disease respond to pharmacologic therapy (Engel and Pedley, 2008). TLE is characterized by a seizure foci that is located within the limbic system (Bartolomei et al., 2005), and commonly begins in childhood or early adulthood. There

is a strong association between developing TLE and having experienced an “initial precipitating event”, such as febrile SE or trauma during the early years of life, followed by a latent period of as long as years before epilepsy actually develops (Mathern et al., 2002; Shukla and Prasad, 2012). Patients with TLE also very commonly have hippocampal sclerosis, first recognized in postmortem specimens over 180 years ago (Bouchet, 1826) and readily detectable using modern radiologic techniques. The pathological findings are hippocampal atrophy, neuronal loss, and gliosis, which is most profound in area CA1. Damage can be either unilateral or bilateral, and can also effect adjacent regions such as the parahippocampal gyrus and amygdala (Engel and Pedley, 2008; Malmgren and Thom, 2012). Whether this neuropathological finding actually is causative of the epilepsy, however, has been debated. Another common finding in hippocampal sclerosis, seen in humans with temporal lobe epilepsy as well as in animal models of this disease, is mossy fiber sprouting (Nadler et al., 1980). This phenomenon involves axons of dentate granule cells forming recurrent excitatory connections onto themselves, and has been hypothesized as a mechanism by which neuronal excitability is enhanced. Its causal contribution to the pathogenesis of temporal lobe epilepsy, however, has not been definitively established (Malmgren and Thom, 2012). As temporal lobe epilepsy is so common, and also commonly resistant to pharmacological treatment, this form of epilepsy has been a focus of study in our lab, and the hypotheses studied in Chapter 2 of this dissertation and (Helgager et al., 2013) are examined within the context of temporal lobe epilepsy.

1.2.2 Models of Epilepsy for Research Purposes

The study of epilepsy would be best conducted in humans who actually have the condition, and clinical trials are obviously an integral last stage in the development of any drug which may be used to treat epilepsy. However, use of animal models of epilepsy which reflect the human condition are invaluable research tools. Ethical concerns would preclude the study in humans of novel, experimental drugs which could potentially have safety issues, as could using invasive techniques to obtain specimens for examination of the molecular and cellular changes that take place in this disease. Furthermore, using animal models are in many cases much more efficient to study epileptic phenomena. Mice and rats, the most commonly used experimental animals, can be obtained in large numbers, and electrical or chemical convulsive stimuli can be administered in a controlled fashion. This results in the development of epilepsy in a predictable manner which is amenable to studying the natural progression of this disease, as well as for examining potential therapies. Finally, development of genetic knockout and transgenic technology, particularly in mice, allows for the controlled study of genetic modifications and how they may influence epilepsy and/or epileptogenesis.

An important factor in any animal model employed for the study of epilepsy is how accurately it emulates the human condition and, for the development of clinical therapies, how predictive it is of a drug being efficacious in humans. Interestingly, many antiepileptic drugs were initially validated through testing their efficacy in suppressing seizures directly induced by convulsant stimuli, such as using electroshock or

pentylenetetrazole (a chemoconvulsant), in normal animals (Loscher, 2002). Such models may accurately model seizures, but fail to emulate epileptogenesis. Efficacy of drugs in these models reflects their anticonvulsant actions, but does not address their ability to intervene in the process of epileptogenesis. Therefore, more accurate animal models of epilepsy are those which model the chronic aspects of this disease, and are also much more optimal for studying the molecular and cellular mechanisms by which this disorder develops (Loscher, 2002). Such models involve the process of actually making an animal epileptic, so that it would ultimately experience spontaneous recurrent seizures (SRSs) which are unprovoked. Furthermore, these models also replicate some of the neuropathology seen in humans with epilepsy, such as hippocampal sclerosis in those models which are thought to emulate TLE.

1.2.2.1 The Pilocarpine Model

The pilocarpine model was first developed and described as in (Turski et al., 1983a; Turski et al., 1983b). In this model, animals are made epileptic through prolonged SE, which features uninterrupted tonic-clonic seizures induced by intraperitoneal injection of pilocarpine. It was first developed in rats, though has subsequently been adapted to mice (Curia et al., 2008). The mechanism by which pilocarpine causes SE appears to be through activation of M1 muscarinic cholinergic receptors, as mice which are genetic knockouts of this receptor fail to develop seizures when injected with pilocarpine (Hamilton et al., 1997). However, after the initial occurrence of SE, seizures seem to be self-sustaining as they are unable to be terminated with atropine, a blocker of

muscarinic receptors (Clifford et al., 1987). Depending on the specific protocol, SE is allowed to spontaneously terminate after several hours, or is stopped using an anticonvulsant, generally a benzodiazepine (Curia et al., 2008). The pilocarpine model is considered to be one of TLE as it emulates many features of the disease. Namely, animals are subjected to an initial precipitating event, SE, and seizures during this episode have been documented to spread to the hippocampus (Turski et al., 1983a). Following termination of SE, there is a latent period which lasts from one to six weeks, after which animals enter a chronic period where they experience SRSs which are usually limbic in nature (Cavalheiro et al., 1991), demonstrating that these animals have developed epilepsy. Animals made epileptic in this model exhibit characteristic pathological findings of hippocampal sclerosis and mossy fiber sprouting (Curia et al., 2008). However, it should be noted that SRSs may be extra-limbic, a possible caveat in using it as a model of TLE (Harvey and Sloviter, 2005). Probably the biggest drawback of using this model is the high mortality encountered during the initial SE event, which has been reported to be around 30-40%, though some have reported even worse outcomes (Curia et al., 2008). This is a particular consideration when using lines of genetically modified mice, which may be in limited supply and difficult to readily generate.

1.2.2.2 The Kainic Acid Model and Kainic Acid Microinfusion Models

Kainic acid was first isolated from *Digenea simplex*, a species of seaweed, and is an agonist of kainic acid receptors (Raol and Brooks-Kayal, 2012). As with the pilocarpine model, it can be administered systemically through intraperitoneal injection

in rats and mice, and results in the development of generalized SE. Animals enter into a latent period following termination of SE, and develop SRSs after approximately a week (Williams et al., 2009). SRSs are generally limbic in nature, the same pathology as found in the pilocarpine model can be found in the hippocampi of animals treated with kainic acid, and for this reason the model is generally considered to be a model of TLE (Nadler et al., 1978; Raol and Brooks-Kayal, 2012; Tauck and Nadler, 1985). However, use of systemic kainic acid as a model of epileptogenesis has been limited by an excessively high mortality rate, as well the fact that a high percentage of animals treated with kainic acid induced SE do not go on to develop SRSs (Leite et al., 2002).

Alternative methods of kainic acid administration involve intraventricular or intrahippocampal infusions, and our lab has successfully adopted a method where kainic acid is infused into the basolateral amygdala through a surgically placed cannula, referred to as the kainic acid microinfusion model (Mouri et al., 2008). This model offers the advantage of directly activating limbic structures, unlike with systemic administration, ensuring that the epileptogenic focus is within the limbic system. Furthermore, mortality in this model is only around 10%, and mice reliably develop SRSs within a week of kainic acid induced SE. This lower mortality during SE and faster progression to developing epilepsy is much shorter and more practical than what is found in the pilocarpine model. Pathology consistent with hippocampal sclerosis, such as neuronal loss, gliosis, and mossy fiber sprouting, are also observed in this model, but this occurs

only on the side where kainic acid is infused. This unilateral hippocampal pathology is also commonly found in patients with temporal lobe epilepsy (Engel and Pedley, 2008).

1.2.2.3 The Kindling Model

The kindling model was discovered by Graham Goddard and colleagues (Goddard, 1967; Goddard et al., 1969) in the late 1960s. It differs from the pilocarpine and kainic acid models described above in that it does not involve giving an animal SE, but rather involves the controlled, chronic elicitation of focal seizures as a means of promoting epileptogenesis. In this model, initially subconvulsive focal electrical stimulations, when applied repeatedly, result in intense focal seizures which eventually generalize (Goddard et al., 1969). In order for kindling to occur, the electrical stimulation must initially elicit a small synchronous firing of neurons, known as an “afterdischarge” (Racine, 1972a). Kindling can be performed from a variety of locations in the brain, but the evolution of activity from brief to prolonged seizures is much more evident when they occur within limbic structures (Engel and Pedley, 2008). Kindling is commonly performed by electrical stimulation from the amygdala, and repeated stimulations evoke progressively more severe seizures which progress through the following behavioral classes (Racine, 1972b): Class 1, facial clonus; Class 2, head nodding; Class 3, unilateral forelimb clonus; Class 4, bilateral forelimb clonus with rearing; Class 5, rearing and falling with loss of postural control. These behaviors are accompanied by progressively longer and more generalized electrographic seizures. An animal is deemed “kindled” after it has progressed to developing Class 5 seizures; this

enhanced response to any further electrical stimuli will persist for the lifetime of that animal, demonstrating that it has undergone epileptogenesis (Engel and Pedley, 2008). In further support of this notion, animals that continue to receive electrical stimulation after developing Class 5 seizures will eventually display SRSs. Particularly later in the kindling process, neuropathological changes reminiscent of hippocampal sclerosis do become observable, such as neuronal death and gliosis, paralleling the condition of TLE (Cavazos et al., 1994; Cavazos et al., 1991).

1.3 Overview of Hippocampal Circuitry

As this dissertation extensively employs histology and microscopy to examine cellular and subcellular structures of hippocampus, a discussion of basic hippocampal circuitry is warranted. The unidirectional glutamatergic, excitatory pathways that underlie the major connections of the hippocampus was first coined the trisynaptic circuit by (Andersen et al., 1971). The major inputs to the hippocampus arise from the entorhinal cortex (Shepherd, 2004). The perforant path, which mostly innervates dendrites of dentate granule cells located in the molecular layer of the dentate gyrus, arises from layer II of the entorhinal cortex. Dentate granule cells project axons, known as mossy fibers, to the proximal dendrites of CA3 pyramidal neurons within stratum lucidum. Mossy fibers possess specialized giant boutons, which also synapse onto particularly enlarged, clustered spines on CA3 neurons known as thorny excrescences. The CA3 pyramidal cells send axons both ipsilaterally and contralaterally to other CA3 neurons, termed associational-commissural projections. They also make numerous

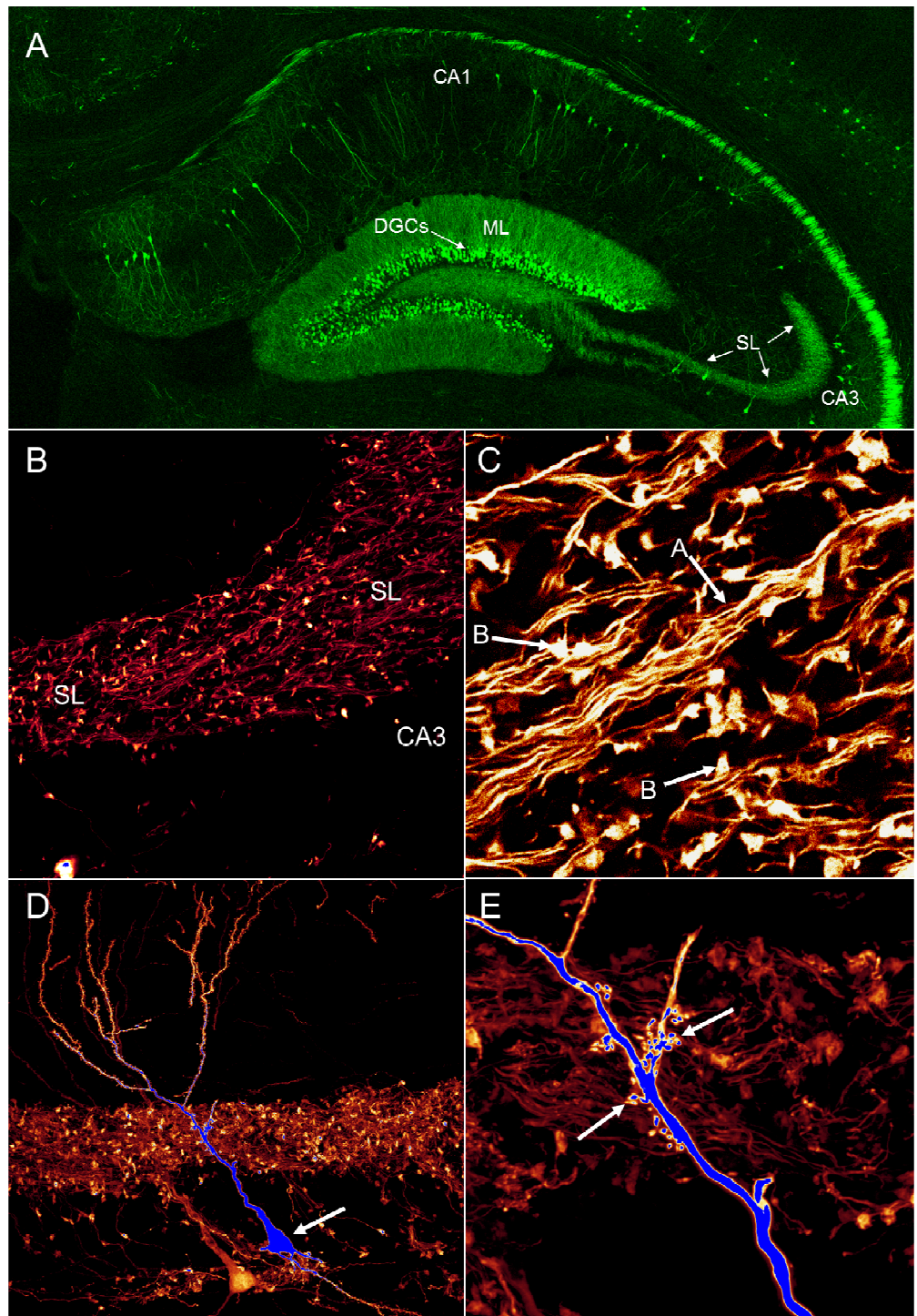


Figure 1: Confocal micrographs of hippocampus in a Thy1-GFP expressing mouse.

A) Low power image of hippocampus. Dentate granule cells (DGCs, arrows point to soma) project their dendrites into the molecular layer (ML) of the dentate gyrus. At this site the dentate granule cells receive input into the hippocampus from axons of entorhinal cortex (not visible). Axons of DGCs, known as mossy fibers, project to stratum lucidum (SL) where synapses are made onto dendrites of CA3 pyramidal cells (CA3). CA3 pyramidal cells in turn project their axons to CA1 pyramidal cells (CA1), which project back to entorhinal cortex. **B&C)** Close up views of stratum lucidum (SL) showing axons of dentate granule cells (A, arrow) which terminate in giant synaptic boutons (B, arrows). **D)** Image of a CA3 pyramidal cell (arrow points to soma), highlighting the entire dendritic tree of this neuron. **E)** The portion of CA3 dendrite within stratum lucidum has multiple thorny excrescences (arrows), large spines onto which giant mossy fiber boutons synapse. Images are pseudocolored projections of z-series acquired through confocal microscopy.

projections, known as Schaffer collaterals, onto CA1 pyramidal neurons. CA1 neurons either project directly back to entorhinal cortex, or project to neurons within subiculum which themselves send connections back to entorhinal cortex. Other projections originating from layer III of entorhinal cortex, termed the temporoammonic pathway, bypass dentate granule cells and CA3 neurons to project mostly onto CA1 pyramidal cell dendrites located within stratum lacunosum moleculare of CA1. It should be noted that this simplified description of excitatory hippocampal projections neglects to discuss myriad connections with multiple different types of interneurons located throughout hippocampus. Furthermore, the hippocampus also receives projections from other brain regions besides entorhinal cortex, such as the amygdala. Confocal micrographs of some of the basic hippocampal regions, cells, and their structures are shown in Figure 1. These micrographs were taken in a Thy1-GFP expressing mouse, in which GFP labels a subset of hippocampal neurons in this animal.

1.4 The Neurotrophin Receptors, TrkB, and Synaptic Plasticity

As the subject of this dissertation focuses on activation of the TrkB receptor, particularly as it relates to increased neuronal excitability facilitating epileptogenesis, the following discussion of the neurotrophin receptors will largely center on TrkB activation and evidence that it contributes to enhanced neuronal excitability.

1.4.1 Overview of the Neurotrophin Receptors and Their Molecular Biology

The tropomyosin-related kinase (Trk) family of neurotrophin receptors are named for the oncogene that resulted in their discovery, a gene which contained a translocation of a portion of non-muscle tropomyosin with a piece of a novel tyrosine kinase (Barbacid et al., 1991). This novel tyrosine kinase was subsequently named the TrkA receptor, and the other two tyrosine kinase receptors in this family, TrkB and TrkC, were identified shortly thereafter. The prototypical ligands for these receptors are the neurotrophins, homodimeric proteins of about 14 kDa which are synthesized and thought to be released by neurons and some non-neuronal tissues, particularly in response to neuronal activity (Huang and Reichardt, 2001; Lessmann and Brigadski, 2009). Interestingly, the neurotrophin ligand for TrkA, nerve growth factor (NGF), predated identification of its receptor by several decades. In the mid-20th century, this ligand had been demonstrated to be critical to survival of sympathetic neurons (Cowan, 2001). It was shown to be internalized in a receptor-dependent fashion and transported down axons using an energy-dependent process, having both local effects on nerve growth cones as well as

nuclear-dependent actions which influenced gene expression (Huang and Reichardt, 2001). It was not until 1991, however, that definitive evidence was provided showing that NGF acted through binding to the TrkA receptor (Kaplan et al., 1991; Klein et al., 1991). Brain-derived neurotrophic factor (BDNF) was originally isolated from pig brain by (Barde et al., 1982), and demonstrated to be the major ligand for TrkB, though neurotrophin-4 (NT-4) may also activate this receptor. Neurotrophin-3 (NT-3) is the major ligand for TrkC, though it can also bind and activate TrkA and TrkB (Barbacid, 1995). The neurotrophins have also been demonstrated to bind to the low affinity neurotrophin receptor p75^{NTR}, a member of the tumor necrosis factor (TNF) family (Huang and Reichardt, 2003). This receptor reduces the ability of NT-3 to activate TrkA and TrkB, and NT-4 to activate TrkB, making the three neurotrophin receptors more selective for NGF, BDNF, and NT-3 (Huang and Reichardt, 2003). Additionally, p75^{NTR} can have both prosurvival and apoptotic actions depending on the cell. However, a consistent finding is that p75^{NTR} leads to cell death in the absence of Trk receptors (Dechant and Barde, 1997).

Neurotrophins and their receptors were originally identified as being necessary for the survival of developing neurons. For example, NGF was identified using *in vitro* studies as necessary for the survival and differentiation of sympathetic and some dorsal root ganglion neurons in the peripheral nervous system, and mice that are genetic knockouts for NGF were born severely deficient in both of these neuronal populations (Lindsay, 1996). TrkC appeared to be particularly important for the survival and

development of large fiber proprioceptive neurons in the peripheral nervous system, with TrkC knockout mice also being deficient in these cell populations (Lindsay, 1996). Signaling through all of these receptors, however, has subsequently been shown to be critical for diverse neuronal processes including survival and proliferation, remodeling and growth of axons and dendrites, and synaptic plasticity (Huang and Reichardt, 2001). In support of the critical role for these receptors in the nervous system, *in situ* hybridization as well as northern analysis has demonstrated virtually ubiquitous expression throughout both the central and peripheral nervous systems (Lindsay, 1996). More than one receptor type is usually expressed in a single neuron, and there are some general developmental and regional expression patterns. TrkB and TrkC are expressed by almost all neurons in the central nervous system, whereas TrkA expression is confined to cholinergic neurons in the striatum and basal forebrain (Lindsay, 1996). In the peripheral nervous system, neurotrophin receptors are expressed in all neurons with the notable exception of the parasympathetic neurons of the ciliary ganglia (Lindsay, 1996). Expression of the neurotrophins largely parallels that of their receptors.

Neurotrophin receptors are activated in a manner typical of tyrosine kinase receptors. Binding of a neurotrophin molecule to the ectodomain of the neurotrophin receptor induces its dimerization, resulting in phosphorylation of multiple tyrosine residues within its intracellular domain (Barbacid, 1995; Cunningham and Greene, 1998). As the subject of this dissertation is TrkB, these intracellular residues will be referred to with respect to their precise residue number within this receptor, though they are common

to all Trk receptors. Phosphorylation of these residues is thought to occur in a lockstep fashion, beginning with tyrosine residues 705 and 706 (pY705/706), causing kinase activation. This leads to autophosphorylation of residues 515 and 816 (pY515 and pY816), which in turn bind and activate alternate signal transduction cascades. pY515 recruits the Shc adaptor protein through phosphotyrosine binding domains, ultimately resulting in activation of the Ras-mitogen-activated protein kinase (MAPK) pathway. Through a complex set of protein interactions, this residue also signals phosphatidylinositol 3-kinase (PI3K), which results in activation of the protein kinase Akt (Minichiello, 2009). These downstream signaling pathways of pY515 have been suggested to mediate actions of neurotrophin receptors related to survival signaling and suppression of apoptosis in neurons (Hetman and Xia, 2000). pY816 recruits phospholipase-C γ 1 (PLC- γ 1) resulting in production of inositol-1,4,5-trisphosphate (IP3) and diacylglycerol (DAG) (Minichiello, 2009). IP3 results in release of Ca^{2+} from intracellular stores, resulting in activation of Ca^{2+} /calmodulin dependent kinases, whereas DAG activates protein kinase C (PKC). Downstream signaling from pY816 is thought to mediate the actions of neurotrophins effecting synaptic plasticity, as will be described in more detail later in this section. A basic schematic of TrkB signaling is illustrated in Figure 2.

Neurotrophin receptors must be at the membrane in order to bind their extracellular ligands, are thought to be internalized into endosomes in response to

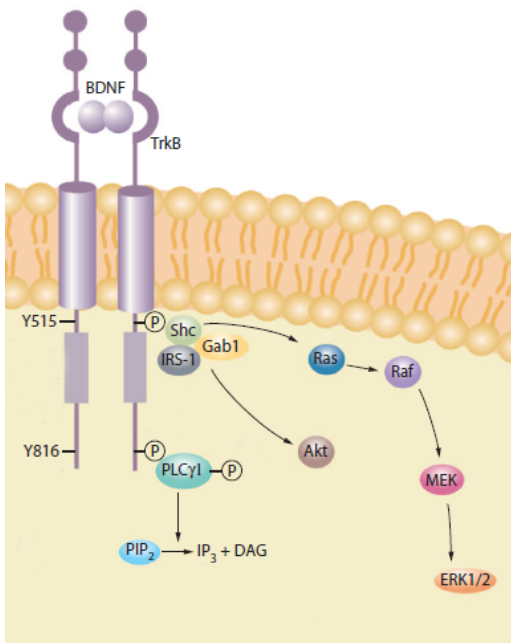


Figure 2: Schematic of TrkB, its important tyrosine signaling residues, and downstream signaling pathways.

Figure adapted from (McNamara et al., 2006).

activation, and once internalized may continue to signal from this locale (Howe and Mobley, 2005). Retrograde transport of neurotrophin receptors in complex with their ligands have been described in axons, and may be a means by which signals are conveyed from synapse to nucleus (Bhattacharyya et al., 1997; Niewiadomska et al., 2011; Watson et al., 1999a). Forms of TrkB and TrkC receptors have also been identified which lack their intracellular signaling domains, and thus are unable to activate any signaling cascades. The role of these truncated receptors is not clear, however they have been hypothesized to act by competing for dimerization with full-length receptors, thus acting in a dominant negative fashion. In support of this hypothesis, mice overexpressing a

truncated form of TrkC have similar neuronal losses as observed in TrkC knockout animals (Eide et al., 1996; Palko et al., 1999).

1.4.2 Transactivation of Neurotrophin Receptors

In addition to neurotrophin-mediated activation, neurotrophin receptors have been shown to undergo transactivation, a process by which a receptor is activated by a ligand without directly interacting with it (Carpenter, 1999). Neurotrophin receptor transactivation was initially examined by Chao and colleagues, who demonstrated that adenosine, a neurotransmitter, could activate Trk receptors both in PC12 cells and hippocampal cultures through a neurotrophin-independent process (Lee et al., 2002a). Though the mechanism by which transactivation occurs is incompletely understood, use of specific adenosine receptor agonists and antagonists established that this effect was mediated through the adenosine-A_{2A} receptor, which is a G-protein coupled receptor (GPCR). Trk receptor transactivation was blocked by specific inhibitors of Src-family kinases (SFKs), suggesting that these signaling molecules may act downstream of the A_{2A} receptor to mediate Trk receptor phosphorylation. Pituitary adenylate cyclase-activating polypeptide (PACAP), a neuropeptide which also activates a GPCR, transactivated Trk receptors through a similar SFK-dependent mechanism (Lee et al., 2002b). Transactivation of Trk receptors by adenosine and PACAP resulted in activation of downstream effectors, such as MAPK and PLC- γ 1, showing that transactivated neurotrophin receptors also participated in downstream signaling (Lee et al., 2002a). Importantly, transactivation by adenosine and PACAP takes hours after exogenous

application to fully activate Trk receptors, whereas neurotrophin ligands robustly activate their receptors on a time scale of seconds to minutes. Activation of Trk receptors by neurotrophins necessarily must occur at the cell membrane, but transactivation events by adenosine and PACAP may occur predominantly on receptors located at an intracellular locale, such as Golgi membranes (Rajagopal et al., 2004). Trk transactivation has been suggested to have relevance *in vivo*, most notably supported by a study demonstrating that application of A_{2A}-receptor agonists promoted survival of lesioned facial motoneurons in rodents through a process suggested to be dependent on TrkB transactivation (Wiese et al., 2007).

Our laboratory discovered another means by which TrkB receptors can be transactivated, which stemmed from a finding involving activated TrkB within stratum lucidum during epileptogenesis. In mice with a conditional deletion of BDNF, resulting in elimination of this neurotrophin from dentate granule cells and CA3 pyramidal neurons of stratum lucidum, TrkB activation was only partially diminished following seizures, and epileptogenesis was only modestly inhibited (He et al., 2004). Subsequent work employing an NT-4 null mutant mouse demonstrated that absence of this neurotrophin likewise failed to diminish TrkB activation and epileptogenesis (He et al., 2006). This prompted a search for other ligands which could activate this receptor. Studies with epithelial growth factor receptor (EGFR), another tyrosine kinase, found that this molecule could be transactivated by the divalent cation, zinc (Wu et al., 2002).

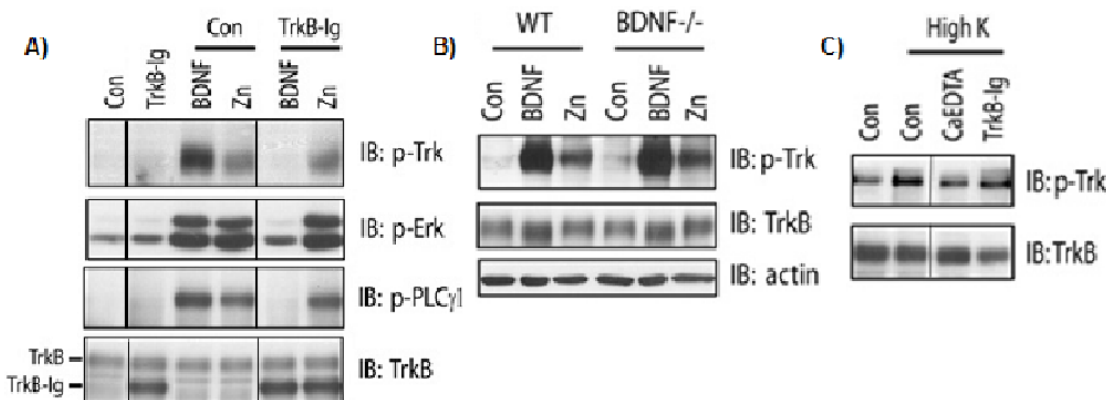


Figure 3: Zinc activates TrkB signaling by a BDNF-independent mechanism.

In the experiments above, cortical neurons cultured from E18 rat pups (A and C) or mouse P1 pups (B) were maintained *in vitro* for 12-14 days. Cell lysates were subjected to immunoblotting with the indicated antibodies after the treatments described. A) Both BDNF and zinc cause TrkB phosphorylation, resulting in phosphorylation of downstream Trk effectors Erk and PLC- γ 1. Addition of TrkB-Ig (2 mg/mL), a BDNF scavenger, occludes BDNF but not zinc activation of Trk. Neurons were treated for 15 minutes with vehicle, BDNF (10 ng/ml) or zinc (100 μ M). B) Zinc activates TrkB in cortical neurons of BDNF $^{-/-}$ mice. Cortical neurons cultured from wild type and BDNF null mutant pups were incubated with vehicle, BDNF (10 ng/mL) or zinc (100 μ M) for 15 minutes. C) Activity facilitates endogenous zinc-induced TrkB activation. High potassium induces Trk phosphorylation, which can be occluded by CaEDTA, a zinc chelator, but not TrkB-Ig. Cortical neurons were preincubated with CaEDTA (1 mM), a zinc chelator, or TrkB-Ig (2 μ g/mL) for 30 minutes. Each of these treatments was continued for an additional 30 minutes in the presence of high (50 mM) K $^{+}$ buffer. TrkB-Ig eliminated BDNF-mediated increases of pTrk in the presence of KCl, demonstrating the efficacy of TrkB-Ig under these experiments conditions. Figure adapted from (Huang et al., 2008).

Because of this finding, our lab hypothesized that zinc may similarly transactivate the TrkB receptor, and this was subsequently demonstrated in neuronal-glial cultures prepared from rodent cortex (Fig. 3A) (Huang et al., 2008). TrkB transactivation after application of exogenous zinc could be observed within five minutes, peaked between 30

and 60 minutes, and declined by 120 minutes, following a kinetic time course more similar to activation of TrkB by BDNF than adenosine or PACAP transactivation. Exogenously applied zinc was found to mediate TrkB phosphorylation in neurons cultured from BDNF knockout mice, demonstrating this phenomenon to be BDNF independent (Fig. 3B) (Huang et al., 2008). The mechanism by which zinc transactivates TrkB, as with adenosine or PACAP transactivation, was found to occur through SFK. To this end, SFK was activated in a manner that paralleled transactivation of TrkB by zinc, and transactivation was blocked by SFK inhibitors. The hypothesized mechanism by which TrkB is transactivated by SFK has to do with the ability of zinc to bind and inhibit another protein kinase, C-terminal Src kinase (Csk) (Sun and Budde, 1999). When uninhibited, Csk will phosphorylate the C-terminal tyrosine residue, Y527, of SFK. pY527 causes intramolecular inhibition of SFK by preventing phosphorylation at its catalytic site, Y416 (Cole et al., 2003; Cooper and Howell, 1993). Thus, the net effect of zinc inhibition of Csk is activation of SFK, and SFK itself can directly phosphorylate and thereby transactivate TrkB (Huang and McNamara, 2010; Huang et al., 2008).

Our laboratory also found that endogenous zinc could activate TrkB in a BDNF independent fashion using the same *in vitro* neuronal preparations described above (Fig. 3C) (Huang et al., 2008). TrkB activation was induced in these experiments by neuronal activity, and chelation of extracellular zinc blocked this activation. As zinc is found within presynaptic vesicles of many glutamatergic neurons throughout the CNS, and most

notably enriched in mossy fibers of stratum lucidum, we hypothesized that endogenous zinc may transactivate TrkB *in vivo* (Frederickson et al., 2005).

1.4.3 The TrkB Receptor and Long Term Potentiation

Long term potentiation (LTP) is the phenomenon whereby brief high-frequency electrical stimulation of a synapse results in persistent augmentation of synaptic strength, usually measured by an increase in EPSPs following the stimulation (Minichiello, 2009). For many years, this phenomenon has been speculated to occur under physiological conditions, and may be a mechanism by which learning and memory take place. LTP has been documented at various synapses within the nervous system, but is most commonly studied at the CA3-CA1 synapse within hippocampus, where Schaffer collaterals of CA3 pyramidal neurons innervate the spines of CA1 pyramidal cells. Induction of LTP at this synapse is NMDA receptor dependent, and expression can be divided into early LTP (E-LTP), where cellular changes occur leading to potentiation, such as trafficking and phosphorylation of AMPA receptors, and late LTP (L-LTP), which involves changes in gene expression and protein synthesis (Minichiello, 2009). At this synapse, considerable work has been performed showing that TrkB and BDNF are involved in E-LTP. In mice that are genetic knockouts of BDNF, E-LTP is impaired at this synapse (Korte et al., 1995), however reintroduction of BDNF through exogenous application or viral transduction successfully restored this defect (Korte et al., 1996; Patterson et al., 1996; Pozzo-Miller et al., 1999). Further work suggested that BDNF may also be important for expression of L-LTP (Korte et al., 1998). Mice with conditional deletions of TrkB from

both CA3 and CA1 pyramidal cells demonstrated impairment of LTP, showing the importance of signaling through this receptor for this phenomenon (Minichiello et al., 1999; Xu et al., 2000). In order to dissect the TrkB signaling pathways important for LTP, mice were generated with tyrosine to phenylalanine (Y→F) mutations of either the Y816 or Y515 residues of TrkB, preventing phosphorylation and downstream activation of signaling pathways from these sites. Interestingly, studies revealed that it was pY816 (Minichiello et al., 2002), which signals through PLC- γ 1, and not pY515 (Korte et al., 2000), which signals through Shc, which is important for LTP. An important distinction is that though TrkB signaling may be necessary for development of LTP, TrkB activation alone induced by application of exogenous BDNF is not sufficient to cause LTP to develop in the absence of high frequency stimulation (Figurov et al., 1996; Lu et al., 2008; Patterson et al., 1996).

A requirement of TrkB and BDNF for normal expression of LTP has also been found at the mossy fiber-CA3 (mf-CA3) synapse, where mossy fiber axons form synapses onto CA3 pyramidal neurons. In contrast to LTP at the CA3-CA1 synapse, LTP at mf-CA3 synapses is induced and expressed by a mechanism intrinsic to the presynaptic dentate granule cell, and involves an increase in glutamate release (Nicoll and Schmitz, 2005; Pan et al., 2011). LTP is impaired at this synapse in mice that are genetic knockouts for TrkB (Huang et al., 2008). Animals expressing a mutant form of TrkB, rendering it sensitive to inhibition by a small molecule, 1NMPP1, also had impaired LTP at this synapse in response to transient inhibition of this receptor by this small molecule

(Huang et al., 2008). Interestingly, as with the CA3-CA1 synapse, it is the PLC- γ 1 signaling pathway through pY816 of TrkB that appears to be important for the effects of TrkB on LTP. Y816F TrkB mutants showed impaired LTP at the mossy fiber-CA3 synapse, whereas Y515F TrkB mutants displayed intact LTP (He et al., 2010).

In addition to LTP deficits, mice lacking the TrkB receptor have also been shown to have deficits in hippocampal-dependent learning, suggesting that neuronal excitability mediated by TrkB may also be critical for this process. Mice with a conditional deletion of TrkB from cells of the hippocampus, as well as other regions of the forebrain, demonstrated deficits in the ability to learn the Morris water maze and other spatial learning tasks (Minichiello et al., 1999). Interestingly, associative learning, also thought to be hippocampal-dependent, was shown to be disrupted in Y816F TrkB mutants, but not in Y515F mutant mice, suggesting that signaling through PLC- γ 1 is critical to this process (Gruart et al., 2007).

1.4.4 The TrkB Receptor and Epilepsy

Given the importance of TrkB in regulating processes of synaptic plasticity and excitability, this receptor has been extensively investigated in terms of its ability to mediate the process of epileptogenesis. Due to the pivotal role that this receptor plays in the pathogenesis of epilepsy, elucidating the cellular and molecular mechanisms by which TrkB mediates this phenomenon has become a primary topic of study by our laboratory. It is our hope that through understanding the mechanisms by which this

receptor mediates the development of epilepsy, novel therapies may be developed which can prevent epileptogenesis through targeting TrkB.

Early work noted increased expression levels of BDNF in models of epilepsy, suggesting that signaling through TrkB may be involved in this disease. Using *in situ* hybridization, BDNF mRNA was increased in rodent hippocampus and other brain structures shortly after SE induced by kainic acid, or following kindling (Ernfors et al., 1991; Isackson et al., 1991). Striking increases in BDNF protein levels, particularly within stratum lucidum, were later observed within hippocampus following kainic acid induced seizures using immunohistochemical methods employing a BDNF-specific antibody (Conner et al., 1997). Subsequently, immunohistochemical methods employing an antibody specific for phosphorylated Trk receptors also demonstrated increases in activated Trk within stratum lucidum (Binder et al., 1999a). This finding was subsequently replicated by numerous studies in various models of epileptogenesis, all demonstrating what appeared to be a region-specific enrichment in activated Trk receptors within stratum lucidum of hippocampus during the development of limbic epilepsy (Danzer et al., 2004; He et al., 2004; He et al., 2002; He et al., 2010). Notably, these increases within stratum lucidum did not occur in models of epileptogenesis in mice with Y515F mutations in TrkB using an antibody recognizing pY515 (He et al., 2002). Increased levels of Trk receptor activation in epilepsy models assayed using Western blot of hippocampus were also blocked in Y816F TrkB mutant mice using an antibody that recognized pY816 of the Trk receptor (He et al., 2010). This demonstrated that the

striking increase observed in phosphorylated Trk receptors in models of epileptogenesis was due to pTrkB

BDNF and TrkB have been demonstrated to be pivotal to the process of epileptogenesis, suggesting that this TrkB signaling within hippocampus and other CNS structures is likely to be integral to the pathogenesis of this disease. Kindling was markedly impaired in mice heterozygous for the BDNF gene (Kokaia et al., 1995). Intraventricular infusion of TrkB-Fc, a BDNF scavenging protein, impaired epileptogenesis in this model (Binder et al., 1999b). Interestingly, infusion of TrkA-Fc or TrkC-Fc, scavengers for NGF or NT-3, respectively, did not affect kindling development in the same study, suggesting that BDNF/TrkB signaling in particular is important for this phenomenon (Binder et al., 1999b). Both transgenic overexpression of BDNF (Croll et al., 1999) and infusion of BDNF into hippocampus (Xu et al., 2004) of rodents enhances the process of limbic epileptogenesis, demonstrating that excess activation of TrkB promotes limbic epilepsy.

All of these studies, while suggesting that BDNF facilitates epileptogenesis by signaling through TrkB, fail to directly show the involvement of this receptor in the development of limbic epilepsy. Compelling evidence that TrkB is directly involved in this process, however, was provided in (He et al., 2004). In this study, TrkB conditional knockout mice, which lack this receptor from regions of forebrain including cells populating stratum lucidum, failed to undergo kindling. Importantly, these animals were still capable of experiencing acute seizures, demonstrating that this observation was not

due to a broader developmental defect in these animals which compromised their ability to experience behavioral seizures. In order to dissect the TrkB signaling pathways important for epileptogenesis, animals with Y515F and Y816F mutations in TrkB were kindled. Interestingly, mice with Y515F mutations kindled normally, whereas kindling was impaired in Y816F animals, demonstrating the importance TrkB signaling through the PLC- γ 1 pathway in the development of epileptogenesis. This is notable given that pY816 signaling has also been demonstrated to be necessary for the development of some forms of LTP.

A recent, intriguing study has demonstrated that even transient inhibition of TrkB signaling can prevent epileptogenesis (Liu et al., submitted). Mice with a mutant TrkB receptor, making it susceptible to reversible inhibition in the presence of a small molecule, 1NMPP1, were given SE through kainic acid microinfusion into the basolateral amygdala. Following this episode, animals were treated with 1NMPP1 for a period of two weeks, after which treatment was discontinued. Almost no SRSs in these animals were detected during 1NMPP1 treatment, whereas TrkB mutants not administered 1NMPP1, or wild type mice given this small molecule, experienced numerous SRSs consistent with the development of epilepsy in these animals. Most notably, even after discontinuation of 1NMPP1 following the two week treatment period, mice susceptible to inhibition of TrkB by this small molecule failed to demonstrate significant numbers of SRSs, even up to six weeks after the initial SE episode. In contrast, animals treated with SE that never experienced TrkB inhibition by 1NMPP1 experienced many SRSs at this

time point. The fact that 1NMPP1 was administered directly after SE in this study is particularly important because TrkB inhibition during the episode could have anticonvulsant effects, confounding the ability to examine its antiepileptogenic effects. These findings demonstrate that transient inhibition of TrkB after an initial precipitating event, such as SE, is actually sufficient to permanently suppress plastic changes resulting in epileptogenesis. Such results suggest that therapies even transiently inhibiting TrkB signaling during the process of epileptogenesis may permanently prevent this process. Development of such potential therapies will therefore be the subject of future studies.

1.5 Zinc in the CNS

The transition metal, zinc, is an essential micronutrient (Sandstead, 2000) which is a critical component of many enzymes and proteins (Berg, 1990). Within the nervous system, zinc is thought to be an important neuromodulator, and is known to affect the activity of many neurotransmitter receptors and signaling proteins (Frederickson et al., 2005). It is shuttled by transporters between cellular compartments and organelles, sequestered within intracellular storage pools, and released in response to various stimuli. Despite its critical functions, however, its excess is thought to be neurotoxic (Choi and Koh, 1998), and its levels must therefore be tightly regulated. Zinc has been implicated in playing a role in a variety of nervous system pathologies including Alzheimer's disease (Sensi et al., 2009) and neurotoxicity following cerebral ischemia (Koh et al., 1996).

Zinc has been found to be enriched in the presynaptic vesicles of certain glutamatergic neurons that populate both limbic and neocortical structures (Sindreu et al., 2003), most notably within boutons of mossy fibers of dentate granule cells, and is co-released with glutamate in response to neuronal activity (Frederickson and Danscher, 1990; Frederickson et al., 2005). This “free” (chelatable) zinc within mossy fibers was first detected by Maske using histochemical methods, who noted a bright red band within stratum lucidum of hippocampus that corresponded to large deposits of this transition metal within mossy fiber boutons (Maske, 1955). Ever since this finding, the precise role of this vesicular zinc in modulating CNS function has been a matter of debate, its functions still incompletely understood. The mechanism by which vesicular zinc becomes enriched at glutamatergic synapses is through a zinc transporter, ZnT3, and it is notable that a Timm’s stain, which detects free transition metals, is abolished in mice that are knockouts for this receptor (Cole et al., 1999). Zinc release from mossy fiber boutons has been visualized using dyes that detect zinc (Qian and Noebels, 2005), and this release was not detected in ZnT3 knockout animals. Concentrations of zinc in the synaptic cleft in response to neuronal activity have been estimated at around 10–30 μ M (Li et al., 2001; Thompson et al., 2000; Ueno et al., 2002). The potential contribution of this synaptically released zinc to TrkB transactivation and epileptogenesis, particularly given the concordance of this synaptically released zinc and pTrkB immunoreactivity within stratum lucidum in models of epilepsy, has been of great interest to our lab. Notably, chelation of zinc has been found to impair LTP at the mf-CA3 synapse (Huang et al.,

2008; Pan et al., 2011), suggesting that TrkB transactivation by vesicular zinc may be critical to development of LTP at this locale. However, the observation that LTP was unimpaired in ZnT3 knockout mice failed to further substantiate this finding (Pan et al., 2011).

A widely studied example of how zinc functions as a neuromodulator is through its inhibition of NMDA receptors (Peters et al., 1987). This is mediated by both a high-affinity binding site on the NR2A subunit, with an IC₅₀ of around 5 nM, as well as a low-affinity, voltage-dependent site on the NR2A subunit with an IC₅₀ which is in the low micromolar range, thought to be important during neuronal activity (Aslamkhan et al., 2002; Coughenour and Barr, 2001; Low et al., 2000). Given concentrations of zinc found under physiological concentrations, the expectation is that this high affinity binding site would be at least partially occupied by zinc, therefore providing tonic inhibition of NMDA receptors (Frederickson et al., 2005). Evidence for this has been provided using zinc chelators, which have been demonstrated to potentiate NMDA currents (Martin et al., 1992; Paoletti et al., 1997; Vogt et al., 2000). A recent study generated a mouse with a mutant high-affinity zinc binding site, rendering zinc unable to bind at this locale. Interestingly, these animals showed enhanced sensitivity to pain as well as allodynia, providing evidence that tonic inhibition of NMDA receptors by zinc has physiological importance (Nozaki et al., 2011). Other examples of the numerous documented neuromodulatory effects of zinc are its ability to inhibit GABA receptors, its proposed

modulation of voltage-gated ion channels, as well as the inhibition of glutamate and dopamine reuptake transporters (Frederickson et al., 2005).

1.5.1 Vesicular zinc and plasticity at the mf-CA3 synapse

Generation of mice that are knockouts for the ZnT3 protein have provided the opportunity to examine the effects of ridding vesicular zinc from neurons that normally co-release this metal along with glutamate from presynaptic vesicles. The ZnT3 transporter is a member of a large family of zinc transporters which mediate zinc efflux from the cytosol, either to intracellular organelles or across the plasma membrane (Palmiter and Huang, 2004). Importantly, the distribution of ZnT3 is restricted to the nervous system, where it is found only in neurons that contain zinc within their synaptic vesicles. Therefore, this genetic knockout provides a clean and specific means of eliminating synaptic zinc (Cole et al., 1999). Given the large amounts of synaptic vesicular zinc found within hippocampus, and the known neuromodulatory effects of this metal, examination of the *ZnT3* knockout largely sought to find deficits in synaptic transmission and neuronal excitability at this locale, as well as deficits in hippocampal-dependent behaviors such as learning.

At first assessment, $ZnT3^{-/-}$ mice were grossly normal, with no differences in body weight, lifespan, or fertility compared to wild type littermates (Cole et al., 1999). Ultrastructural assessment of mossy fiber boutons revealed no abnormalities. Zinc levels were reduced by approximately 20% in the hippocampi and neocortex of these mice, as a result of a lack of synaptic vesicular zinc. Interestingly, mutant mice were shown to be

more sensitive to seizures induced by kainic acid, whereas they were less sensitive to those induced by bicuculline, a GABA_A antagonist (Cole et al., 2000). These effects could potentially reflect disinhibition of both NMDA receptors and GABA_A receptors in the absence of synaptic zinc. Early studies failed to find any deficits in learning when animals were tested in paradigms of hippocampal-dependent learning tasks (Cole et al., 2001), such as the Morris water maze, and basal synaptic transmission as well as LTP was unimpaired at the mossy fiber-CA3 synapse (Lopantsev et al., 2003; Pan et al., 2011). All of this suggested that synaptic transmission and hippocampal function in the absence of synaptic zinc remained grossly normal.

However, further study of *ZnT3* knockout animals revealed that some forms of hippocampal-dependent learning were impaired. Studies conducting more in-depth examinations of hippocampal-mediated learning, such as reversal learning in the Morris water maze and working memory in the rewarded-alternation T-maze task, did find deficits (Martel et al., 2011; Sindreu et al., 2011). Furthermore, *ZnT3* knockouts were found to have deficits in contextual fear discrimination (Martel et al., 2011; Sindreu et al., 2011), contradicting an earlier study (Lopantsev et al., 2003). Interestingly, one of these studies also found that MAPK signaling was impaired in *ZnT3* knockouts, though the mechanism was attributed to the enhanced activation of a phosphatase in the absence of synaptic zinc, not to any decrease in TrkB activation (Sindreu et al., 2011). Furthermore, examination of learning tasks thought to be dependent on the amygdala, which also contains glutamatergic neurons possessing synaptic zinc, found deficits in associative

fear memory and extinction (Martel et al., 2010). Finally, testing spatial memory in older mice (six months of age), as opposed to young mice examined in the previous study (Cole et al., 2001), demonstrated that ZnT3 mutant animals performed significantly worse in the Morris water maze compared to wild type controls (Adlard et al., 2010). Furthermore, the investigators noted decreased levels of proteins involved in synaptic transmission, such as NMDA receptors and TrkB. The investigators hypothesized that vesicular zinc is critical to maintaining normal synaptic function during the aging process.

Despite the fact that LTP did not appear to be impaired in ZnT3 knockout mice at the mf-CA3 synapse, further study revealed qualitative differences in LTP in mutant compared to wild type animals (Pan et al., 2011). As previously discussed, expression of LTP at the mf-CA3 synapse occurs through a presynaptic mechanism of increased glutamate release from mossy fiber boutons (Nicoll and Schmitz, 2005). A means of measuring this is through paired pulse facilitation (PPF), which is inversely related to neurotransmitter release from a synapse (Cowan et al., 2001). Interestingly, LTP at the mf-CA3 synapse in slices from wild type animals is associated with decreased PPF, whereas it was found to be unchanged in *ZnT3* knockout animals, or in the presence of a zinc chelator. Furthermore, mice mutant for *rim1α*, a protein localized to the presynaptic active zone, do not express LTP at the mf-CA3 synapse, as enhanced glutamate release at this synapse in response to LTP-inducing stimuli does not occur (Castillo et al., 2002). Strikingly, however, LTP at this synapse in these mutant animals could be induced in the

presence of a zinc chelator. This, as well as other data within (Pan et al., 2011), demonstrates that LTP at the mf-CA3 synapse in the ZnT3 knockout animal occurs through a novel postsynaptic mechanism, not the conventional presynaptic one. This is particularly interesting in light of the fact that studies have suggested that TrkB is involved in LTP through a presynaptic mechanism, and that work from this dissertation localizes activated TrkB to mossy fiber boutons (Helgager et al., 2013; Xu et al., 2000). All of this evidence demonstrates that zinc plays a critical neuromodulatory role at the glutamatergic synapses where it is released, and that one such component of this role could be TrkB transactivation.

2. The Cellular and Synaptic Location of Activated TrkB in Mouse Hippocampus during Limbic Epileptogenesis

This chapter has been adapted from (Helgager et al., 2013).

2.1 Introduction

Epilepsy is a serious common neurological disorder, afflicting an estimated 1% of the population worldwide (Shorvon, 1996). Limbic epilepsy (synonymous with temporal lobe epilepsy [TLE]) is particularly problematic because it is both common and commonly resistant to optimal contemporary treatment (Arroyo et al., 2002). Clinical observations led Sir William Gowers (1881) to propose that seizures themselves promote progression of epilepsy, a proposal supported by subsequent studies of animal models in which recurrent seizures alone are sufficient to destroy limbic neurons and induce lifelong severe epilepsy (Sayin et al., 2003). An extension of Gowers' hypothesis is that an episode of continuous seizure activity spanning 30 minutes to hours (status epilepticus, SE) is *sufficient* to induce TLE that persists for a lifetime. Indeed SE alone is sufficient to induce TLE in models of both developing and adult rodents (Dunleavy et al., 2010; Loscher, 2002). Circumstantial evidence supports the idea that SE contributes to the pathogenesis of TLE in humans (Annegers et al., 1979; Tsai et al., 2009; VanLandingham et al., 1998).

Understanding how seizures promote induction and/or progression of epilepsy may reveal molecular targets for preventive therapy. Experimental evidence suggests that the neurotrophin, brain-derived neurotrophic factor (BDNF), promotes limbic

epileptogenesis by activation of its cognate receptor, tropomyosin-related kinase B (TrkB). Epileptogenesis was markedly impaired in the kindling model in mice heterozygous for the BDNF gene or in rats following intraventricular infusion of a BDNF scavenging protein (Binder et al., 1999b; Kokaia et al., 1995). Conditional deletion of TrkB in mice abolished limbic epileptogenesis in an animal model induced by recurrent seizures (He et al., 2004), and transient inhibition of TrkB signaling following SE in a mouse model prevented subsequent development of spontaneous recurrent seizures (SRS) (Liu et al., submitted). These findings demonstrate that TrkB is *necessary* for limbic epileptogenesis. Transgenic overexpression of BDNF enhances limbic epileptogenesis (Croll et al., 1999), as does direct infusion of BDNF into hippocampus of adult rodents (Xu et al., 2004), suggesting that excess activation of TrkB by BDNF is *sufficient* to promote limbic epilepsy. Importantly, diverse models of limbic epileptogenesis exhibit enhanced activation of TrkB (Binder et al., 1999a; Danzer et al., 2004; He et al., 2004; He et al., 2002; He et al., 2010) as evidenced by a surrogate measure, namely increased tyrosine phosphorylation (Segal et al., 1996). Collectively, these findings underscore the importance of elucidating the cellular consequences of enhanced TrkB activation because these are likely to promote limbic epileptogenesis.

Establishing the cellular and subcellular locale of the enhanced TrkB activation evident during limbic epileptogenesis is necessary to elucidate its cellular consequences. Using an antibody that recognizes the phosphorylated tyrosine 816 (pY816) of TrkB together with cellular markers and confocal microscopy, we examined the anatomic

locale of pY816 TrkB immunoreactivity in a model of limbic epileptogenesis involving SE induced by microinfusion of the chemoconvulsant kainic acid (KA) into the basolateral amygdala of adult mice (Araki et al., 2002; Li et al., 2008; Mouri et al., 2008). Advantages of this model include low mortality, as well as the reliable induction of spontaneous recurrent seizures and hippocampal pathology similar to humans with TLE (Mathern et al., 1997). Notably, work employing mice with mutations in either of two key TrkB tyrosine signaling residues, Y816 and Y515, revealed that Y816, but not Y515, is critical for the development of epilepsy (He et al., 2002; He et al., 2010), underscoring the rationale for examining the phosphorylation of this particular tyrosine residue of TrkB during epileptogenesis. The present study reveals evidence of enhanced TrkB activation in two populations of neurons within hippocampal circuitry—dentate granule cells and CA1 pyramidal cells. The enhanced TrkB activation was localized in part to excitatory synapses in each of these neuronal populations. Importantly, the model employed in this study is the same one used to demonstrate that transient TrkB inhibition following SE prevented the development of SRS (Liu et al., submitted), suggesting that TrkB signaling from these locales is likely to be critical for the development of limbic epilepsy.

2.2 Materials and Methods

2.2.1 Thy1-GFP Expressing Mice

C57/BL6 mice which express a green fluorescent protein (GFP) transgene under control of the Thy1 promoter were a generous gift from Dr. Guoping Feng (Duke University School of Medicine, Durham, NC). These mice were of either the M or O line,

as described previously (Feng et al., 2000). Animals used for experiments were bred from mice hemizygous for the Thy1-GFP allele crossed to wild type C57/BL6 mice from a local colony, the founders of which were originally obtained from Charles River (Wilmington, MA). Thy1-GFP animals were crossed to the local colony for at least five generations before use in experimentation. Thy1 belongs to the Ig superfamily and is expressed in both neuronal as well as non-neuronal cells, and both lines express GFP in a subset of dentate granule cells, as well as CA3 and CA1 pyramidal cells. Importantly for the purpose of this study, these cells represent typical granule and pyramidal cells in that their dendritic, axonal, and somatic morphologies reflect patterns observed using other techniques (Ramón y Cajal, 1911). Dentate granule cell mossy fiber axons expressing GFP can be visualized, and their giant boutons are easily identifiable based on their location within stratum lucidum, their continuity with the axon, and their large size (8-17 μ m²) (Amaral and Dent, 1981). The dendritic processes and spines of GFP-expressing pyramidal neurons within hippocampus, though more sparse, are also readily observable. These mice have been used previously as a means of examining the cellular morphology of hippocampal neurons, as well as for colocalization analyses similar to those performed in this study (Copanaki et al., 2010; Danzer et al., 2008; Danzer and McNamara, 2004; Walter et al., 2007).

2.2.2 Induction of SE

All animal procedures described were approved for use by the Institutional Animal Care and Use Committee (IACUC) at Duke University, and conformed to

National Institutes of Health and Duke University institutional guidelines for the care and use of animals. Animals were maintained on 12 hour light/dark cycles. Littermate GFP-expressing and non-expressing mice were included in experiments, and an effort was made to pair control and SE treated animals of the same GFP genotype whenever possible. Mice that died during treatment or that did not develop SE were discarded from the experiment.

2.2.2.1 SE Induced by Microinfusion of KA

A model of limbic epileptogenesis whereby SE was induced by microinfusion of KA into the basolateral amygdala was adopted for the majority of experiments conducted in this study, and has been extensively characterized in C57/BL6 mice (Araki et al., 2002; Li et al., 2008; Moura et al., 2008). This model was selected for several reasons: a) animals usually develop SE; b) animals undergoing SE uniformly develop spontaneous recurrent seizures after a seizure free latent period of 3-6 days; c) mortality is low; d) unlike systemic administration of KA in C57/BL6 mice (Schauwecker and Steward, 1997), hippocampal sclerosis similar to that of human TLE develops in the hippocampus ipsilateral to the amygdala into which KA is infused. The unilaterality of the hippocampal damage also provides the advantage of an intra-animal control not present in other models.

It should be noted, however, that prominent cell death is not found directly following SE induced by KA microinfusion into amygdala in C57/BL6 mice (Kasugai et al., 2007), such as at the time point examined in this study, but rather occurs over

subsequent days and weeks (Araki et al., 2002; Li et al., 2008; Mouri et al., 2008). In the present study, pY816 immunoreactivity was examined under conditions where cell damage should be minimal, as the presence of significant amounts of dead tissue would have confounded the ability to accurately quantify pY816 immunoreactivity in the remaining viable neuropil. This was exemplified in two KA treated animals in this study that were found to have disruption of the cytoarchitecture within stratum lucidum accompanied by a loss of pY816 staining, and were subsequently discarded from analysis (see below). The paucity of cell death in this study is reinforced by the presence of GFP+ pyramidal cells and their processes in KA treated Thy1-GFP mice; no obvious differences in their numbers or morphology were evident in NS compared to KA infused animals.

A total of 34 mice undergoing infusion of KA or NS into the right amygdala were used in this portion of the study. Both male and female C57BL/6 mice aged 3-6 months old and weighing at least 20 g were anesthetized with 60 mg/kg pentobarbital (Lundbeck, Deerfield, IL) via intraperitoneal injection and placed in a stereotactic frame. Animals were surgically implanted with a guide cannula (1.1 mm posterior, 2.9 mm lateral to Bregma; Plastics One, Roanoke, VA), following which a bipolar electrode was inserted into the contralateral dorsal hippocampus (2.0 mm posterior, 1.6 mm lateral to Bregma, depth of 1.5 mm below dura). Mice were allowed to recover postoperatively for at least three days. Before microinfusions, digital EEG recording commenced from the previously placed hippocampal electrode (Grass Technologies, West Warwick, RI). An

injection cannula (Plastics One) was inserted through the guide cannula at a depth of 4.6 mm below dura so as to target basolateral amygdala. Through this cannula, a total of 21 mice to be given SE received infusions of 0.3 µg of KA (Sigma, St. Louis, MO) in 0.5 µL of normal saline (NS) which was infused over a period of five minutes using a motorized infusion/withdrawal pump (Harvard Apparatus, Holliston, MA). A total of 13 mice to be used as surgical controls were infused with an equivalent volume of vehicle, NS, in the same fashion. The EEG was subsequently monitored for electrographic seizure activity, and mice were simultaneously observed for the development of behavioral SE. SE was defined as in (Danzer and McNamara, 2004): partial or whole body clonus, myoclonic jerks, rearing and falling, shivering, and/or loss of posture that was uninterrupted by normal behavior. Animals that developed SE were monitored until three hours after the first recorded electrographic seizure, at which time they were sacrificed, as described below, along with littermates that had been treated as surgical controls. Of the 21 animals infused with KA, four did not survive for the full three hours of SE, whereas another three failed to develop SE.

2.2.2.2 SE Induced by Pilocarpine

A total of 15 male and female C57/BL6 mice 2-3 months of age, generated as described above, were used in the portion of the study that examined pY816 immunoreactivity within CA1 of hippocampus. Mice received methylscopolamine nitrate (1 mg/kg by intraperitoneal injection) (Sigma), in order to block peripheral effects of the subsequent pilocarpine treatment. Fifteen minutes later, animals to be given SE

were injected with pilocarpine (375 mg/kg, intraperitoneal) (Sigma), whereas those to be used as controls were injected with NS. In total, 11 mice received pilocarpine treatment and four NS. Pilocarpine treated mice were observed for the development of behavioral SE as described above. An additional dose of pilocarpine (75 mg/kg, intraperitoneal) was administered to animals that failed to develop SE by 50 minutes following the initial pilocarpine injection. Animals were allowed to remain in SE for three hours at which time diazepam (10 mg/kg, intraperitoneal) (Hospira, Lake Forest, IL) was given to terminate seizure activity. Control animals also received diazepam. Animals were sacrificed, along with NS treated controls, at six hours following onset of SE. Of the 11 animals injected with pilocarpine, four did not survive the full SE episode and two failed to develop SE. In a separate experiment, a total of 12 animals (six pilocarpine and six NS) were treated in a similar fashion in order to quantify and examine the cellular distribution of pY816 immunoreactivity within stratum lucidum.

2.2.3 Preparation of Brain Specimens for Immunohistochemistry

Animals treated as above were anesthetized with 100 mg/kg pentobarbital by intraperitoneal injection and underwent transcardial perfusion through the left ventricle with a solution of ice-cold PBS, pH 7.4, containing 1 U/mL heparin (Sigma) and 2 mM sodium orthovanadate (Sigma), at a rate of 10 ml/min for one minute. This was followed by a seven minute perfusion with ice-cold 4% paraformaldehyde (Sigma) and 2 mM sodium orthovanadate in PBS, pH 7.4. Brains were removed and postfixed overnight at 4°C in the same solution, after which they underwent cryoprotection for 36 hours in a

solution of 30% sucrose, 2 mM sodium orthovanadate in PBS at pH 7.4 and 4°C. Brains were verified as being appropriately cryoprotected when they sank in this solution. Brains were then frozen by slow immersion in 2-methylbutane (J.T. Baker, Phillipsburg, NJ) cooled to -20°C with dry ice, and stored at -80°C until cryosectioning. Sections were cut at a thickness of 40 µm, placed in cryoprotection solution, and stored at -80°C until immunostaining. In animals that received KA microinfusions to induce SE, sections containing the cannula tract were examined to confirm that microinfusion had targeted the basolateral amygdala.

Any brains with misplaced cannulas or that were found to contain blood in the hippocampi upon sectioning, indicating a suboptimal perfusion, were discarded from further processing. Furthermore, sections from two animals treated with SE by KA microinfusion revealed disruption of the cytoarchitecture within stratum lucidum compared to control animals as determined by Nissl stain, probably a result of particularly severe SE (Fig. 5B; arrows). For this reason, these animals were discarded from the final quantitative analysis. The region of disrupted cytoarchitecture revealed striking paucity of pY816 staining compared to control mice (Fig. 5C; arrows), however it should be noted that inclusion of these animals would not have altered the statistical significance level of any results of this study.

2.2.4 Antibody Characterization

Details of antibodies employed in this study are provided in Table 1 (Primary Antibodies) and Table 2 (Secondary Antibodies). These antibodies were characterized in terms of their specificity as follows:

Table 1: Primary antibodies employed in study.

| Target | Immunogen | Source | Working Dilution |
|--|--|---|------------------|
| Phosphorylated tyrosine residue 816 (pY816) of TrkB Receptor | LQNLAKASPVpYLDI, corresponding to amino acids 806-819 of mouse TrkB. | McNamara Laboratory; Rabbit Polyclonal. | 1:2000 |
| Green Fluorescent Protein (GFP) | GFP-BSA | Millipore; Mouse Monoclonal; MAB3580. | 1:1000 |
| MAP2 | Rat brain microtubule-associated proteins (MAPs). | Sigma; Mouse Monoclonal; M4403. | 1:500 |
| Tau-1 | Purified denatured bovine microtubule associated proteins. | Millipore; Mouse Monoclonal; MAB3420. | 1:1000 |

Table 2: Secondary Antibodies Employed in Study.

| Secondary Antibody | Source | Working Dilution |
|---|---------------------|------------------|
| Alexa Fluor 555 Goat Anti-Rabbit IgG (H+L), highly cross-adsorbed | Invitrogen; A-21429 | 1:1000 |
| Alexa Fluor 488 Goat Anti-Mouse IgG (H+L), highly cross-adsorbed | Invitrogen; A-11029 | 1:500 |
| Alexa Fluor 633 Goat Anti-Mouse IgG (H+L), highly cross-adsorbed | Invitrogen; A-21052 | 1:500 |

Rabbit polyclonal antibody which recognizes phosphorylated tyrosine residue 816 of the TrkB receptor (pY816) was generated using the peptide LQNLAKASPV**p**YLDI, corresponding to amino acids 806-819 of mouse TrkB , and was used in all experiments at a 1:2000 dilution following IgG purification using protein-A beads. Importantly, the specificity of this antibody was previously established for immunohistochemistry (He et al., 2010). This was evidenced by demonstrating a significant reduction in immunoreactivity in stratum lucidum of genetically modified mice with a substitution of phenylalanine for tyrosine at the 816 residue (Y816F) of TrkB compared to wild type controls, as shown in Supplementary Figure 1 of (He et al., 2010).

A mouse monoclonal antibody recognizing GFP (1:1000; Millipore, Temecula, CA) was found to augment GFP fluorescence. This was tested by incubating GFP-expressing mouse brain sections with this antibody, followed by an Alexa Fluor-555 conjugated secondary antibody, which fluoresces red. Augmented (red) and endogenous (green) GFP fluorescence could be seen to overlap when viewed using an epifluorescent microscope. Mouse monoclonal MAP2 (1:500; Sigma) and tau (1:1000; Millipore) antibodies were employed as tissue markers of dendrites and axons, respectively (Binder et al., 1985; Huber and Matus, 1984). MAP2 antibody was found to label what appeared to be dendrites throughout mouse brain, confirmed by the fact that dendritic shafts of GFP+ CA1 and CA3 pyramidal cells were found to colocalize with MAP2 immunoreactivity within CA3 stratum lucidum and CA1 stratum radiatum when examined in Thy1-GFP mice. Tau immunoreactivity was found to colocalize with GFP+

mossy fiber axons in stratum lucidum, and was also excluded from GFP+ dendrites that could be identified within this structure.

2.2.5 Immunohistochemistry

NS and SE treated littermates were always incubated in parallel using the same solutions and conditions. All incubations took place at 4°C in 5% normal goat serum (Invitrogen, Carlsbad, CA) in PBS, pH 7.4, with 2 mM sodium orthovanadate. Floating sections were permeabilized for one hour in 0.5% Triton-X100 (GE Healthcare, Chalfont St. Giles, UK), and solutions of primary antibodies added for 36 hours. Alexa Fluor 555 conjugated goat anti-rabbit (1:1000; Invitrogen) and, for colocalization experiments, Alexa Fluor 488 or 633 conjugated goat anti-mouse secondary antibodies (1:500; Invitrogen) were then applied for six hours. Adjacent sections not treated with primary antibody were also run in parallel for each animal as negative controls. Sections were wet-mounted on Superfrost Plus slides (Erie Scientific, Portsmouth, NH) and stepped through serial dehydration solutions of two minutes each of 50%, 70%, 85%, 95%, 100%, and 100% ethanol, followed by 20 minutes incubation in xylene (VWR, Radnor, PA) before coverslipping.

2.2.6 Confocal Microscopy and Data Analysis

2.2.6.1 Imaging Parameters

Imaging was performed with a Leica (Nussloch, Germany) DMIRE2 inverted microscope with a 10x (numerical aperture, 0.4) air or 63x (numerical aperture, 1.4) oil

immersion objective equipped with a Leica TCS SL confocal system. All images were acquired with the pinhole set to 1.0 Airy units. All images shown for visual comparison between treatment groups or used for quantitative analysis were acquired so as to prevent systematic differences in image intensities between mouse genotypes. To this end, sections to be compared within an experiment were incubated together and imaged using the same laser intensity and detection settings during the same imaging session, thereby permitting relative densitometry measurements to be made between treatment groups. Because overall staining intensities necessarily varied between staining experiments, confocal settings were adjusted optimally for each experiment so that all image intensities fell within the dynamic range of detection of the device.

Low power (10x objective, total of 100x magnification) images of hippocampus are average projections of *z*-series “stacks” taken through the entire thickness of the hippocampal section. Unless otherwise stated, high power (63x objective, total of 630x magnification) images are average projections of *z*-series taken through a 1 μm depth of hippocampus where pY816 staining was of greatest intensity. Average projections were used because they best reflect representative staining intensities in the *z*-plane for quantification of immunoreactivity. Images depicting colocalizations were confirmed in the *x*, *y*, and *z* dimensions. The focal plane thickness is a significant factor in the *z*-dimension. For the 63x objective used in this study, assuming ideal conditions and 488 nm of light, *z* resolution is stated to be 235 nm (Leica). The resolution in the *x-y* plane is stated to be 180 nm (Leica). All image quantification described was performed on raw

images which were not adjusted for brightness or contrast. However, brightness and/or contrast were optimized in all images shown within this chapter in order to best convey relevant features. In images of pY816 immunoreactivity used for comparison, brightness and contrast were adjusted equally between images.

2.2.6.2 Quantification of pY816 Immunoreactivity

Analysis of imaging data was performed by an investigator blinded to treatment group. The program ImageJ (Abramoff, 2004) was used for data analysis. All quantitative data are presented as mean \pm SEM, analyzed by 1-way ANOVA with significance values between individual groups determined by *post-hoc* Bonferroni's test or Student's t-test.

For quantification of stratum lucidum immunoreactivity for animals in the KA model of SE, one hippocampal image including the CA3b regions of stratum lucidum and stratum radiatum, taken both ipsilateral and contralateral to the side of infusion, was used from each animal acquired at both low power (100x) and high power (630x). If there was any discrepancy in stratum lucidum brightness between sections, that with the brightest stratum lucidum immunoreactivity was used. Low power quantification of pY816 immunoreactivity within stratum lucidum was performed by outlining a square region of interest (ROI) in the CA3b region, of uniform dimension for all images sampled, and taking the average intensity within this region. The average intensity of an ROI of equal dimension was taken within stratum radiatum of CA3, reflective of background immunoreactivity, and subtracted from the stratum lucidum value so as to compensate for

differences in background staining intensity between animals. Other hippocampal regions quantified at low power (100x) were analyzed in the same fashion. Quantification of stratum lucidum values in pilocarpine treated mice was done as in the KA model, except only one stratum lucidum was quantified per mouse. In the rare instance where a notable discrepancy was observed in pY816 stratum lucidum immunoreactivity between hemispheres, the side with the brightest immunoreactivity was used. Quantification at high power (630x) focused on specific areas within stratum lucidum that were enhanced in pY816 immunoreactivity and shown to correspond to axon tracts in colocalization experiments. Representative regions enriched in pY816 immunoreactivity were outlined as ROIs until 50,000 pixels in total area were reached or exceeded, and the average intensity of this area quantified. The average intensity of stratum radiatum of CA3 that was included in the same micrograph was also taken, and subtracted from the value obtained from stratum lucidum in order to compensate for variations in background staining. Signal within stratum radiatum was used for normalization for several reasons: a) signal within stratum radiatum immunoreactivity was always substantially lower than stratum lucidum; b) signal within stratum radiatum was found to be of the same average intensity when compared between control and SE treated animals at both low power (100x) and high power (630x) (data not shown); c) the CA3 pyramidal cell dendrites which populate this region were found not to contain significant amounts of pY816 immunoreactivity (Fig. 11E; CA3 SR; also observe CA3 stratum radiatum in Fig. 5A).

For quantification of other regions within hippocampus, the investigator counted the total numbers of individual neuronal processes discerned within a given region within an image. In mice treated with the KA microinfusion model, two images were taken both ipsilateral and contralateral to the site of infusion in each of the following regions for every animal: CA1 stratum radiatum, CA1 stratum oriens, CA1 stratum lacunosum moleculare, CA3 stratum radiatum, CA3 stratum oriens, and the suprapyramidal and infrapyramidal molecular layers of dentate gyrus. In mice treated with the pilocarpine model, two images from each side were taken from each of the regions above, and those that appeared to display the greatest number of neuronal processes were used for analysis. In order to quantify how far within apical dendritic shafts of CA1 pyramidal cells the pY816 immunoreactivity extended into stratum radiatum, individual GFP+ apical shafts that could be traced through the vertical extent of stratum radiatum were imaged in a KA infused animal in the hippocampus ipsilateral to microinfusion. In those dendritic shafts that contained pY816 immunoreactivity, measurements were made of both the distance from the soma that this immunoreactivity was observed, and the total dendritic length within stratum radiatum of CA1. From these measurements, the percent of the total length of the dendritic shaft containing pY816 immunoreactivity was calculated.

Quantification of synaptic pY816 immunoreactivity employed just the subset of mice that expressed Thy1-GFP (5 KA and 5 NS out of 9 KA and 9 NS). Sections from these animals treated in the KA microinfusion model were imaged within a given region both ipsilateral and contralateral to the side of infusion. For quantification of pY816

immunoreactivity within giant mossy fiber boutons of stratum lucidum, *z*-series were acquired at 200 nm intervals over a total depth of 1 μm . For quantification of immunoreactivity within dendritic spines of stratum radiatum of CA1, stratum oriens of CA1, stratum lacunosum moleculare of CA1, stratum radiatum of CA3, and the outer two thirds of the suprapyramidal and infrapyramidal molecular layers, *z*-series were taken at 250 nm intervals over a total depth of 2 μm . Note that pY816 antibody generally penetrated sections only superficially, but this was particularly pronounced within stratum lucidum, limiting the depth in which immunoreactivity could be imaged in this region more than the others. Individual spines and boutons from each of these regions were checked for pY816 immunoreactivity in the *x*, *y*, and *z* planes, and scored as being positive if they appeared to contain at least one discrete immunoreactive puncta, even if only in one *z*-section. This immunoreactivity needed to occupy at least 20% of the area of a bouton, whereas for a spine the majority of its area needed to be filled.

2.3 Results

2.3.1 Enhanced pY816 Immunoreactivity within Stratum Lucidum Following Kainic Acid Status Epilepticus (KA-SE)

Initial studies centered on characterization of the intensity of pY816 immunoreactivity within stratum lucidum in the KA model. As KA microinfusion directly activates limbic structures on the side in which it is infused (Araki et al., 2002), pY816 immunoreactivity was examined in stratum lucidum both ipsilateral and contralateral to the side of infusion. Littermate mice were infused with either normal

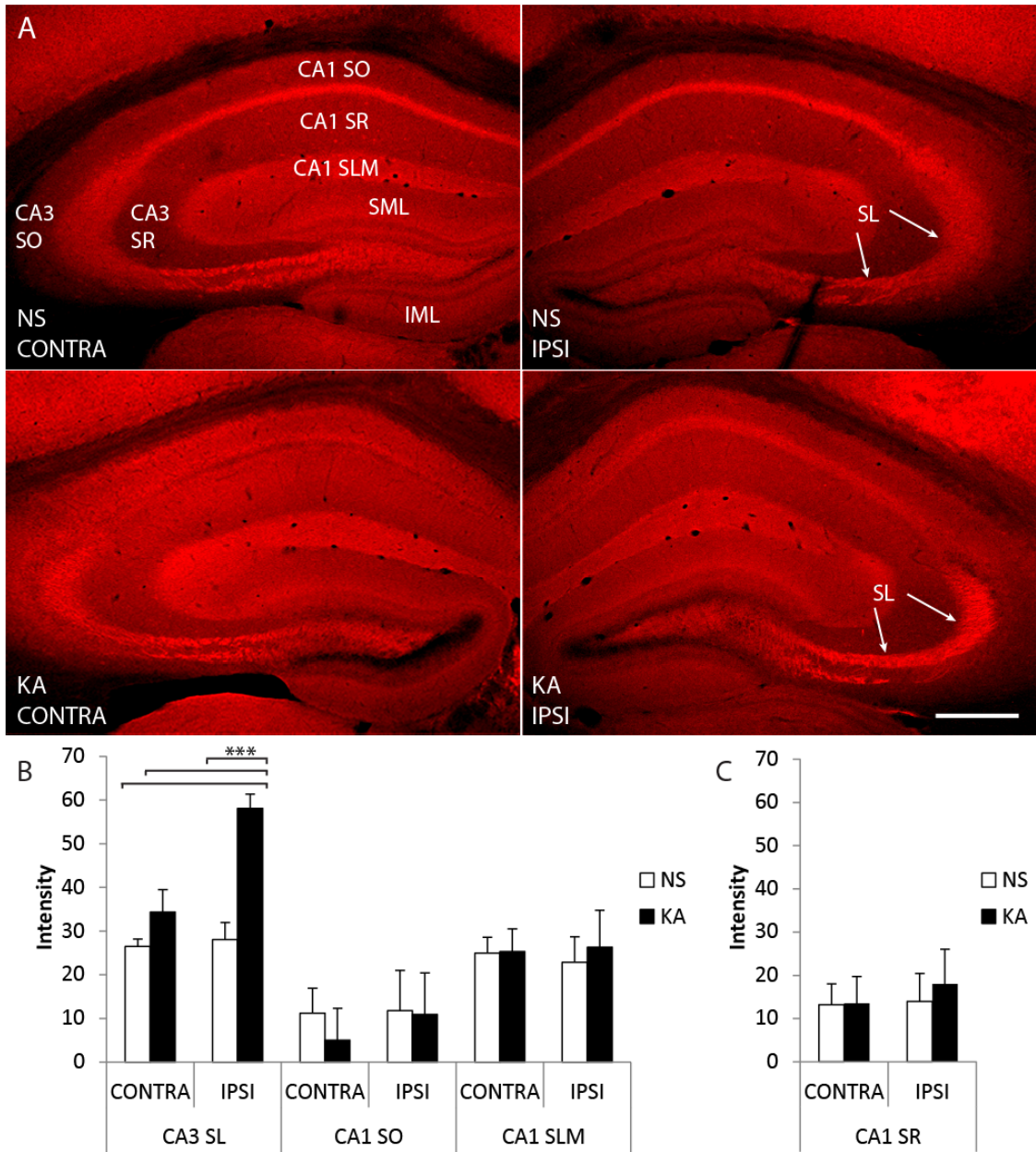


Figure 4: Immunoreactivity labeling phosphorylated tyrosine 816 (pY816) of TrkB is enhanced within stratum lucidum (SL) following kainic acid (KA) induced status epilepticus (SE), observed preferentially in the hippocampus ipsilateral to KA microinfusion.

A) Representative images of hippocampi stained with pY816 from animals infused with normal saline (NS, top) or given SE (KA, bottom) through microinfusion of KA into right amygdala (KA-SE). Hippocampi both ipsilateral (IPSI, right) and contralateral (CONTRA, left) to the side of infusion are shown. A noticeable increase in SL immunoreactivity can be discerned in the KA animal compared to NS on the side of infusion (IPSI, arrows point to SL). Other regions within hippocampus that are referred to within the text are labeled for reference in (A): stratum radiatum of CA3 (CA3 SR), stratum oriens of CA3 (CA3 SO), stratum radiatum of CA1 (CA1 SR), stratum oriens of CA1 (CA1 SO), stratum lacunosum moleculare of CA1 (CA1 SLM), the suprapyramidal molecular layer of dentate gyrus (SML), and the infrapyramidal molecular layer of dentate gyrus (IML). Each image is a montage of two images taken at low magnification (100x). Scale bar = 300 μ m. **B)** Low power (100x) quantification of pY816 intensity in various regions from hippocampi both ipsilateral (IPSI) and contralateral (CONTRA) to microinfusion. A 2.1-fold, highly significant increase ($p<0.001$, one-way ANOVA; $p<0.001$, post-hoc Bonferroni's test) was observed in CA3b SL of KA treated animals ($n=9$) compared to NS ($n=9$) on the side ipsilateral to infusion, whereas on the contralateral side the increase was only 1.3-fold ($p>0.05$, post-hoc Bonferroni's test). Analysis of CA1 SO and CA1 SLM did not demonstrate any significant differences in pY816 intensity between NS and KA treated mice on either side. **C)** Analysis of CA1 SR did not demonstrate differences in pY816 intensity between NS and KA treated animals either ipsilateral (IPSI) or contralateral (CONTRA) to infusion. All quantification is presented as mean intensity values \pm SEM; all data were analyzed by one-way ANOVA and post-hoc Bonferroni's test; *** $p<0.001$.

saline (NS) or KA, and those receiving the latter treatment allowed to seize for three hours following the first electrographic seizure, as recorded from a bipolar electrode in CA1 of the hippocampus contralateral to the side of infusion. At this time mice were sacrificed along with their NS controls and coronal sections containing dorsal hippocampi were stained with pY816 antibody. Visual inspection at low magnification (100x) revealed striking increases of pY816 immunoreactivity in stratum lucidum ipsilateral to KA microinfusion compared to contralateral stratum lucidum or to NS treated mice (Fig. 4A; compare KA IPSI to others, arrows point to stratum lucidum).

Quantification of pY816 immunoreactivity within CA3b of stratum lucidum using low

power (100x) images revealed approximately a 2-fold increase ipsilateral to KA infusion (n=9) compared to NS littermates (n=9) (Fig. 4B; CA3 SL; p<0.001); by contrast, only a 1.3-fold increase was observed contralateral to KA infusion (p>0.05). Thus, pY816 immunoreactivity was preferentially increased within stratum lucidum ipsilateral to the KA infused amygdala, a site at which immunoreactivity in all KA treated mice (n=9) exceeded that of either side in NS treated littermates. Furthermore, in all but one KA treated animal (n=8), pY816 immunoreactivity was greater ipsilaterally than contralaterally. Except for stratum radiatum of CA1 (see below), no overt changes in pY816 TrkB immunoreactivity were evident in other regions of hippocampus following KA-SE, consistent with past reports (Binder et al., 1999a; Danzer et al., 2004; He et al., 2004; He et al., 2002; He et al., 2010); quantification within stratum oriens and stratum lacunosum moleculare of CA1 revealed no significant differences in immunoreactivity between NS (n=9) and KA (n=9) infused animals (Fig. 4B; CA1 SO and CA1 SLM).

Stratum lucidum was also visualized at high magnification (630x) in sections from the same NS (n=9) and KA (n=9) treated mice as above (Fig. 5A). This revealed discrete patches of pY816 immunoreactivity within CA3b of stratum lucidum, which appeared noticeably brighter in hippocampi ipsilateral to infusion in KA treated animals (Fig. 5A; compare IPSI KA to others, arrows mark areas of enhanced immunoreactivity), confirming observations at low magnification (100x). Importantly, the pattern of pY816 immunoreactivity was similar in NS and KA treated animals, suggesting that the cellular locale was similar in experimental and control conditions.

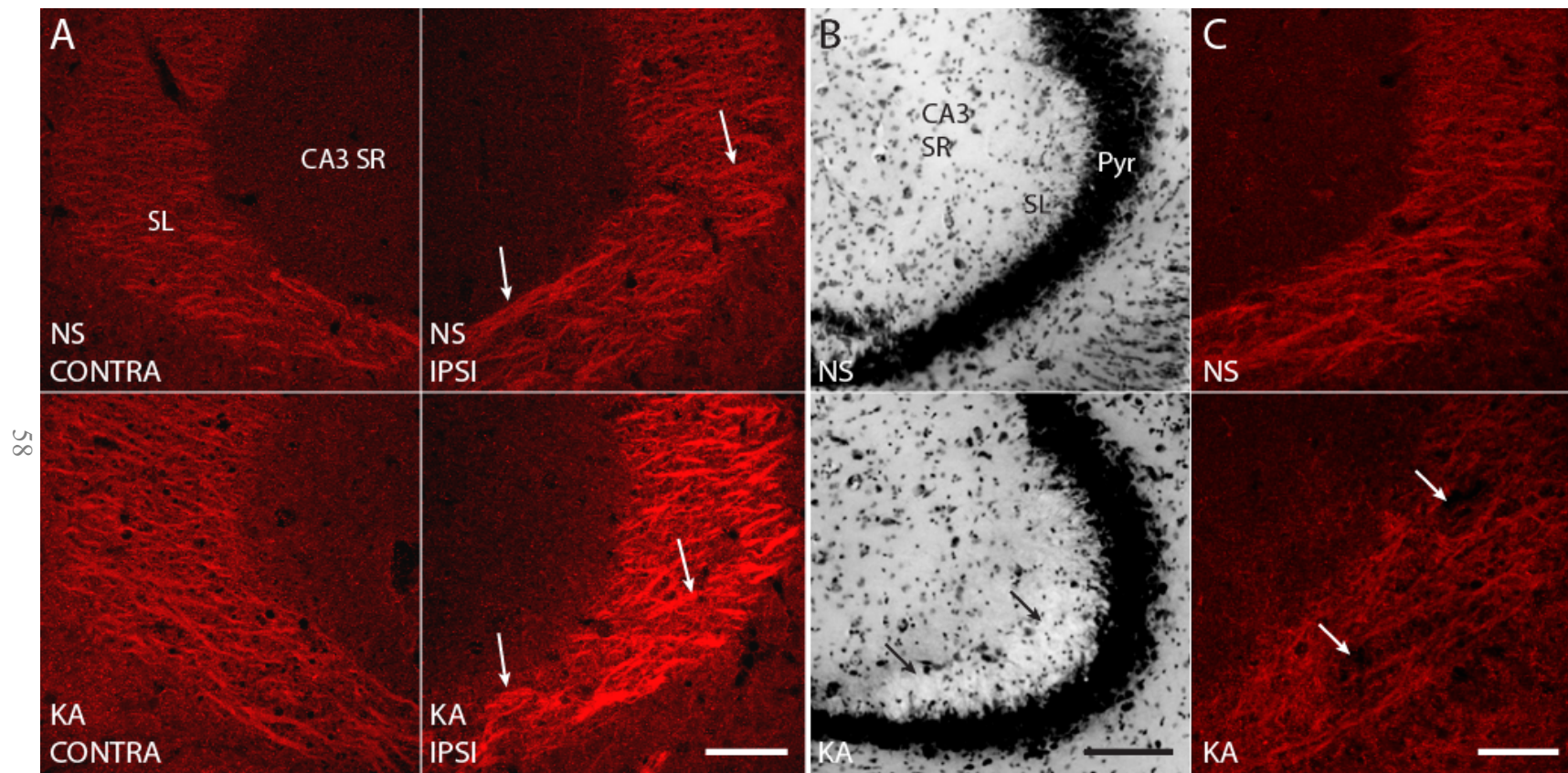


Figure 5: High magnification (630x) images reveal discrete patches of pY816 immunoreactivity within SL, enhanced preferentially on the side ipsilateral to KA microinfusion.

A) Representative high magnification (630x) images of SL from CA3b in NS (top) and KA (bottom) treated mice, both ipsilateral (IPSI, right) and contralateral (CONTRA, left) to microinfusion. Arrows point to discrete patches of pY816 immunoreactivity that could be discerned within SL, and a noticeable increase in intensity of these immunoreactive areas can be seen in the KA treated animal ipsilateral to infusion compared to NS (IPSI, right). Scale bar = 50 μ m. **B)** Nissl stain of the CA3 region from a KA treated mouse (KA) showing disruption of SL cytoarchitecture (arrows). The SL damage observed is representative of that found in two animals discarded from analysis due to this issue. Note the normal appearing SL in the NS treated littermate (NS). Pyr is CA3 pyramidal cell layer. Scale bar = 100 μ m. **C)** pY816 staining from the same hippocampi as in (B) demonstrates a relative paucity of stain in the KA treated animal (KA, arrows) within SL compared to its NS infused littermate (NS). Scale bar = 50 μ m.

2.3.2 Localization of Stratum Lucidum pY816 Immunoreactivity to Mossy Fiber Axons Following KA-SE

To further explore the cellular and subcellular locations of the discrete patches of pY816 TrkB immunoreactivity in stratum lucidum observed at high magnification (630x), sections from NS and KA infused animals examined above were co-labeled with pY816 antibody and various markers of cellular structures, and confocal microscopy used to examine colocalization. To survey pY816 immunoreactivity within mossy fiber axons and giant boutons, a transgenic mouse that expresses green fluorescent protein (GFP) under control of the Thy1 promoter was employed for a subset of the KA microinfusion experiments (Feng et al., 2000). Subsets of dentate granule cells are labeled with GFP in these mice, and GFP fills the processes of these cells so that mossy fiber axons and their giant boutons can be directly visualized (Danzer et al., 2008; Danzer and McNamara, 2004). pY816 immunoreactivity prominently colocalized with GFP-labeled mossy fiber axons in CA3b of stratum lucidum in both NS (n=5) and KA (n=5) mice (Fig. 6A, B; arrows). This immunoreactivity was finely granular but appeared relatively

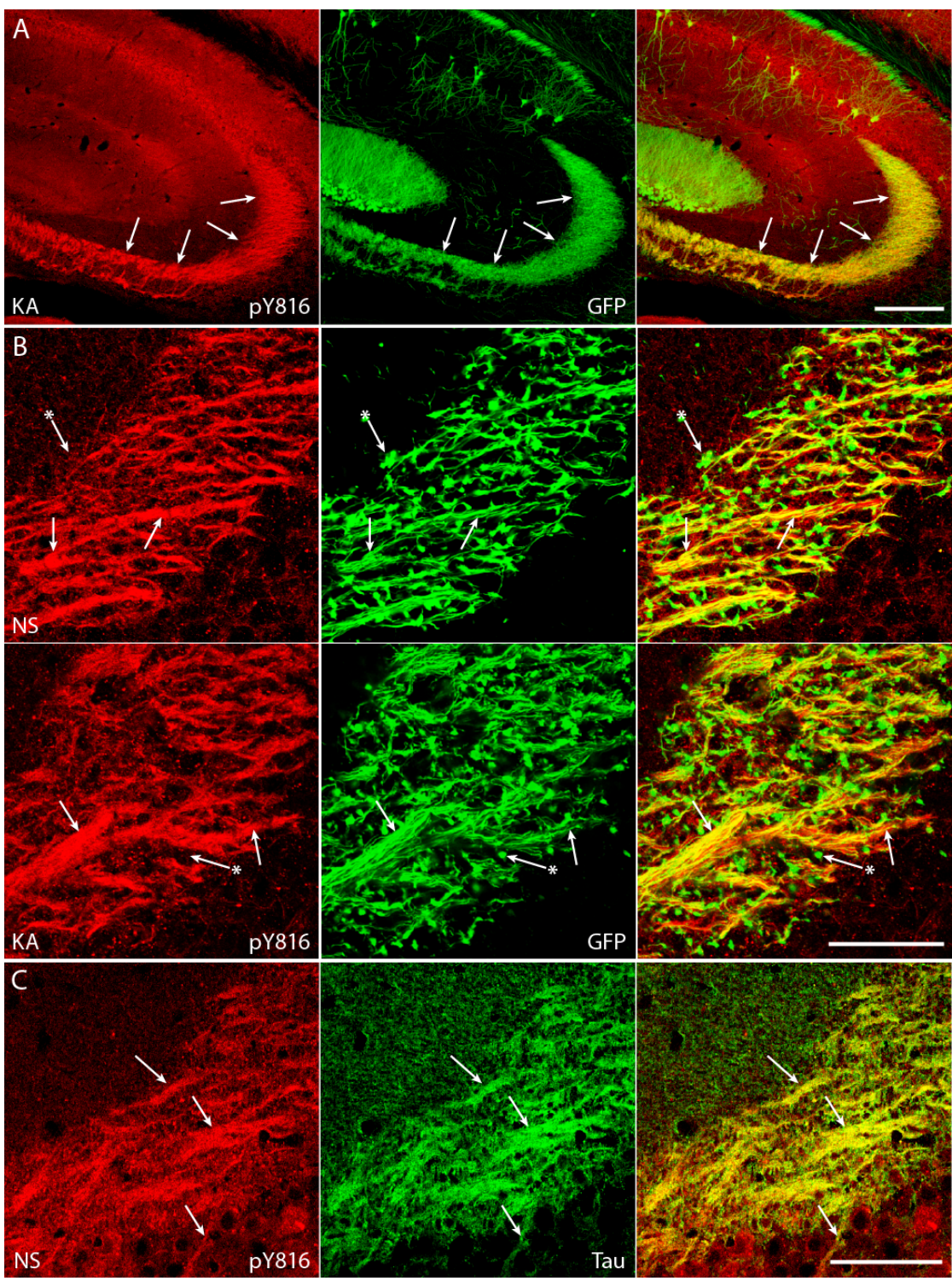


Figure 6: pY816 TrkB immunoreactivity colocalizes with axons of dentate granule cells (DGCs) in SL of hippocampus under both NS conditions and following KA-SE.

A) Images of CA3 region of hippocampus from a KA treated animal demonstrates striking overlap of enhanced pY816 immunoreactivity (red; arrows) with GFP-labeled mossy fibers (green; arrows) that populate SL. Merged pY816 and GFP is shown in the rightmost panel. Scale bar = 200 μ m. **B)** Images from CA3b of SL of sections stained with pY816 (red) that also contain GFP (green) under conditions of NS infusion (NS) and following KA-SE (KA). A subset of mossy fiber axons of DGCs (green; arrows) are filled with GFP, and can be seen to colocalize with pY816 (red; arrows) under both NS and KA conditions. In contrast, most mossy fiber boutons (green; arrows with asterisks) do not contain prominent pY816 immunoreactivity (red; arrows with asterisks) compared to axons. Note that the distribution of immunoreactivity does not change between NS and KA treated animals. Merged pY816 and GFP is shown in the rightmost panels. Scale bar = 50 μ m. **C)** Images from CA3b of SL from a control animal stained with pY816 (red) and tau (green), an axonal protein. Tau stained mossy fiber axon tracts (green; arrows) prominently colocalize with pY816 (red; arrows). Merged pY816 and Tau is shown in the rightmost panel. Scale bar = 50 μ m.

homogeneous throughout the axons. A subset of giant boutons of mossy fiber axons exhibited pY816 immunoreactivity in both NS and KA treated animals (see below), though most did not contain prominent immunoreactivity (Fig. 6B; arrows with asterisks).

Though GFP-expressing mice permit visualization of fine structures of dentate granule cells, only a subset of mossy fiber axons are labeled with GFP, and therefore the full extent of pY816 overlap with mossy fiber axons could not be appreciated. To circumvent this limitation, axons were visualized with an antibody to the protein tau, which selectively labels axons (Binder et al., 1985). Striking overlap of tau and pY816 immunoreactivity in the CA3b region of stratum lucidum was evident in a control mouse (Fig. 6C; arrows), further supporting axonal localization of pY816. Difficulties in detecting tau immunoreactivity following SE precluded its study in KA treated animals.

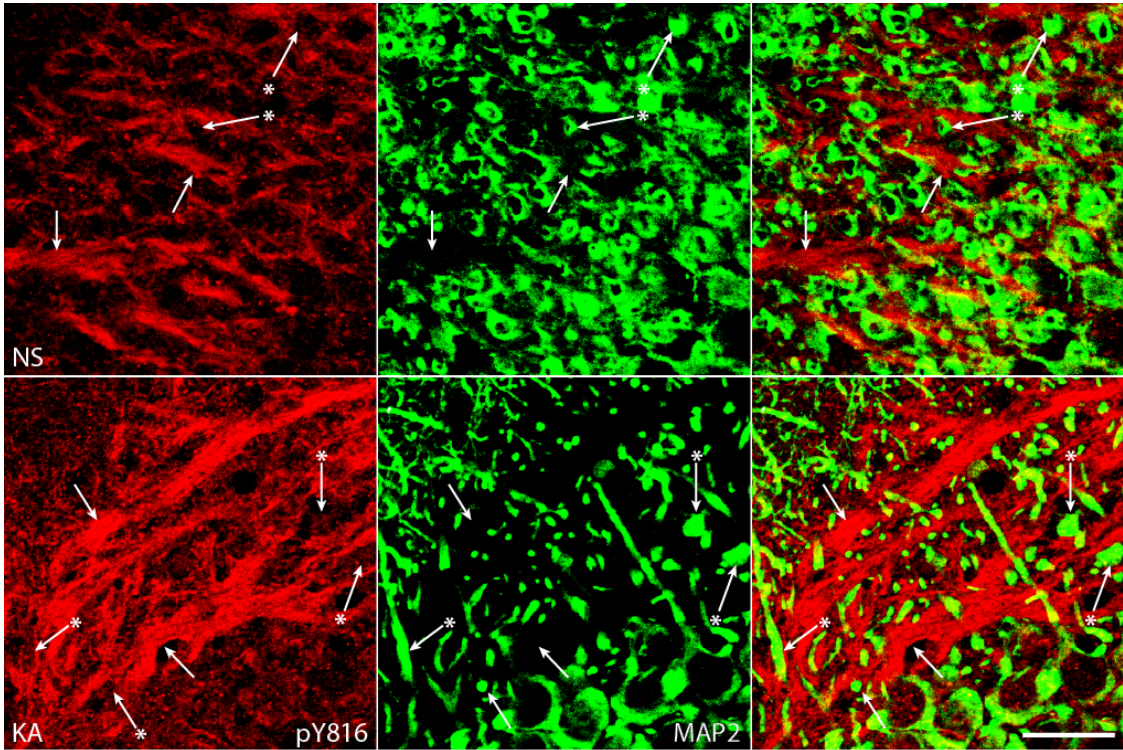


Figure 7: pY816 TrkB immunoreactivity does not prominently colocalize with MAP2 stained dendrites of CA3 pyramids under either NS conditions or following KA-SE.

Images from CA3b of SL of pY816 stained sections (red) co-stained with MAP2 (green), a marker of dendrites, under conditions of NS infusion (NS) and following KA-SE (KA). Linear patches of pY816 immunoreactivity (red; arrows), demonstrated to colocalize with mossy fiber axons (Fig. 6), do not colocalize with MAP2 (green; arrows). Furthermore, MAP2 labeled dendrites of CA3 pyramidal cells (green; arrows with asterisks) do not contain prominent pY816 immunoreactivity (red; arrows with asterisks). No apparent differences are observed in the cellular distributions of pY816 immunoreactivity between NS and KA treated animals. Merged pY816 and MAP2 is shown in rightmost panels. Scale bar = 20 μ m.

To determine whether pY816 immunoreactivity is detectable within dendrites of CA3 pyramidal cells which populate stratum lucidum and onto which giant boutons of dentate granule cells form synapses, an antibody for MAP2 was employed. The MAP2 protein is selectively expressed in dendrites (Huber and Matus, 1984) which were oriented largely perpendicular in CA3b of stratum lucidum in coronal sections (Fig. 7; MAP2 panels, arrows with asterisks). In sharp contrast to axonal markers, no prominent overlap of pY816 and MAP2 immunoreactivity was detected in either NS (n=3) or KA (n=3) treated animals (Fig. 7). Collectively, these findings demonstrate that pY816 immunoreactivity is largely confined to mossy fiber axons and boutons under both basal conditions and following KA-SE, not within dendrites of CA3 pyramids.

In these same NS and SE treated mice, imaging was also performed within the CA3c region of stratum lucidum, located more proximally to hilus than the CA3b portion. Not surprisingly, the cellular distribution of pY816 was the same as in the CA3b region. However, CA3 pyramidal cell dendrites were found to run in parallel to the plane of section in this portion of stratum lucidum, whereas mossy fiber axons run obliquely to the section plane. The different orientation of these structures provided an alternative perspective by which the cellular distribution of pY816 could be visualized, which also clearly illustrated pY816 exclusion from MAP2-labeled CA3 pyramidal cell dendrites. Representative confocal images obtained from this area are shown in Figure 8.

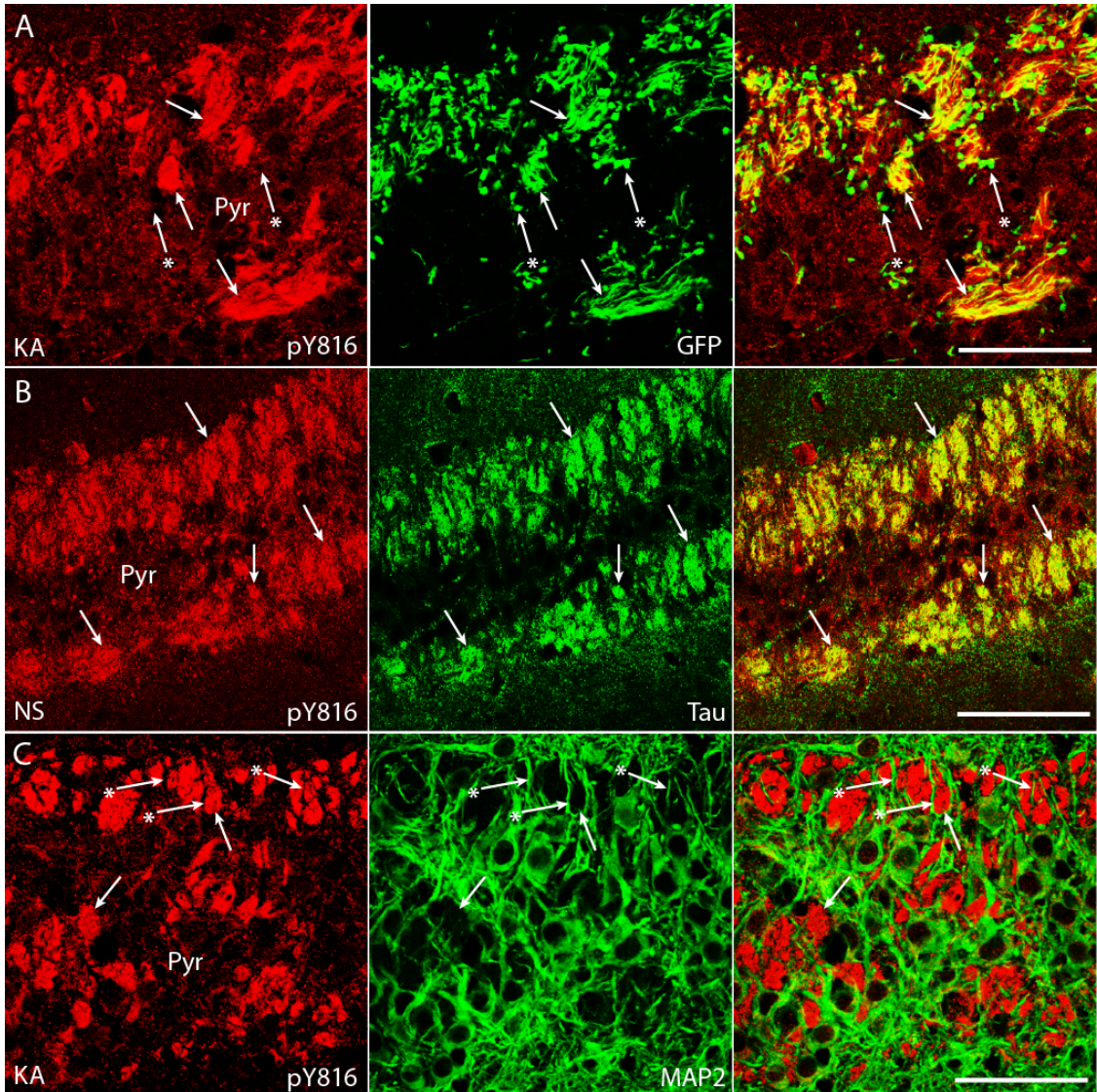


Figure 8: Colocalization of pY816 TrkB immunoreactivity with cellular markers within the CA3c region of SL.

A) In the CA3c region of SL in a KA-treated mouse, mossy fiber axons (green; arrows) can be seen to run largely oblique to the plane of section in bundles that are strongly enriched in pY816 immunoreactivity (red; arrows). Boutons (green; arrow with asterisk) are largely devoid of immunoreactivity (red; arrow with asterisk). A similar result was obtained in NS treated animals (data not shown). Merged pY816 and GFP is shown in the rightmost panel. Scale bar = 50

μm . B) pY816 (red) reveals striking overlap with Tau (green), a marker for axons. Arrows point to clear regions of colocalization. Merged pY816 and Tau is shown in the rightmost panel. Scale bar = 75 μm . C) A MAP2 stain (green) labels dendrites of CA3 pyramidal cells (arrows with asterisks) running parallel to the plane of section. These MAP2 stained dendrites surround patches of pY816 immunoreactivity (red; arrows) presumably composed of mossy fiber axons, but themselves do not contain significant amounts of pY816 immunoreactivity (red; arrows with asterisks). Merged pY816 and MAP2 is shown in the rightmost panel. Scale bar = 50 μm . Pyr marks the CA3 pyramidal cell layer.

2.3.3 Quantification of pY816 Immunoreactivity Within Axons of Stratum Lucidum Following KA-SE

Given the localization of pY816 immunoreactivity within stratum lucidum to axons of dentate granule cells, additional quantification of immunoreactivity within these structures was performed at high power (630x) in the same NS (n=9) and KA (n=9) treated mice used for the low power (100x) quantification (Fig. 5A shows representative 630x images). Unlike the low power (100x) quantification performed above, this high power (630x) quantification specifically measured immunoreactivity found within axon tracts of stratum lucidum (see Materials and Methods), thus focusing on the anatomical locale where pY816 immunoreactivity was most prominent. Quantification revealed a significant increase of pY816 immunoreactivity on the side ipsilateral to KA infusion of approximately 2-fold (NS = 51.5 ± 8.4 , KA = 105.1 ± 8.1 , mean \pm SEM, intensity units); by contrast, an increase of 1.5-fold was detected contralaterally (NS = 53.9 ± 8.1 , KA = 78.9 ± 7.9 , mean \pm SEM, intensity units). As with the low power (100x) quantification, this difference was significant only on the side ipsilateral to KA infusion ($p < 0.001$, one-way ANOVA; $p < 0.001$ ipsilateral NS vs. ipsilateral KA, $p < 0.001$ contralateral NS vs.

ipsilateral KA, *post-hoc* Bonferroni's test). The high power (630x) quantification mirrored the low power (100x) in that immunoreactivity ipsilateral to infusion was greater than contralateral in KA infused mice in all but the one animal where this was not observed with low power (100x) quantification (n=8); in all KA infused animals (n=9), the pY816 immunoreactivity in stratum lucidum ipsilateral to KA infusion exceeded that on either side in NS infused littermates.

2.3.4 Localization of Stratum Lucidum pY816 Immunoreactivity to Mossy Fiber Axons Following Pilocarpine SE

To determine whether this cellular and subcellular location of pY816 TrkB was generalizable to other models of epileptogenesis, additional mice underwent three hours of SE induced by systemically administered pilocarpine (n=6), and were matched with NS injected littermate controls (n=6). A subset of these animals contained a Thy1-GFP transgene. Consistent with past reports (He et al., 2010), a significant increase in pY816 immunoreactivity was observed within stratum lucidum of pilocarpine treated animals compared to controls when quantified at low power (100x) (Fig. 9A, B). In contrast to the KA microinfusion model, however, this increase was observed to be bilateral in nature (data not shown). As in the KA microinfusion model, pY816 immunoreactivity exhibited striking colocalization with GFP-labeled mossy fiber axons but not with dendrites labeled with MAP2 following pilocarpine SE (Fig. 9C, D). A subset of giant boutons of mossy fiber axons also exhibited pY816 immunoreactivity in pilocarpine SE treated animals (Fig. 9C, arrow with asterisk). Thus, pY816 immunoreactivity exhibits

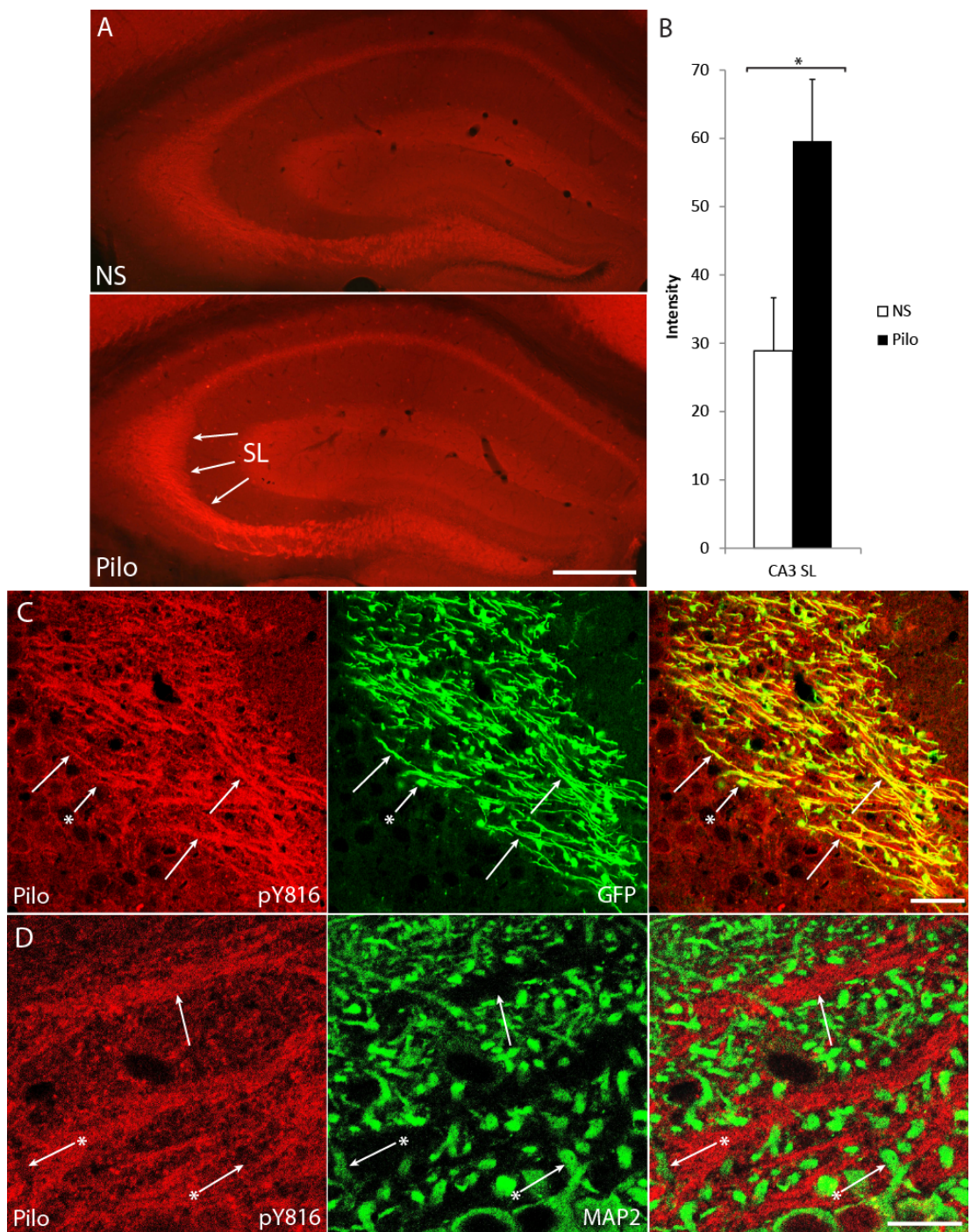


Figure 9: pY816 immunoreactivity increases within SL following pilocarpine SE, and colocalizes with axons of DGCs.

A) Representative images of hippocampi stained with pY816 from a mouse that experienced three hours of SE induced by intraperitoneal (IP) injection of pilocarpine (Pilo) and its littermate control that received IP normal saline (NS). A noticeable increase in pY816 immunoreactivity can be seen within SL of the pilocarpine treated animal (Pilo; arrows point to SL). Each image is a montage of two confocal images acquired at low magnification (100x). Scale bar = 300 μ m. **B)** Low power (100x) quantification of pY816 immunoreactivity within SL of NS (n=6) and pilocarpine (n=6) treated mice. A 2-fold, significant increase ($p<0.05$, Student's t-test) in immunoreactivity was observed in pilocarpine treated animals compared to controls. As in KA versus NS infused mice, no significant differences in pY816 intensity between NS and pilocarpine treated animals was apparent in other hippocampal regions by visual inspection at low power (100x). **C)** In a pilocarpine treated animal (Pilo), pY816 (red; arrows) is enriched in GFP-labeled mossy fiber axons (green; arrows). A minority of boutons (green; arrow with asterisk) also contained some pY816 immunoreactivity (red; arrow with asterisk), though the majority were devoid. Similar distributions of pY816 immunoreactivity were observed in NS injected animals (data not shown). Merged pY816 and GFP is shown in the rightmost panel. Scale bar = 25 μ m. **D)** MAP2 labeled CA3 dendrites (green; arrows with asterisks) do not prominently colocalize with pY816 (red; arrows with asterisks) in a pilocarpine (Pilo) treated mouse. Areas of enriched pY816 immunoreactivity (red; arrows) are largely devoid of MAP2 labeled dendrites (green; arrows). A similar distribution of pY816 immunoreactivity was observed in NS injected animals. Merged pY816 and MAP2 is shown in the rightmost panel. Scale bar = 15 μ m.

similar patterns of cellular localization following SE in two distinct models of epileptogenesis.

2.3.5 Enhanced pY816 Immunoreactivity Within Synaptic Mossy Fiber Boutons Following KA-SE

A subset of GFP+ giant boutons of mossy fibers in stratum lucidum in Thy1-GFP mice exhibited pY816 immunoreactivity (Fig. 10A; arrow demarks a pY816+ bouton, arrow with asterisk demarks a bouton not prominently immunoreactive). In contrast to the finely granular pattern of pY816 immunoreactivity within mossy fiber axons, the immunoreactivity within boutons was punctate in nature. To determine whether

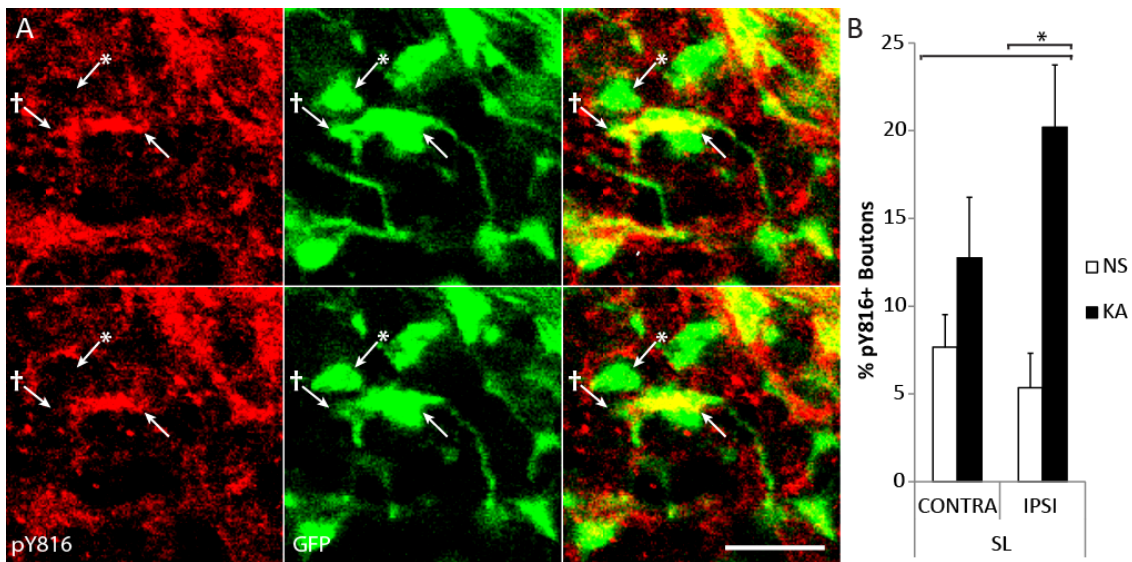


Figure 10: pY816 TrkB immunoreactivity is enhanced within synaptic mossy fiber boutons in SL following KA-SE, observed preferentially in the hippocampus ipsilateral to infusion.

A) Confocal micrographs of two z-sections (top panels, z-section one; bottom panels, z-section two) taken at a 1 μ m increment containing GFP+ mossy fiber boutons (green; arrow and arrow with asterisk) within SL ipsilateral to infusion in a KA treated animal. One bouton contains obvious pY816 immunoreactivity (red; arrow), whereas an adjacent bouton does not contain prominent pY816 (red; arrow with asterisk). Merged pY816 and GFP is shown in rightmost panels. A pY816 puncta within the bouton (top; arrow with dagger) disappears as the portion of the bouton containing it leaves the focal plane (bottom; arrow with dagger). Scale bar = 3.3 μ m. **B)** Quantification of percentages of GFP+ boutons in SL found to contain pY816 immunoreactivity in Thy1-GFP-expressing mice under NS (n=5) and KA (n=5) treated conditions, both ipsilateral (IPSI) and contralateral (CONTRA) to the side of infusion. In boutons ipsilateral to KA infusion, a 3.8-fold ($p<0.01$, one-way ANOVA; $p<0.05$, post-hoc Bonferroni's test) increase in the numbers of pY816+ boutons was observed compared to NS treated animals. On the contralateral side, there was only a 1.9-fold ($p>0.05$) increase in the number of boutons containing immunoreactivity. A total of 901 boutons were analyzed under NS conditions, 934 under KA conditions. Quantification is presented as mean % of neuronal processes \pm SEM; all data analyzed by one-way ANOVA and post-hoc Bonferroni's test; * $p<0.05$.

immunoreactivity within giant boutons increased during epileptogenesis, GFP+ boutons were imaged in the subset of mice treated with NS (n=5) or KA-SE (n=5) that expressed Thy1-GFP. A stack of *z*-sections were scored for pY816 immunoreactivity by a blinded investigator; a bouton was deemed positive if it contained a discrete pY816 puncta that filled at least 20% of the bouton in at least one *z*-section. A total of over 1800 boutons were scored in this fashion.

Under basal conditions, a small fraction (average of 6.5%) of GFP+ boutons in stratum lucidum exhibited pY816 immunoreactivity. Strikingly, the fraction of GFP+ boutons exhibiting pY816 immunoreactivity increased approximately 4-fold in the stratum lucidum ipsilateral to the amygdala infused with KA (Fig. 10B; NS = $5.4 \pm 2.0\%$, KA = $20.2 \pm 2.9\%$, mean \pm SEM; $p < 0.05$); a 1.9-fold increase was evident in stratum lucidum in the contralateral hippocampus (NS = $7.7 \pm 1.9\%$, KA = $14.7 \pm 3.0\%$, mean \pm SEM; $p > 0.05$). The increased fraction of pY816 immunoreactive synaptic boutons paralleled the increase of mossy fiber axonal immunoreactivity in that it was most prominent in the hippocampus ipsilateral to the KA infused amygdala. Towards this end, more boutons were labeled with pY816 in the stratum lucidum ipsilateral to KA infusion than on the contralateral side in all KA treated mice examined (n=5). Furthermore, percentages of boutons labeled on the ipsilateral side in all KA treated mice (n=5) were always greater than the percentages labeled in NS infused littermates on either side relative to infusion.

2.3.6 Localization of pY816 Immunoreactivity within Apical Dendritic Shafts of CA1 Pyramidal Cells Following KA-SE

Although no significant increases in pY816 TrkB immunoreactivity were detected in low power (100x) analyses of stratum radiatum of CA1 following SE induced by KA microinfusion (Fig. 4C), high power (630x) analyses of sections from these same mice revealed increases within neuronal processes populating this region in KA treated animals (n=9) compared to those infused with NS (n=9) (Fig. 11A; arrows point to pY816+ dendritic shafts). The failure to detect an increased intensity of the CA1 stratum radiatum region in low-power analyses following SE is because only a subset of these processes exhibited increased immunoreactivity. This increased pY816 immunoreactivity was found to colocalize with a subset of GFP+ apical dendritic shafts of CA1 pyramidal cells (Fig. 12A; arrows), identified as such based on the fact that they emanated from cell bodies in the stratum pyramidale in the direction of stratum lacunosum moleculare (Ramón y Cajal, 1911). Like the pY816 immunoreactivity within stratum lucidum, pY816 immunoreactive apical dendritic shafts of CA1 pyramidal cells were most prominent in the hippocampus ipsilateral to the KA-infused amygdala (Fig. 11A; compare bottom right panel to others). Counting the number of pY816-immunoreactive processes detected in a total of two high power (630x) fields taken from stratum radiatum of CA1 (Fig. 11B; CA1 SR) revealed a 3.6-fold increase on the side ipsilateral to KA microinfusion compared to NS controls ($NS = 19.3 \pm 2.6$, $KA = 70.2 \pm 13.2$, mean \pm SEM, number of pY816+ neuronal processes; $p < 0.01$); contralaterally, a

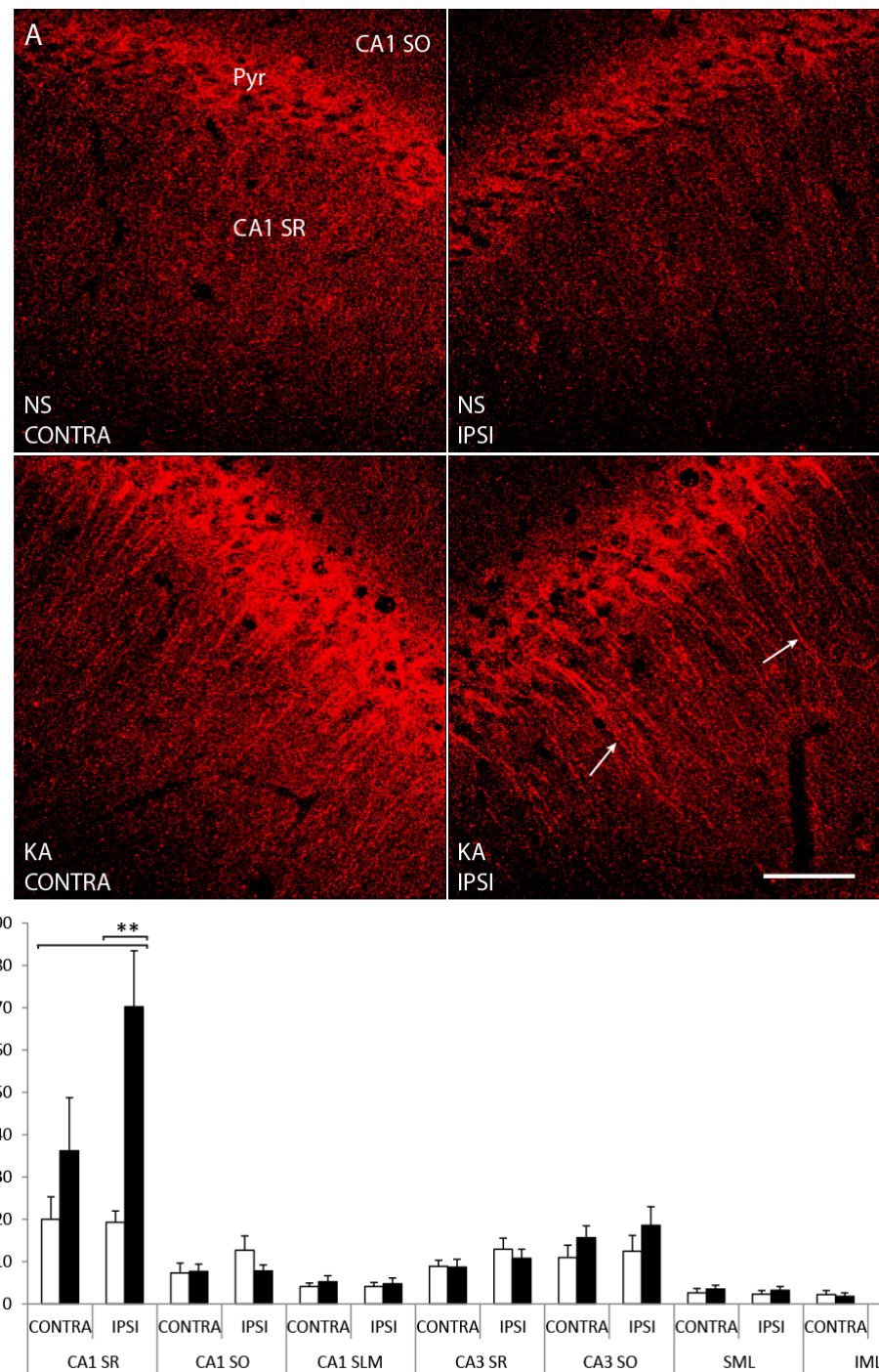


Figure 11: pY816 TrkB immunoreactivity is enhanced within apical dendrites of SR of CA1 following KA-SE, observed preferentially in the hippocampus ipsilateral to infusion.

A) Representative high power (630x) images of CA1 SR (region marked top left) from sections stained with pY816. Animals were infused with either NS (top) or KA (bottom), and images taken from hippocampi both ipsilateral (IPSI, right) and contralateral (CONTRA, left) to the side of infusion. Apical dendrites of CA1 pyramidal cells labeled with pY816 immunoreactivity can be observed under SE conditions, most prominently on the side ipsilateral to KA infusion (bottom right; arrows). Note that dendrites appear most immunoreactive in the region of SR more proximal to CA1 pyramidale (Pyr, marked top left). Scale bar = 50 μ m. **B)** Quantification of total numbers of neuronal processes observed in two high magnification (630x) images taken from NS (n=9) and KA (n=9) treated animals, both ipsilateral and contralateral to the side of infusion. In CA1 SR ipsilateral to KA infusion, a 3.6-fold ($p<0.01$, one-way ANOVA; $p<0.01$, post-hoc Bonferroni's test) increase in the numbers of discerned neuronal processes was observed compared to NS treated animals. On the contralateral side, there was only a 1.8-fold ($p>0.05$) increase in the number of pY816 apical dendrites stained. Quantification in the same fashion of CA1 SO, CA1 SLM, CA3 SR, CA3 SO, SML, and IML in hippocampi taken both ipsilateral and contralateral to infusion also demonstrated no significant differences in the numbers of discerned neuronal processes between NS and KA conditions on either side (CA1 SO $p=0.342$, CA1 SLM $p=0.885$, CA3 SR $p=0.462$, CA3 SO $p=0.449$, SML $p=0.758$, IML $p=0.557$ by one-way ANOVA). Quantification is presented as mean number of neuronal processes \pm SEM; all data analyzed by one-way ANOVA and post-hoc Bonferroni's test; ** $p<0.01$.

1.8-fold increase in number of pY816-immunoreactive processes was detected (NS = 20.0 ± 5.3 , KA = 36.2 ± 12.5 , mean \pm SEM, number of pY816+ neuronal processes, $p>0.05$). In all but one KA-SE treated animal (n=8), more immunoreactive processes were observed on the side ipsilateral to infusion than on the contralateral side, or on either side in NS infused littermates. In the one KA infused animal where these observations did not hold, no dendritic processes were detected in stratum radiatum of CA1 on either side, despite a clear lateralized increase in pY816 immunoreactivity within stratum lucidum compared to NS infused littermates.

Localization of pY816 immunoreactivity to apical dendritic shafts of CA1 pyramidal cells in KA treated animals exhibited striking anatomic specificity. That is, basal dendritic shafts of CA1 pyramidal cells did not exhibit prominent pY816 immunoreactivity (Fig. 12A; arrows with asterisks) nor were significant differences detected in stratum oriens of CA1 between NS (n=9) and KA (n=9) treated animals in the hippocampus either ipsilateral or contralateral to the infused amygdala (Fig. 11B; CA1 SO; ipsilateral: NS = 12.7 ± 3.4 , KA = 7.8 ± 1.5 , contralateral: NS = 7.3 ± 2.3 , KA = 7.7 ± 1.8 , mean \pm SEM, number of pY816+ neuronal processes). Likewise, stratum lacunosum moleculare contains the distal apical dendritic arbors of CA1 pyramidal cells, and this region exhibited few pY816+ neuronal processes (data not shown). No significant differences in the numbers of pY816+ neuronal processes were detected in this region between NS (n=9) and KA (n=9) treated animals (Fig. 11B; CA1 SLM; ipsilateral: NS = 4.1 ± 1.0 , KA = 4.8 ± 1.3 , contralateral: NS = 4.1 ± 0.8 , KA = 5.2 ± 1.5 , mean \pm SEM, number of pY816+ neuronal processes). Finally, little pY816 immunoreactivity was detected in either apical or basal dendritic shafts of CA3 pyramids (in CA3 stratum radiatum and stratum oriens respectively) nor in apical dendritic shafts of dentate granule cells in either the suprapyramidal or infrapyramidal molecular layers of dentate gyrus (data not shown); no significant differences in the numbers of discerned neuronal processes between NS (n=9) and KA (n=9) infused animals were found in any of these regions (Fig. 11B; CA3 SR, CA3 SO, SML, and IML). Importantly, in each of the above regions, abundant GFP-labeled dendritic shafts were evident in Thy1-GFP

animals (data not shown). Thus, apical but not basal dendritic shafts of CA1 pyramidal cells exhibited pY816 immunoreactivity under basal conditions, and this immunoreactivity increased following KA-SE; the immunoreactivity was detected within the proximal dendritic tree within stratum radiatum but not in the most distal portion within stratum lacunosum moleculare. Likewise, minimal pY816 immunoreactivity was detectable within the dendritic arbors of CA3 pyramids and dentate granule cells, nor were differences detected in NS compared to KA treated animals.

2.3.7 Localization of pY816 Immunoreactivity Within Apical Dendritic Shafts of CA1 Pyramidal Cells Following Pilocarpine SE

Similar increases of pY816 labeling of apical dendritic shafts of CA1 pyramidal cells were evident in mice after three hours of SE induced by intraperitoneal injection of pilocarpine. That is, a 6.2-fold increase in the number of pY816-immunoreactive apical shafts of CA1 pyramidal cells was evident in pilocarpine treated animals (n=5) compared to NS (n=4) (NS = 12.3 ± 3.3 , Pilocarpine = 76.4 ± 12.0 , mean \pm SEM, number of pY816+ neuronal processes; $p < 0.01$ by Student's t-test). In contrast to the KA-SE model, apical shaft staining increased bilaterally within both hippocampi in all pilocarpine treated mice (n=5) when compared to NS injected littermates (data not shown). As in the KA-SE model, examination of other regions within hippocampus revealed no detectable differences in the total number of pY816+ basal dendrites observed in stratum oriens of CA1 following SE, nor in any of the other hippocampal regions quantified in the KA-SE model (data not shown).

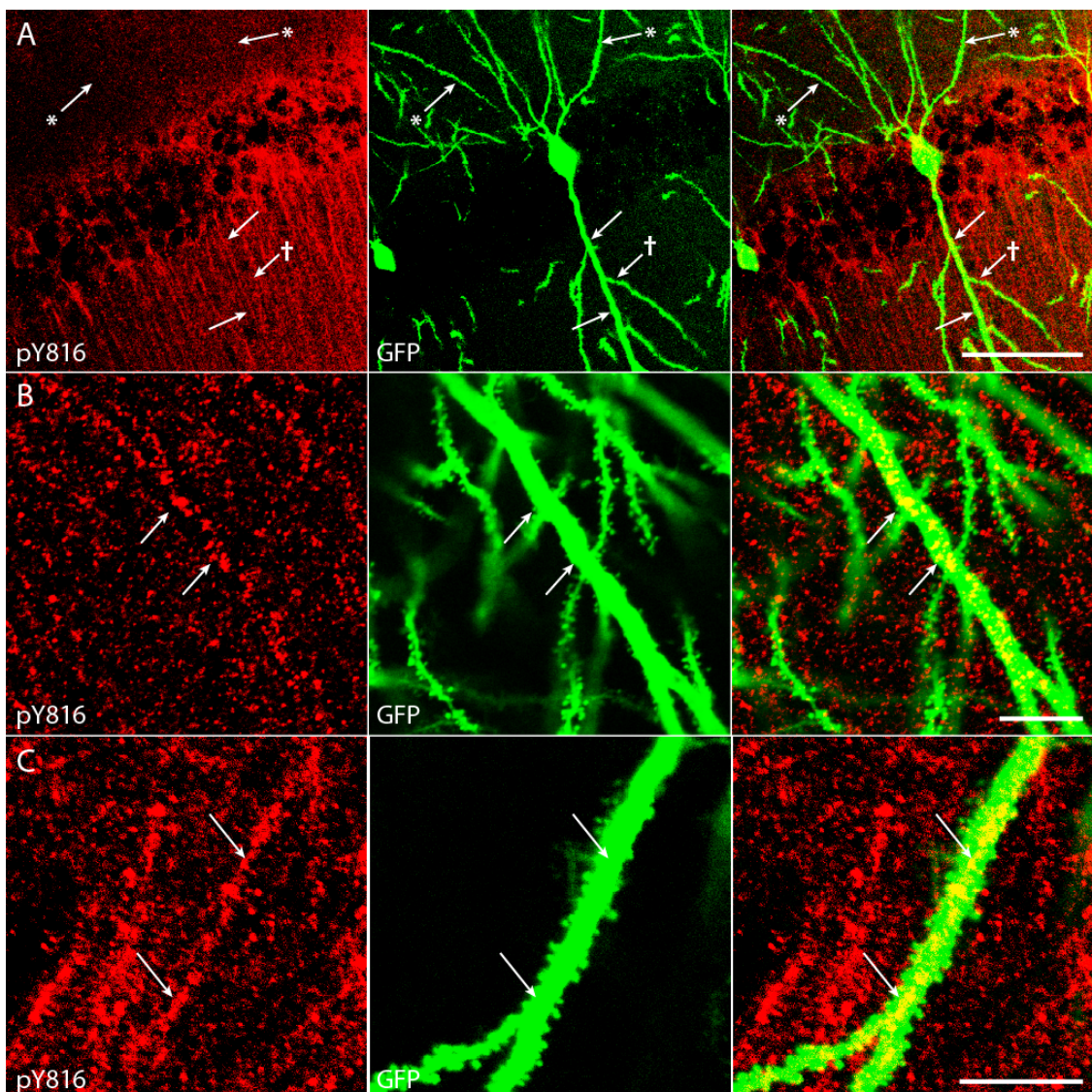


Figure 12: pY816 TrkB immunoreactivity is intracellular and punctate within the dendritic shaft of proximal apical dendrites of CA1 pyramidal cells.

A) The primary apical dendrite of a GFP+ CA1 pyramidal neuron (green; arrows) contains clear pY816 immunoreactivity (red; arrows) within its aspinous proximal shaft, whereas a secondary dendritic branch (green; arrow with dagger) does not contain prominent immunoreactivity within its shaft (red; arrow with dagger). Basal dendritic processes (green; arrows with asterisks) clearly do not contain pY816 immunoreactivity (red; arrows with asterisks). Merged pY816 and

GFP is shown in the rightmost panel. Image is a maximum projection (displaying the region of highest intensity) of multiple confocal scans taken at 0.4 μ m increments in the z-plane. Scale bar = 50 μ m. B) Close-up of a proximal, aspinous portion of a GFP+ apical dendritic process (green; arrows) with intracellular, punctate pY816 immunoreactivity (red; arrows) within the shaft. Merged pY816 and GFP is shown in the rightmost panel. Scale bar = 10 μ m. C) A spiny portion of a GFP+ apical dendrite (green; arrows) also displaying intracellular, punctate pY816 immunoreactivity (red; arrows) within the shaft. Merged pY816 and GFP is shown in the rightmost panel. Scale bar = 10 μ m.

2.3.8 Characterization of pY816 Immunoreactivity Within Apical Dendritic Shafts of Pyramidal Cells in CA1 Following KA-SE

The finding of increased pY816 immunoreactivity within apical dendritic shafts of CA1 pyramidal cells warranted further analysis of its location within these structures. Colocalization analysis with GFP+ shafts in hippocampi of KA-SE treated mice (n=5) revealed immunoreactivity that appeared intracellular and punctate (Fig. 12A-C; arrows). Further inspection of the distribution of pY816 immunoreactivity within apical dendritic shafts of CA1 pyramidal cells in SE treated animals in the KA microinfusion model revealed that this punctate immunoreactivity appeared most prominently within the portion proximal to the soma, becoming sparser and more difficult to identify with increased distance from stratum pyramidale (Fig. 11A; KA). Sections stained with MAP2 from KA-SE treated mice (n=3) revealed apical shafts of CA1 pyramidal cells projecting throughout the entire stratum radiatum, and continuing into stratum lacunosum moleculare (Fig. 13A; arrows). Thus, this finding was not a result of large differences in the numbers of apical dendritic shafts populating proximal versus distal stratum radiatum, or because these shafts were not running parallel to the plane of section. As stated previously, few pY816+ neuronal processes were counted in stratum lacunosum

moleculare and no increase was detected following SE (Fig. 11B; CA1 SLM), demonstrating that pY816 immunoreactivity was also not prominent within the most distal dendritic shafts of CA1 pyramidal cells that populate this region of hippocampus. pY816 immunoreactivity was generally most prominent within the primary apical shaft, with immunoreactivity much less noticeable within secondary branches (Fig. 12A; arrow with dagger). Interestingly, the most proximal segments of primary apical dendrites of CA1 pyramidal cells are generally aspinous (Papp et al., 2001), and immunoreactivity was found within the shafts of these aspinous portions (Fig. 12B; arrows), demonstrating that this immunoreactivity existed even when glutamatergic synapses were not in immediate proximity. However, dendritic immunoreactivity was also readily discernible on some spiny portions of dendritic shaft (Fig. 12C; arrows).

To quantify the distance that pY816 immunoreactivity within the apical dendritic shaft was most prominent within stratum radiatum, GFP+ dendritic shafts containing pY816 immunoreactivity that could be traced throughout the entire vertical span of stratum radiatum were imaged, and the distance that this immunoreactivity was detectable within stratum radiatum was measured (Fig. 13B). In six such apical shafts taken from the ipsilateral hippocampus of a KA infused animal, pY816 immunoreactivity was detected an average of 78.7 μ m from the soma. In contrast, mean total dendritic shaft length within stratum radiatum was found to be 235.8 μ m. Thus, pY816 immunoreactivity was readily detectable throughout only about 32% of the total apical shaft length within stratum radiatum (Fig. 13C). All of these findings demonstrate that

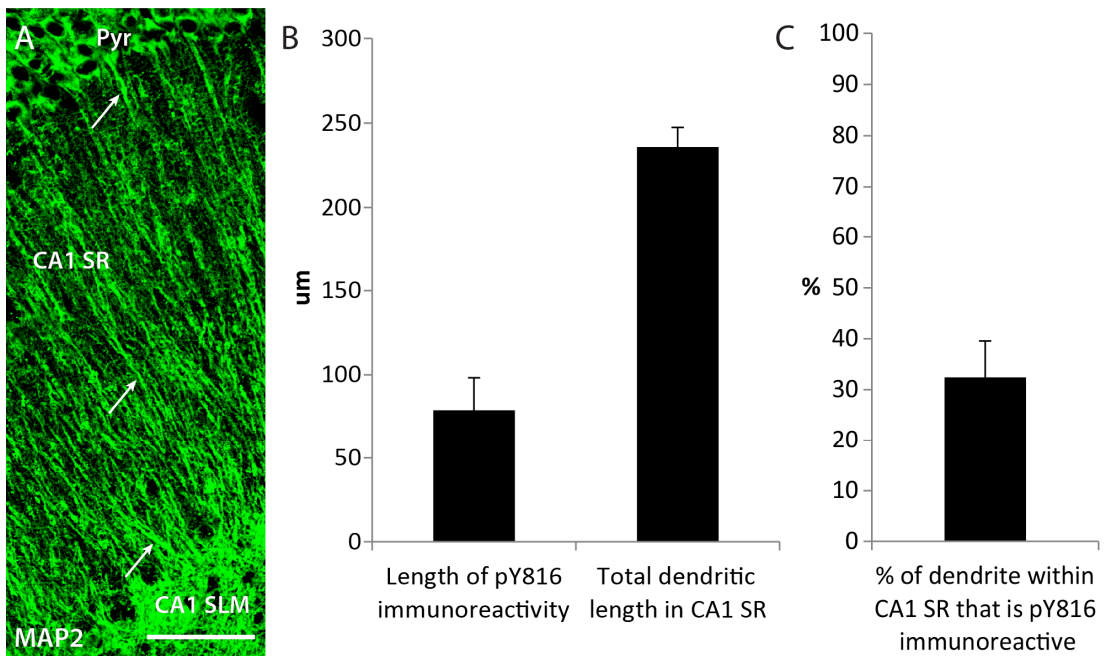


Figure 13: pY816 TrkB immunoreactivity is enriched preferentially within the portion of the apical dendritic shaft of CA1 pyramidal cells more proximal to soma.

A) Image of the entire longitudinal span of CA1 SR, from pyramidale (Pyr) to CA1 SLM, stained with MAP2. Prominent dendritic shaft labeling by MAP2 can be seen within the entire vertical span of CA1 SR (arrows), showing that apical dendrites remain within the focal plane throughout. Scale bar = 50 μ m. B) Quantification of the total distance that pY816 immunoreactivity in GFP+ apical dendritic shafts was found to extend distally into CA1 SR in a KA treated animal, measured from soma (n=6 dendritic shafts). Only GFP+ dendritic shafts that were also found to be pY816+ were used in this analysis. The entire lengths of these GFP+ dendrites were imaged until their intersection with SLM, and total dendritic length from soma to SLM was also quantified. pY816 immunoreactivity was found to extend an average of 78.7 ± 19.4 μ m into the shaft, whereas average dendritic length was found to be 235.8 ± 11.7 μ m. C) Quantification of the percent of total dendritic length that pY816 immunoreactivity was found to occupy (n=6), using measurements made from the same dendritic shafts as in (B). Immunoreactivity was found, on average, within 38 ± 7 % of the most proximal portion of pY816+ apical dendritic shafts within CA1 SR. Error bars represent SEM.

pY816 TrkB immunoreactivity is enhanced within proximal shafts of apical dendrites of CA1 pyramidal cells following SE, and appears intracellular and punctate within these structures.

2.3.9 Enhanced pY816 Immunoreactivity Within Dendritic Spines of Pyramidal Cells in CA1 Stratum Radiatum Following KA-SE

The localization of pY816 immunoreactive puncta to presynaptic boutons of mossy fiber axons within stratum lucidum raised the question as to whether pY816 immunoreactivity within CA1 might be localized to synaptic specializations of the apical dendrites of CA1 pyramidal cells. Small specializations of apical dendrites of CA1 pyramidal cells indicative of spines were evident in Thy1-GFP mice in both NS and KA infused animals. Moreover, analysis of pY816 immunoreactivity within stratum radiatum of CA1 revealed that, in addition to signal corresponding to apical dendritic shafts, the entire region was also filled with many small puncta. Inspection of GFP+ spines of apical dendrites in Thy1-GFP mice revealed that a subset colocalized with pY816 puncta (Fig. 14A; arrows). To quantify colocalization of pY816 immunoreactivity with GFP+ dendritic spines in CA1 stratum radiatum, z-stacks were acquired and spines scored as positive or negative for pY816 by a blinded observer; a spine was scored as positive if filled with a pY816 immunoreactive puncta in at least one z-section. Over 1800 spines were examined in the same NS (n=5) and SE (n=5) Thy1-GFP animals used previously in this study. The percentages of pY816+ spines in CA1 stratum radiatum in NS and KA treated mice both ipsilateral and contralateral to infusion was then determined (Fig. 14B;

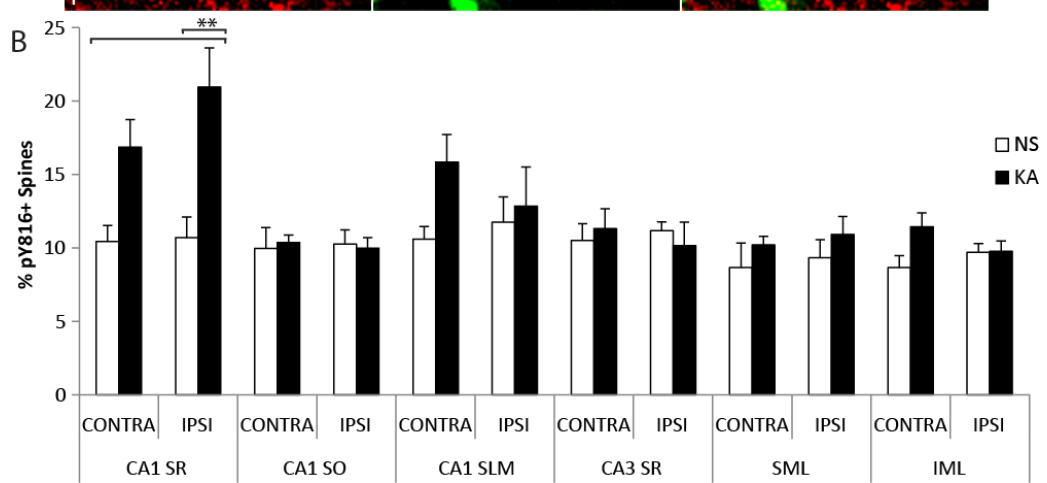
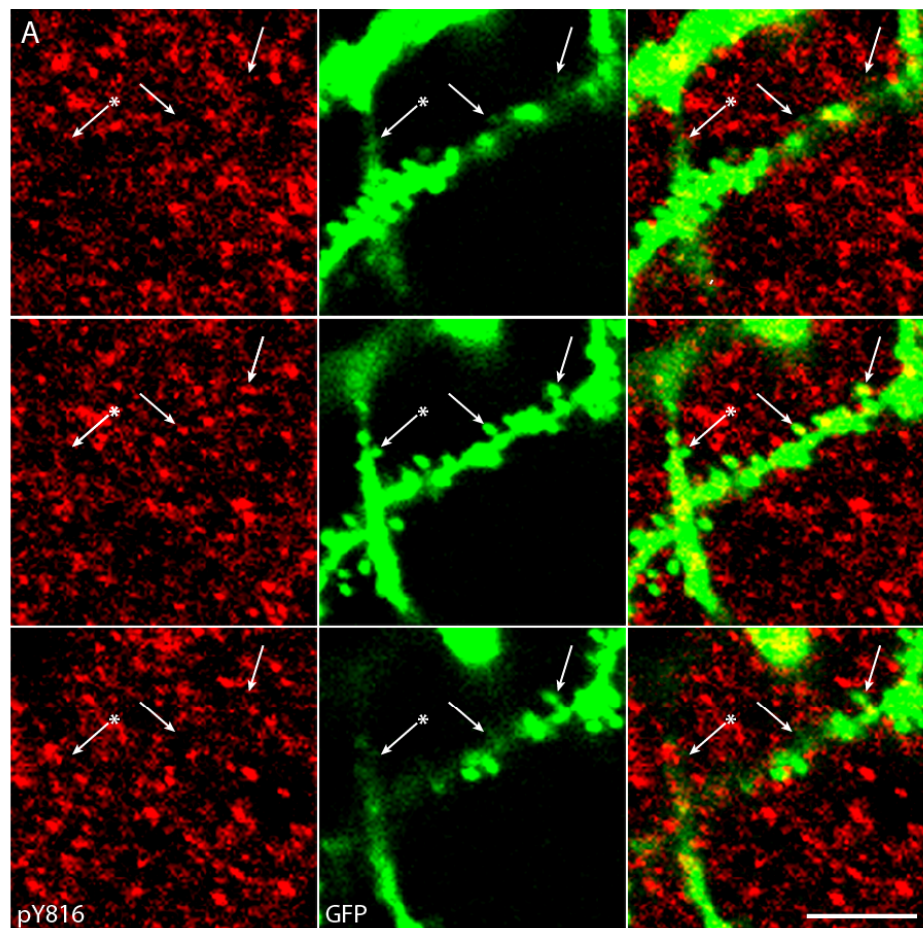


Figure 14: pY816 TrkB immunoreactivity is enhanced within dendritic spines in CA1 SR following KA-SE, observed preferentially in the hippocampus ipsilateral to infusion.

A) Confocal micrographs from CA1 SR from a Thy1-GFP mouse treated with KA. Three z-sections are shown taken at 750 nm increments above (top panels), within (middle panels), and below (bottom panels) two GFP+ spines (middle, green panel; arrows) of an apical dendrite that contain small pY816 puncta (middle, red panel; arrows). Other spines (middle, green panel; arrow with asterisk) do not appear to contain pY816 (middle, red panel; arrow with asterisk). Note colocalization of pY816 with spines in the z-plane (observe panels from top to bottom and note arrows), such that these pY816 puncta are observable within the spine but not above or below it. Merged pY816 and GFP images are shown in the rightmost panels. Scale bar = 2.5 μ m. **J) Quantification of percentages of GFP+ spines found to contain pY816 immunoreactivity in Thy1 GFP-expressing mice in CA1 SR, CA1 SO, CA1 SLM, CA3 SR, the outer two-thirds of SML, and the outer two-thirds of IML.** This was quantified under both NS (n=5) and KA (n=5) conditions, both ipsilateral (IPSI) and contralateral (CONTRA) to the side of infusion. In spines of CA1 SR ipsilateral to KA infusion, a 2.0-fold increase in the numbers of pY816+ spines was observed compared to NS treated animals ($p<0.01$, one-way ANOVA; $p<0.01$, post-hoc Bonferroni's test). The contralateral side demonstrated a more modest, 1.6-fold increase which was not significant. Data are from 994 spines analyzed under NS conditions, 1020 spines analyzed under KA conditions. No significant differences in the numbers of pY816+ spines were found in any of the other regions analyzed (CA1 SO $p=0.993$, 2097 spines; CA1 SLM $p=0.272$, 2428 spines; CA3 SR $p=0.899$, 2263 spines; SML $p=0.604$, 1940 spines; IML $p=0.128$, 1958 spines, one-way ANOVA). Quantification is presented as mean % of neuronal processes \pm SEM; all data analyzed by one-way ANOVA and post-hoc Bonferroni's test; ** $p<0.01$.

CA1 SR). Importantly, no overt differences in spines were noticeable between conditions (data not shown).

Under basal conditions, a small fraction (approximately 10%) of spines of proximal apical dendrites of CA1 pyramidal cells exhibited pY816 immunoreactivity. The fraction of GFP+ spines exhibiting pY816 immunoreactivity approximately doubled in the apical dendrites of CA1 pyramidal cells in the hippocampus ipsilateral to the amygdala infused with KA (NS = $10.7 \pm 1.4\%$, SE = $21.0 \pm 2.7\%$, mean \pm SEM; $p<0.01$); a 1.6-fold increase was detected in the hippocampus contralateral to the infused amygdala

($NS = 10.4 \pm 1.1\%$, $SE = 16.9 \pm 1.9\%$, mean \pm SEM, $p > 0.05$). The percentage of pY816 colocalization with spines in stratum radiatum of CA1 in KA infused animals was always greater in hippocampus ipsilateral to the infused amygdala compared to contralateral and this value always exceeded that found in either hippocampus of NS infused littermates ($n=5$). Thus, similar to giant boutons of the mossy fiber-CA3 synapse, pY816 immunoreactivity was found to increase in spines of the CA3-CA1 synapse following SE induced by KA microinfusion, and this effect was lateralized to the side ipsilateral to infusion.

As GFP+ spines could also be visualized in stratum oriens of CA1 and stratum lacunosum moleculare in these same mice (data not shown), similar analyses were conducted in these regions (Fig. 14B; CA1 SO and CA1 SLM). Similar to stratum radiatum of CA1, pY816 puncta could be discerned within these regions and colocalized with a subset (approximately 10%) of GFP+ spines (data not shown). However, unlike stratum radiatum of CA1, no significant differences in the numbers of pY816 immunoreactive spines on basal dendrites within stratum oriens of CA1 were detected between NS ($n=5$) and KA animals ($n=5$), either ipsilateral or contralateral to infusion (ipsilateral: $NS = 10.3 \pm 1.0\%$, $KA = 10.0 \pm 0.7\%$, contralateral: $NS = 10.0 \pm 1.4\%$, $KA = 10.4 \pm 0.5\%$, mean \pm SEM; $p > 0.05$). Similar results were obtained with quantification of spines of apical dendrites of CA1 pyramidal neurons within stratum lacunosum moleculare (ipsilateral: $NS = 11.7 \pm 1.7\%$, $KA = 12.9 \pm 2.7\%$, contralateral: $NS = 10.6 \pm 0.9\%$, $KA = 15.9 \pm 1.9\%$, mean \pm SEM; $p > 0.05$; $n=5$ mice per treatment group). Thus,

pY816 activation within spines of CA1 pyramidal neurons following SE appeared to be confined to the proximal apical dendrites within stratum radiatum, just as increased pY816+ immunoreactivity was also only found within this portion of the dendritic tree of CA1 pyramidal neurons.

Finally, GFP+ spines of CA3 pyramids were readily discerned within stratum radiatum of CA3, and spines of dentate granule cells could be imaged in the dentate gyrus (data not shown). This afforded the opportunity to quantify pY816 immunoreactivity in spines within these other important neuronal populations of hippocampus. Quantification of spines in CA3 stratum radiatum demonstrated that about 10% of spines were found to contain significant pY816 immunoreactivity, but no differences were found between NS (n=5) and KA (n=5) conditions on either side relative to infusion (Fig. 14B; CA3 SR; p>0.05). For spines of the molecular layer of dentate gyrus, the outer two-thirds of this region was quantified, as this is the portion that receives perforant path innervation from entorhinal cortex and is robustly activated during limbic seizures. Quantification of both suprapyramidal and infrapyramidal molecular layers demonstrated that approximately 9% of imaged spines contained pY816 immunoreactivity in NS treated mice (n=5), and there was no significant increase in this percentage in KA-SE treated animals (n=5) (Fig. 14B; SML and IML; p>0.05). Thus, enhanced pY816 immunoreactivity within synaptic spines appeared to be confined only to stratum radiatum in hippocampus following KA-SE, the only region where increases in pY816 immunoreactivity were found in dendritic shafts after SE. Furthermore, the only regions where increases in immunoreactivity

within synaptic boutons or spines was detected were also the only regions where increases in pY816 immunoreactivity within axons or dendritic shafts was detected, namely stratum lucidum and stratum radiatum of CA1.

2.4 Discussion

This study tested the hypothesis that enhanced pTrkB immunoreactivity evident in the hippocampus in multiple animal models was localized to the mossy fibers of dentate granule cells. To test this hypothesis, confocal microscopy was employed to examine colocalization of pY816 immunoreactivity with axonal and dendritic markers, and with GFP expressed in hippocampal neurons of Thy1 GFP mice following SE. Four principal findings emerged: (1) pY816 immunoreactivity in stratum lucidum was found within mossy fiber axons and giant presynaptic boutons of dentate granule cells of control adult mice. (2) A robust increase of pY816 immunoreactivity was detected within both of these structures following SE. (3) Unexpectedly, pY816 immunoreactivity was also found within the shafts and spines of apical dendrites of CA1 pyramidal cells of control adult mice. (4) pY816 immunoreactivity was also robustly enhanced within these structures following SE. Collectively, these findings provide evidence that SE induces enhanced activation of TrkB at two distinct excitatory synapses within hippocampal circuitry. This enhanced TrkB activation is well positioned to regulate the plasticity of these synapses, an attractive cellular mechanism underlying epileptogenesis.

The results reveal that activated TrkB within hippocampus is most prominent within stratum lucidum, and robustly increases within this region following KA-SE. The

activated TrkB within stratum lucidum was localized to the axons and giant boutons of the mossy fibers of dentate granule cells by colocalization of pY816 immunoreactivity with GFP expressed in these neurites, and confirmed by colocalization with the axonal marker, tau. Whereas all mossy fiber axons appeared to contain activated TrkB, only a small minority (5%) of mossy fiber boutons contained activated TrkB under basal conditions. Notably, a striking 4-fold increase was found in the percentage of mossy fiber boutons containing activated TrkB in the hippocampus ipsilateral to KA infusion. These results confirm earlier work that reported increased pTrkB immunoreactivity in stratum lucidum during epileptogenesis, yet was unable to identify the cellular structures containing this immunoreactivity (Binder et al., 1999a; Danzer et al., 2004; He et al., 2004; He et al., 2002; He et al., 2010). The present results are also consistent with recent ultrastructural evidence localizing pY816 immunoreactivity to mossy fiber axons and a minority (5%) of boutons within SL under basal conditions (Spencer-Segal et al., 2011); pY816 immunoreactivity within boutons was most often affiliated with small synaptic vesicles opposite the synaptic contact.

The abundance of activated TrkB found in stratum lucidum correlates with high levels of expression of ligands known to activate it. The highest levels in forebrain of the canonical TrkB ligand, BDNF, are found within stratum lucidum, where its expression is increased during epileptogenesis (Conner et al., 1997; He et al., 2004; Yan et al., 1997). Unexpectedly, increases of activated TrkB within stratum lucidum were identified during epileptogenesis despite conditional deletion of BDNF (He et al., 2004), a finding leading

to the discovery that the divalent cation, zinc, can transactivate TrkB in the absence of BDNF (Huang and McNamara, 2010; Huang et al., 2008). Synaptic vesicles of mossy fiber boutons contain copious stores of zinc, presumably released during neuronal activity, suggesting a role for this metal in contributing to TrkB activation at this locale (Cole et al., 1999; Qian and Noebels, 2005). pTrkB within mossy fiber boutons is likely to have been activated at the synaptic membrane by one of these ligands. The pTrkB within axons may be in transit back to the soma; transport of pTrk-ligand complexes have been previously described in axons and may promote communication of TrkB signaling from synapse to cell body (Bhattacharyya et al., 1997; Watson et al., 1999a) in a manner similar to NGF-TrkA signaling (Niewiadomska et al., 2011).

The discovery of activated TrkB within shafts of apical dendrites and spines of CA1 pyramidal cells following epileptogenesis was unexpected based upon previous work (Binder et al., 1999a; Danzer et al., 2004; He et al., 2004; He et al., 2002; He et al., 2010). Use of less sensitive antibodies together with quantitative analyses conducted solely at low magnification (100x) accounts for this finding previously escaping detection. Indeed, quantification at low power (100x) in stratum radiatum of CA1 in the present study revealed no significant differences between NS and KA treated animals, despite robust increases following KA when pY816+ dendritic shafts and spines were quantified at high power (630x). These results are consistent with ultrastructural evidence localizing pY816 immunoreactivity to dendritic shafts of CA1 pyramidal cells and a minority (5%) of spines within stratum radiatum of CA1 under basal conditions

(Spencer-Segal et al., 2011); notably, activated TrkB was clustered next to the postsynaptic density. Light microscopic studies have also colocalized pTrkB immunoreactivity with a subset of PSD-95 (5%) in stratum radiatum of CA1, and the fraction of pTrkB colocalizing with PSD-95 increased approximately 2-fold following an unsupervised learning paradigm (Chen et al., 2010a; Chen et al., 2010b). These values are similar to those detected under basal conditions in the present study. Notably, BDNF and synaptic zinc are readily detectable within stratum radiatum of CA1, but are present in lower amounts than in stratum lucidum, correlating with the less robust pY816 immunoreactivity detected in this region (Conner et al., 1997; Yan et al., 1997). Like in mossy fiber boutons, TrkB at the spine is likely to be activated by one of these ligands, and pTrkB within dendritic shafts may be undergoing retrograde transport to the soma.

The restricted localization of activated TrkB induced by SE raises multiple questions. Why is the activation not more widespread? And what accounts for its activation within synapses at these two sites? With respect to the first question, we suspect that enhanced TrkB activation does indeed occur at sites outside the hippocampus and perhaps even at additional sites within hippocampus. The present study examined TrkB activation at a single point in time, following 3 hours of SE; study at additional times following SE might reveal additional sites of TrkB activation. Moreover, an antibody with greater sensitivity may have revealed additional sites of TrkB activation even at 3 hours. With respect to the second question, we favor the explanation that enhanced release of BDNF and/or zinc from presynaptic terminals of axons of the dentate

granule cells and CA3 pyramidal cells is responsible for TrkB activation in mossy fiber boutons and CA1 pyramidal cell spines respectively. That is, SE, the inducing stimulus, is characterized by enhanced firing of populations of neurons which would be expected to trigger release of BDNF and zinc which are packaged in synaptic vesicles. The localization of activated TrkB to synapses is consistent with this idea. The bilateral tonic and clonic motor activity of the induced seizures notwithstanding, the lateralization of activated TrkB preferentially to the hippocampus ipsilateral to the infused amygdala is consistent with enhanced neuronal activity within these circuits, a proposal consistent with direct projection ipsilaterally—but not contralaterally—from the basal nucleus of amygdala to CA3 and CA1 of hippocampus (Pikkarainen et al., 1999).

This idea may also account for the localization of pY816 immunoreactivity to the spines and shafts of proximal apical dendrites, while sparing the spines and shafts of basilar dendrites and of the distal portion of apical dendrites within stratum lacunosum-moleculare. The observed distribution of TrkB activation implies that afferents innervating the apical dendrites of CA1 pyramidal cells were activated during KA-SE to a greater extent than those innervating the basilar dendrites. Interestingly, axons of CA3 pyramidal neurons positioned closer to dentate gyrus (CA3c) project preferentially to superficial layers of stratum radiatum of CA1 (located closer to stratum lacunosum moleculare) (Ishizuka et al., 1990). In contrast, axons of CA3 pyramidal cells located closer to CA1 (in CA3a) project preferentially to proximal apical dendrites of CA1 pyramidal cells and to basilar dendrites in stratum oriens. These differential patterns of

anatomic projections support the possibility that preferential firing of subpopulations of CA3 pyramidal cells during KA-SE may promote release of TrkB ligands from subpopulations of synapses formed by CA3 axons on spines of proximal apical dendrites of CA1 pyramidal cells, thereby accounting for the observed pattern of pY816 immunoreactivity.

Activation of TrkB within these hippocampal neuronal populations likely promotes epileptogenesis, though study of this process in mutant mice carrying cell type specific deletions of TrkB will be required to provide definitive answers. Lesion studies implicate hippocampal circuitry in epileptogenesis triggered by stimulation of amygdala in the kindling model as evidenced by striking inhibition following knife cuts of entorhinal cortex or selective destruction of the dentate granule cells (Dasheiff and McNamara, 1982; Savage et al., 1985). With respect to how TrkB activation at these locales may contribute to the development of epilepsy, one cellular consequence of activated TrkB in mossy fibers that might promote epileptogenesis is long term potentiation (LTP). Both *ex vivo* and *in vivo* studies of animal models support the idea that LTP of excitatory synapses between principal cells contributes to limbic epileptogenesis (Sutula and Steward, 1987), the hypothesis being that potentiation of these synapses may facilitate propagation of seizure activity via synaptically coupled neuronal populations throughout the limbic system and beyond.

The excitatory synapse formed by mossy fiber boutons with spines of CA3 pyramids undergoes LTP which is notable in that mechanisms underlying its induction

and expression reside presynaptically (reviewed by Nicoll and Schmitz, 2005; Pan et al. 2011; but see Yeckel et al. 1999). Mossy fiber-CA3 LTP is eliminated by inhibition of TrkB kinase (Huang et al., 2008) and by inhibition of TrkB-mediated activation of phospholipase C gamma-1 (PLC γ 1) signaling through pY816 (He et al., 2010), the same residue critical for epileptogenesis. Interestingly, study of hippocampal slices isolated from animals following KA induced seizures *in vivo* revealed that LTP of the mossy fiber-CA3 synapse was occluded, suggesting that this synapse had undergone LTP *in vivo* (Goussakov et al., 2000). Collectively, it seems plausible that enhanced activation of TrkB in mossy fibers may contribute to LTP of this synapse *in vivo* during epileptogenesis. The axonal localization of pY816 immunoreactivity within stratum lucidum is also consistent with the possibility that TrkB-PLC γ 1 signaling within these structures, through evoking rises in cytosolic calcium, is positioned to promote LTP by activating type 2 ryanodine receptors. These ER-bound channels mediate calcium-induced calcium release (CICR) from internal stores, and themselves open in response to rises in calcium (Verkhratsky, 2005). These receptors have been localized to mossy fiber axons (Shimizu et al., 2008) in a distribution similar to pY816 found in this study. Mossy fiber-CA3 LTP is inhibited by ryanodine (Bortolotto et al., 2003), consistent with the idea that type 2 ryanodine receptor activation may be a consequence of pY816 signaling. Interestingly, epileptic seizures are one manifestation of mice genetically engineered to express leaky type 2 ryanodine receptors (Lehnart et al., 2008).

Like activated TrkB within mossy fiber boutons, one cellular consequence of the enhanced TrkB activation within spines of CA1 pyramidal cells may be LTP of synapses formed by Schaffer collateral axon terminals onto these structures (Huang et al., 2008; Minichiello et al., 1999). TrkB activation at these synapses has been implicated in both LTP and hippocampal-dependent associative learning (Gruart et al., 2007). Like the mossy fiber-CA3 synapse, mutation of Y816, but not Y515, inhibited induction of LTP of the Schaffer collateral-CA1 synapse (He et al., 2010; Korte et al., 2000; Minichiello et al., 2002), the same residue implicated in promoting epileptogenesis. Furthermore, in immunohistochemical studies examining pTrkB using brain slices treated with LTP-inducing stimuli at the Schaffer collateral-CA1 synapse, increases in numbers of pTrkB-immunoreactive puncta were observed in CA1 stratum radiatum (Lu et al., 2011), and enhanced colocalization of pTrkB puncta with PSD-95 was found in brain slices after such a stimuli (Chen et al., 2010b). The location of activated TrkB within spines of CA1 pyramidal neurons is optimally positioned to promote a postsynaptic LTP of this synapse. Whereas the pTrkB found within dendritic spines in the present study is well positioned to regulate synaptic function (Lu, 2003), the function of pTrkB within shafts is less obvious. If pTrkB within dendritic shafts is in transit back to the soma, it may ultimately affect key transcriptional regulators, such as CREB, implicated in the expression of the late phase of LTP, which is protein synthesis dependent and also mediated by TrkB (Minichiello, 2009).

In summary, the present work demonstrates that epileptogenesis is associated with a highly specific pattern of enhanced activation of TrkB within hippocampus. Among the diverse populations of neurons within hippocampus, enhanced activation of TrkB was identified only within dentate granule cells and CA1 pyramidal neurons, suggesting that the functional consequences of its activation are multifocal yet discrete within limbic circuitry. The localization within these populations was highly specific, involving the axons of the granule cells and apical, but not basal, dendritic shafts of CA1 pyramidal neurons. While localization to synapses was common to each population of neurons, the localization was to presynaptic boutons of the granule cell axons and to postsynaptic spines of the CA1 pyramidal cells. One plausible cellular consequence of enhanced TrkB activation is increased efficacy of excitatory synapses between principal neurons, a cellular event likely pivotal to the pathogenesis of limbic epilepsy.

3. The Contribution of Vesicular Zinc to Transactivation of TrkB in Stratum Lucidum of Mouse Hippocampus

3.1 Introduction

TrkB is a tyrosine kinase receptor in the tropomyosin-related kinase (Trk) family of neurotrophin receptors which is critical to neuronal processes including survival, differentiation, and synaptic plasticity (Chao et al., 2006; Huang and Reichardt, 2001; McAllister et al., 1999; Poo, 2001). The importance of this receptor in diverse neuronal processes, as well as its involvement in several diseases of the nervous system (Barbacid, 1995; Chao et al., 2006; McNamara et al., 2006), underscores the importance of understanding the ligands which mediate its activation. The canonical neurotrophin ligand that activates TrkB is brain derived neurotrophic factor (BDNF) (Barbacid, 1995). Binding of BDNF to the ectodomain of TrkB induces phosphorylation at intracellular tyrosine residues, resulting in receptor activation and downstream signal transduction (Barbacid, 1995; Cunningham and Greene, 1998). Antibodies that recognize specific epitopes of phosphorylated tyrosine residues on TrkB (pTrkB) therefore can be used as surrogate measures of receptor activation (Segal et al., 1996). BDNF is highly enriched in stratum lucidum of hippocampus, an area where dentate granule cells synapse on CA3 pyramidal neurons (Yan et al., 1997). BDNF is thought to be released following neuronal activity, and striking increases in BDNF protein expression have been observed following seizures (Danzer and McNamara, 2004; He et al., 2004; Lessmann and Brigadski, 2009; Yan et al., 1997). In rodent models of epilepsy, antibodies recognizing

pTrkB reveal enriched immunoreactivity in stratum lucidum using immunohistochemical methods (IHC) (Binder et al., 1999a; He et al., 2004; He et al., 2002; He et al., 2010). This temporal and spatial concordance of increased BDNF expression and pTrkB immunoreactivity led to the hypothesis that BDNF was activating this receptor under these conditions. Unexpectedly, however, in mice with a conditional deletion of BDNF from cells of stratum lucidum, this enhanced pTrkB immunoreactivity persisted (He et al., 2004). These findings suggested that another ligand may be contributing to TrkB activation under these conditions, and prompted a search for another such molecule.

Transactivation is a process by which a ligand activates its receptor without interacting directly with it (Carpenter, 1999). The divalent cation, zinc, has been found to transactivate another tyrosine kinase receptor, epidermal growth factor receptor (EGFR), which led to the hypothesis that zinc may also be capable of TrkB transactivation (Wu et al., 2002). To this end, our laboratory found that exogenous zinc can activate the TrkB receptor in neuronal-glial cultures prepared from rodent cortex through a mechanism independent of BDNF (Huang et al., 2008). Endogenous zinc, under conditions of increased neuronal activity, was also found to promote TrkB transactivation *in vitro* (Huang et al., 2008). Zinc is present in glutamate-containing synaptic vesicles of axon terminals throughout hippocampus and neocortex, and is incorporated into these vesicles by zinc transporter protein-3 (ZnT3), expressed only on the membranes of presynaptic vesicles of glutamatergic neurons that concentrate this metal (Palmiter and Huang, 2004). Vesicular zinc is particularly enriched in boutons of dentate granule cells *in vivo*, where it

is found in the highest quantities in the nervous system, and is co-released with glutamate in an activity dependent fashion (Choi and Koh, 1998; Frederickson and Danscher, 1990; Frederickson et al., 2005). TrkB activation is necessary for LTP at the mossy fiber-CA3 synapse, and chelation of extracellular zinc prevents development of this LTP (Huang et al., 2008). All of these findings suggest that both vesicular zinc and BDNF may contribute to activation of TrkB within stratum lucidum. Whether this synaptic pool of zinc activates TrkB *in vivo*, however, remains to be tested.

The objective of this study was to examine the contribution of vesicular zinc to TrkB transactivation within stratum lucidum of hippocampus under physiological conditions, and to compare this contribution to that of the canonical TrkB ligand, BDNF. In order to do this, two strains of genetically modified mice were utilized : (1) a conditional knockout of BDNF which eliminates this molecule from stratum lucidum (He et al., 2004), allowing examination of TrkB activation in the absence of BDNF, and (2) a complete genetic knockout of ZnT3 (Cole et al., 1999), which completely eliminates vesicular zinc from mossy fibers and other CNS neurons, allowing for the study of TrkB activation in the absence of synaptic zinc stores. Breeding these lines together resulted in generation of mice which were deficient in both BDNF and vesicular zinc within stratum lucidum, and thus allowed for the study of TrkB activation in the absence of both BDNF and synaptic zinc. As presented in Chapter 2 of this dissertation and (Helgager et al., 2013), an antibody detecting an activated form of TrkB, that which is phosphorylated on tyrosine residue 816 (pY816) of the receptor, found it to be enriched within important

cellular and synaptic structures within stratum lucidum. As immunoreactivity was readily detectable within these structures under physiological conditions, use of this antibody offered an ideal means by which to assay levels of activated TrkB at these cellular locales in the absence of synaptic zinc and/or BDNF.

3.2 Materials and Methods

3.2.1 Generation of BDNF Mutant, ZnT3 Mutant, and ZnT3/BDNF Double Mutant Mice

BDNF mutant mice were generated as described (Monteggia et al., 2004; Zhu et al., 2001), a gift from the lab of Luis Parada (University of Texas Southwestern Dallas, TX). Cre/loxP technology (Gu et al., 1994) was utilized in these animals, and to this end exon five of the *BDNF* gene was flanked by two *loxP* sites (“floxed”) so that it would be deleted in the presence of Cre recombinase. These animals were backcrossed for at least seven generations into a C57/BL6 background at which time they were bred to transgenic mice, also backcrossed in the same fashion, expressing Cre recombinase under the control of a *synapsin-1* promoter (Syn-Cre). Mice homozygous for *BDNF* floxed alleles which also contain Syn-Cre ($\text{Syn-Cre}^+/\text{BDNF}^{\text{flox/flox}}$) will have BDNF protein eliminated from a subset of CNS neurons. In the hippocampus this results in elimination of *BDNF* gene expression in virtually all dentate granule cells and CA3 pyramidal neurons and in a subset of CA1 pyramidal cells (see Figure 1 of He et al., 2004). These conditional knockout animals will henceforth be referred to as $\text{BDNF}^{-/-}$ mice. $\text{BDNF}^{-/-}$ animals were generated for experiments as outlined in Fig. 15A, yielding litters in which approximately

50% of animals do not contain Syn-Cre ($\text{Syn-Cre}^-/\text{BDNF}^{\text{flox}/\text{wt}}$ or $\text{Syn-Cre}^-/\text{BDNF}^{\text{flox}/\text{flox}}$) and therefore express BDNF at wild type levels, henceforth referred to as $\text{BDNF}^{+/+}$ mice, 25% are $\text{BDNF}^{+/-}$, and 25% $\text{BDNF}^{-/-}$ (He et al., 2004).

ZnT3 mutant mice, generated as described in (Cole et al., 1999), were obtained from the Jackson Laboratory (Bar Harbor, ME) and backcrossed for seven generations into a C57/BL6 background, the founders of which were originally obtained from Charles River (Wilmington, MA). These animals contain a targeted deletion in which exons 1-4 of the *ZnT3* gene have been replaced with a cassette containing *nlacZ* and *neo^r*. Mice homozygous for this mutant allele ($\text{ZnT3}^{-/-}$) express no ZnT3 protein. By breeding those heterozygous for the mutant allele ($\text{ZnT3}^{+/-}$) together, litters can be generated that are approximately 25% wild type ($\text{ZnT3}^{+/+}$), 50% heterozygotes ($\text{ZnT3}^{+/-}$), and 25% $\text{ZnT3}^{-/-}$ (Fig. 15B).

ZnT3/BDNF double mutant animals ($\text{ZnT3}^{-/-}/\text{Syn-Cre}^+/\text{BDNF}^{\text{flox}/\text{flox}}$) were generated using a similar breeding strategy as for generation of $\text{BDNF}^{-/-}$ mice. Specifically, $\text{ZnT3}^{-/-}/\text{Syn-Cre}^-/\text{BDNF}^{\text{flox}/\text{flox}}$ animals were mated with $\text{ZnT3}^{-/-}/\text{SynCre}^+/\text{BDNF}^{\text{flox}/\text{wt}}$ mice (Figure 15C). As with generation of *BDNF* mutant animals, this breeding resulted in litters in which approximately 50% of mice do not express Syn-Cre and therefore express BDNF protein at normal levels, though are knockouts of *ZnT3* ($\text{ZnT3}^{-/-}/\text{Syn-Cre}^-/\text{BDNF}^{\text{flox}/\text{wt}}$ or $\text{ZnT3}^{-/-}/\text{Syn-Cre}^-/\text{BDNF}^{\text{flox}/\text{flox}}$), 25% are heterozygous for the BDNF allele ($\text{ZnT3}^{-/-}/\text{Syn-Cre}^+/\text{BDNF}^{\text{flox}/\text{wt}}$), whereas 25% are *ZnT3/BDNF* double knockouts, henceforth referred to as $\text{ZnT3}^{-/-}\text{BDNF}^{-/-}$ mice. Double mutant

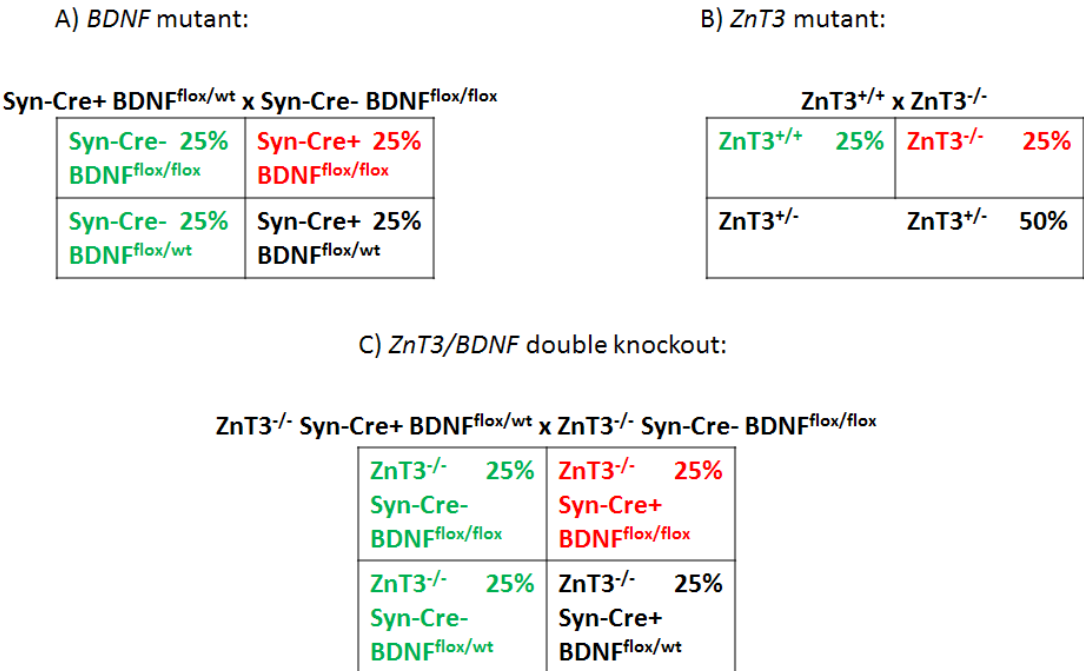


Figure 15: Breeding strategies for generating *BDNF*, *ZnT3*, and *ZnT3/BDNF* mutant and double mutant mice.

Animals were crossed as described in A, B, and C above. Red denotes the genotype of the mutant (A, devoid of BDNF; B, devoid of synaptic zinc) or double mutant (C, devoid of both BDNF and synaptic zinc), whereas green denotes the genotype(s) of the littermate controls. Note that in (A) and (B), the control animals express normal levels of BDNF and synaptic zinc, whereas in (C) the control mice express normal levels of BDNF but are devoid of synaptic zinc. wt = wild type allele, flox = floxed BDNF allele, Syn-Cre+ = Cre recombinase positive, Syn-Cre- = Cre recombinase negative.

animals were always compared to mice that are single knockouts for either *BDNF* or *ZnT3*, referred to in this context as *ZnT3^{+/+} BDNF^{-/-}* (*ZnT3^{+/+}/Syn-Cre⁺/BDNF^{flox/flox}*) or *ZnT3^{-/-} BDNF^{+/+}* (*ZnT3^{-/-}/Syn-Cre⁻/BDNF^{flox/wt}* or *ZnT3^{-/-}/Syn-Cre⁻/BDNF^{flox/flox}*) animals.

All mice used in experiments were 3-6 months of age and genotyped for *ZnT3*, *BDNF* floxed alleles, and Syn-Cre at least twice to confirm their genotypes. Comparisons between *BDNF*^{+/+} vs. *BDNF*^{-/-} and between *ZnT3*^{-/-} *BDNF*^{+/+} vs. *ZnT3*^{-/-} *BDNF*^{-/-} were performed using littermates, as the breeding strategy enabled this. In the case of *ZnT3*^{+/+} vs. *ZnT3*^{-/-} single knockout comparisons, littermate controls were used in some experiments and mice age-matched within 1.5 months of age of one another were used in others; similar results were obtained using both strategies. For *ZnT3*^{+/+} *BDNF*^{-/-} vs. *ZnT3*^{-/-} *BDNF*^{-/-} comparisons, the breeding strategy necessitated that age-matched mice within 1.5 months of age of one another were used.

3.2.2 Preparation of Brain Specimens for Immunohistochemistry

Animals generated as described above were anesthetized with 100 mg/kg pentobarbital (Lundbeck, Deerfield, IL) by intraperitoneal injection and underwent transcardial perfusion through the left ventricle with a solution of ice-cold PBS, pH 7.4, containing 1 U/mL heparin (Sigma, St. Louis, MO) and 2 mM sodium orthovanadate (Sigma), at a rate of 10 ml/min for one minute. This was followed by a seven minute perfusion with ice-cold 4% paraformaldehyde (Sigma) and 2 mM sodium orthovanadate in PBS, pH 7.4. Brains were removed and postfixed overnight at 4°C in the same solution, after which they underwent cryoprotection for 36 hours in a solution of 30% sucrose, 2 mM sodium orthovanadate in PBS at pH 7.4 and 4°C. Brains were verified as being appropriately cryoprotected when they sank in this solution. Brains were then frozen by slow immersion in 2-methylbutane (J.T. Baker, Phillipsburg, NJ) cooled to at

least -20°C with dry ice, and stored at -80°C until cryosectioning. Sections were cut at a thickness of 40 µm, placed in cryoprotection solution, and stored at -80°C until immunostaining.

3.2.3 Immunohistochemistry

Rabbit polyclonal antibody which recognizes phosphorylated tyrosine residue 816 of the TrkB receptor (pY816) was generated using the peptide LQNLAKASPV

pYLDI, corresponding to amino acids 806-819 of mouse TrkB, and was used in all experiments at a 1:2000 dilution following IgG purification using protein-A beads. Importantly, the specificity of this antibody was previously established by demonstrating a significant reduction in immunoreactivity in stratum lucidum of genetically modified mice with a substitution of phenylalanine for tyrosine at the 816 residue (Y816F) of TrkB compared to wild type controls, as shown in Supplementary Figure 1 of (He et al. 2010).

Mouse monoclonal antibodies recognizing synapsin-1 (1:500; Synaptic Systems, Goettingen, Germany) and tau (1:1000; Millipore, Temecula, CA) were employed for colocalization experiments. Mice of the genotypes to be compared in a given experiment were always incubated in parallel using the same solutions and conditions. All incubations took place at 4°C in 5% normal goat serum (Invitrogen, Carlsbad, CA) in PBS, pH 7.4, with 2 mM sodium orthovanadate. Floating sections were permeabilized for one hour in 0.5% Triton-X100 (GE Healthcare, Chalfont St. Giles, UK), and solutions of primary antibodies added for 36 hours. Alexa Fluor 555 goat anti-rabbit (1:1000; Invitrogen) and, for colocalization experiments, Alexa Fluor 488 or 633 goat-anti-mouse

secondary antibodies (1:500; Invitrogen) were then applied for six hours. Adjacent sections not treated with primary antibody were also run in parallel for each animal as negative controls. Sections were wet-mounted on Superfrost Plus slides (Erie Scientific, Portsmouth, NH) and stepped through serial dehydration solutions of two minutes each of 50%, 70%, 85%, 95%, 100%, and 100% ethanol, followed by 20 minutes incubation in xylene (VWR, Radnor, PA) before coverslipping.

3.2.4 Confocal Microscopy and Data Analysis

3.2.4.1 Imaging Parameters

Imaging was performed with a Leica (Nussloch, Germany) DMIRE2 inverted microscope with a 10x (numerical aperture, 0.4) air or 63x (numerical aperture, 1.4) oil immersion objective equipped with a Leica TCS SL confocal system. All images were acquired with the pinhole set to 1.0 Airy units. All images used for quantitative analysis or shown for visual comparison between genotypes were acquired so as to prevent systematic differences in image intensities. To this end, sections from mice which were incubated together within a given staining experiment were imaged using the same laser intensity and detection settings during the same imaging session, allowing relative densitometry measurements to be made between animals of different groups. Because overall staining intensities varied among experiments, confocal settings were adjusted optimally for each experiment so that all image intensities fell within the dynamic range of detection of the device.

Low power (10x objective, total of 100x magnification) images of hippocampus are average projections of *z*-series “stacks” taken through the entire thickness of the hippocampal section. Unless otherwise stated, high power (63x objective, total of 630x magnification) images are average projections of *z*-series taken through a 1 μm depth of hippocampus where pY816 staining was of greatest intensity. Average projections were used because they best reflect representative staining intensities in the *z*-plane for quantification of immunoreactivity. Images depicting colocalizations were confirmed in the *x*, *y*, and *z* dimensions. The focal plane thickness is a significant factor in the *z*-dimension. For the 63x objective used in this study, assuming ideal conditions and 488 nm of light, *z* resolution is stated to be 235 nm (Leica). The resolution in the *x*-*y* plane is stated to be 180 nm (Leica). All image quantification described was performed on raw images which were not adjusted for brightness or contrast. However, brightness and/or contrast were optimized in all images shown within this chapter in order to best convey relevant features. In images of pY816 immunoreactivity used for comparison, brightness and contrast were adjusted equally between images.

3.2.4.2 Quantification of pY816 Immunoreactivity within Stratum Lucidum of Hippocampus

Analysis of imaging data was performed by an investigator blinded to treatment group. The program ImageJ (Abramoff, 2004) was used for data analysis. All quantitative data are presented as mean \pm SEM, analyzed by Student’s t-test.

Quantification of pY816 immunoreactivity within stratum lucidum was performed using images acquired at high power (630x). Hippocampal images including the CA3b regions of stratum lucidum and stratum radiatum were acquired bilaterally, for a total of two images per animal. Quantification focused on specific areas within stratum lucidum that were enhanced in pY816 immunoreactivity and shown to correspond to axon tracts in colocalization experiments (Helgager et al., 2013). Representative regions enriched in pY816 immunoreactivity were outlined as regions of interest (ROIs) until 40,000 pixels in total area were reached or exceeded in a given image, and the average intensity of this area quantified. The average intensity of stratum radiatum of CA3 that was included in the same micrograph was also analyzed, and subtracted from the value obtained from stratum lucidum in order to compensate for variations in background staining. This procedure was performed for both images acquired from each hippocampus in a given animal, and the results averaged to yield one value per mouse. Signal within stratum radiatum was used to normalize for overall staining intensity because signal within stratum radiatum was always substantially lower than stratum lucidum, was found to be of the same average intensity when compared between animals of different genotypes (data not shown), and the CA3 pyramidal cell dendrites which populate this region were found not to contain significant amounts of pY816 immunoreactivity.

Quantification of synaptic pY816 immunoreactivity within stratum lucidum utilized a synapsin-1 antibody, a specific marker of synapses (De Camilli et al., 1983; Fletcher et al., 1991; Moore and Bernstein, 1989), as described above. Z-series were

acquired at 200 nm intervals over a total depth of 1 μ m at 1.7x digital zoom, with three images taken per hippocampus, yielding a total of six images per animal. Individual synapsin-1 puncta were checked for pY816 immunoreactivity in the x , y , and z planes, and scored as being positive if they appeared to contain at least one discrete immunoreactive puncta, even if only in one z -section. This immunoreactivity needed to occupy at least 20% of the area of a bouton. 50 puncta were quantified per image, with a total of 300 synapsin-1 puncta per animal, and the percent of synapsin-1 puncta found to colocalize with pY816 computed.

3.2.5 Preparation of Brain Specimens for Western Blot and ELISA

Mice were anesthetized with 100 mg/kg pentobarbital by intraperitoneal injection and decapitated. Mouse heads were swiftly dipped into liquid nitrogen three times in order to cool the brain during the dissection process, and placed on a cold ice pack. Both hippocampi were dissected and placed into ice cold lysis buffer (137 mM NaCl [Sigma], 20 mM Tris [pH 7.6; Merck, Whitehouse Station, NJ], 1% NP40 [Sigma], 10% glycerol [Merck], 1 mM PMSF [Sigma], 2 mM sodium orthovanadate, and a Complete Mini protease inhibitor tablet [Roche, New Mannheim, Germany]). The hippocampi were then homogenized using a motorized tissue homogenizer and centrifuged at 4°C at 14,000 RPM. The amount of total protein in the supernatant was quantified using a Micro BCATM Protein Assay Kit (Pierce, Rockford, IL). For Western blot, samples were diluted while on ice to a final concentration of 1 mg/mL using lysis buffer and 6x SDS-PAGE sample buffer (350 mM Tris [pH 6.8], 30% glycerol, 1% SDS [Crystalgen, Plainview,

NY], 6% β -mercaptoethanol [Sigma], and 0.2 mg/mL bromophenol blue [Sigma]), the latter mixed into the sample so that it was at 1x concentration. For ELISA, samples were diluted with PBS-V to a final concentration of 5 mg/mL. As acid treatment will increase yield of BDNF (Okragly and Haak-Frendscho, 1997), the pH of the sample was adjusted to <3.0 with 1N HCl for 20 minutes at room temperature, after which it was placed on ice and brought to a pH of approximately 7.0 using 1N NaOH. Samples were then diluted to a concentration of 2.5 mg/mL using the Block & Sample buffer provided with the BDNF E_{max}[®] ImmunoAssay System (Promega, Madison, WI) used to assay BDNF levels (see below).

3.2.6 Western Blot

10 μ g of samples previously prepared for Western blot were loaded onto SDS-PAGE gels containing 8% polyacrylamide (Bio-Rad, Hercules, CA). The gels were electrophoresed at 90 Volts until the loading dye reached the bottom of the gel, and transferred onto nitrocellulose membranes (Whatman, Dassel, Germany) for 1.5 hours at 90 Volts. Membranes were then blocked with 5% bovine serum albumin (Sigma) in Tris buffered saline (TBS) for half an hour. Membranes were incubated with primary antibodies probing for one of the following proteins: TrkB (rabbit polyclonal, 1:2000; Chemicon, Temecula, CA), pY816 of the TrkB receptor (rabbit monoclonal, 1:1000; AbCam, Cambridge, MA), or β -actin (rabbit polyclonal, 1:5000; Sigma). Membranes were washed five times with TBS containing 0.05% Tween-20 (TBS-T; Amresco, Solon, Ohio), following which they were incubated with peroxidase conjugated goat anti-rabbit

IgG secondary antibody (1:5000; The Jackson Laboratory) for one hour. Following five additional washes with TBS-T, membranes were probed using ECL™ Western Blotting Analysis System (GE Healthcare, Pittsburgh, PA), imaged in the dark on Biomax MR film (Kodak, Rochester, NY), and developed.

3.2.7 BDNF ELISA

The BDNF E_{max}® ImmunoAssay System (Promega), a sandwich ELISA assay, was used to measure hippocampal BDNF levels. In brief, a 96-well plate was coated with monoclonal mouse antibody (1:1000) overnight at 4°C, after which it was blocked at room temperature using the Block & Sample Buffer provided. Samples prepared as described above were incubated in triplicate along with serial titrations (7.8-500 pg/mL) of the BDNF standard provided for two hours at room temperature. The wells were then evacuated and washed with TBS-T, and incubated with a chicken polyclonal antibody recognizing BDNF (1:500) for two hours at room temperature. Following evacuation and wash with TBS-T, the wells were incubated with a peroxidase conjugated, anti-IgY secondary antibody (1:200) for one hour at room temperature. The wells were again evacuated and washed with TBS-T, following which the TMB One Solution provided was added and allowed to incubate at room temperature for 10 minutes. Following this incubation, an equal volume of 1N HCl was added to the wells to stop color development, and a SpectraMax 190 Absorbance Microplate Reader (Molecular Devices, Sunnyvale, CA) used to record absorbance of the wells at 450 nm. The average BDNF concentration

(pg/mL) was calculated for each sample based on this absorbance reading, which was then converted to ng of BDNF per gram of total protein (ng/g).

3.3 Results

3.3.1 Decreased Axonal and Synaptic pY816 Immunoreactivity within Stratum Lucidum in BDNF^{-/-} Mice

Initial studies examined the contribution of the canonical TrkB ligand, BDNF, to activation of TrkB within stratum lucidum of hippocampus. To this end, pY816 immunoreactivity was assayed within stratum lucidum in BDNF wild type (BDNF^{+/+}) and knockout (BDNF^{-/-}) mice using confocal microscopy. Analysis concentrated on the cellular and synaptic structures within stratum lucidum known to be enriched in pY816—axons and synapses of mossy fibers (Chapter 2 of this dissertation; Helgager et al. 2013).

Survey of the hippocampus at low power (100x) in wild type animals demonstrated that pY816 immunoreactivity was particularly abundant within stratum lucidum (Fig. 16A), confirming previous results (Helgager et al. 2013). High power (630x) images revealed discrete pY816 immunoreactive patches which colocalized with tau protein (Fig. 16B), a marker of axons, showing that this pY816 immunoreactivity corresponded anatomically to mossy fibers (Binder et al., 1985). Notably, reductions of stratum lucidum immunoreactivity were evident in BDNF^{-/-} compared to BDNF^{+/+} mice at low power (Fig. 17A), a pattern due to decreased axonal pY816 immunoreactivity within mossy fibers of BDNF^{-/-} animals as detected in high magnification images (Fig. 17B). To quantify this reduction, high power images of stratum lucidum were acquired

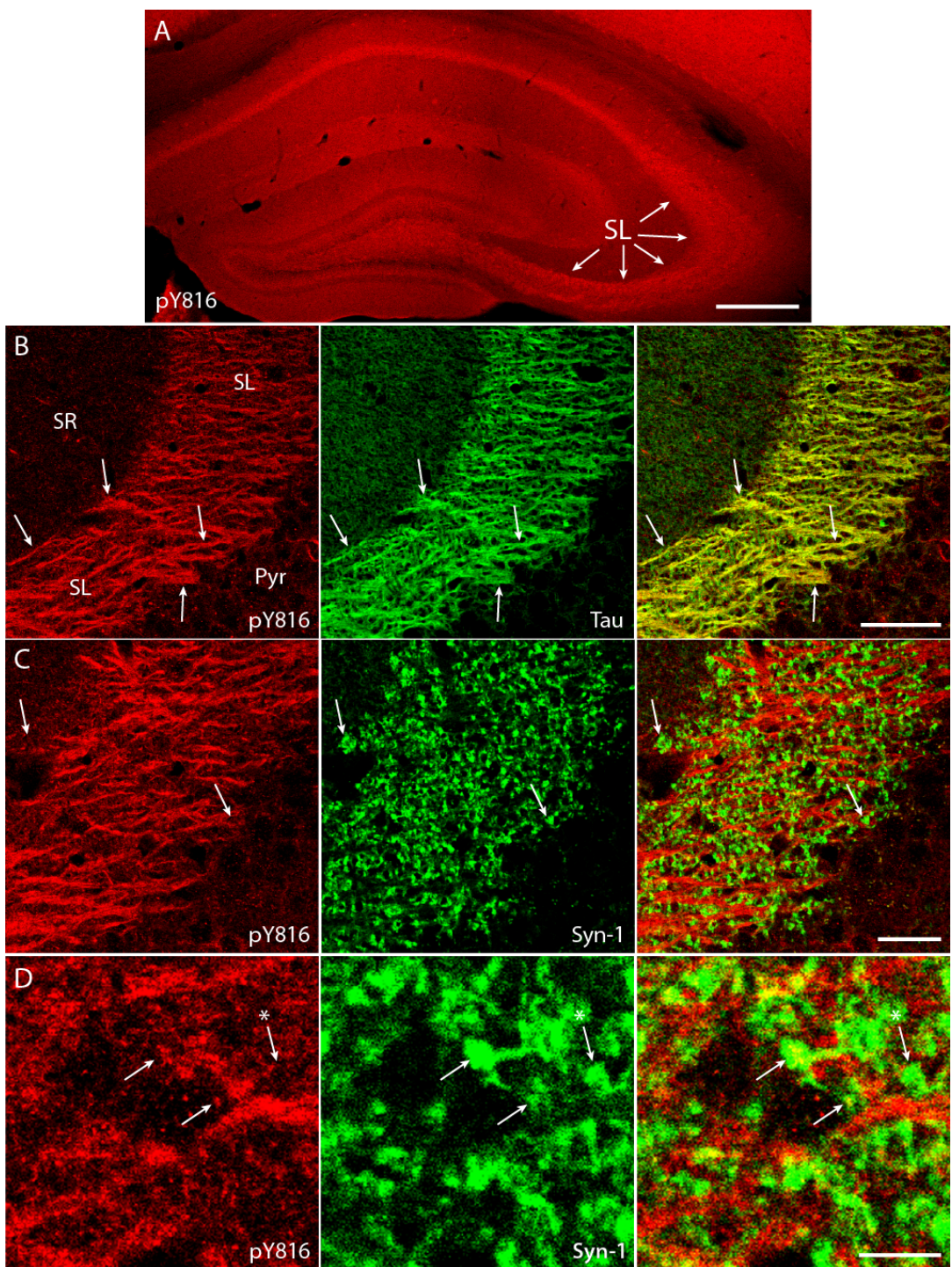


Figure 16: pY816 TrkB immunoreactivity is enriched in mossy fiber axons and synapses within stratum lucidum (SL) of mouse hippocampus.

A) Image of an entire mouse hippocampus in a wild type animal, stained with pY816. The SL region (arrows) appears particularly enriched in pY816 immunoreactivity. Image is a montage of two images taken at low magnification (100x). Scale bar = 300 μ m. **B) High power (630x) images of SL of hippocampus stained for pY816 (red) and tau (green), an axonal marker.** Discrete patches of pY816 immunoreactivity (red; arrows) overlap with tau labeled axons (green; arrows), demonstrating mossy fiber axons of dentate granule cells are particularly enriched in pY816 immunoreactivity. Merged pY816 and tau is shown in the rightmost panel. SR = stratum radiatum of CA3, Pyr = CA3 pyramidal cell layer. Scale bar = 50 μ m. **C) Confocal micrographs showing SL stained with pY816 (red) and synapsin-1 (green), a marker of synapses.** The majority of synapsin-1 puncta (green; arrows) do not appear to contain substantial pY816 (red; arrows). Merged pY816 and synapsin-1 are shown in the rightmost panel. Scale bar = 30 μ m. **D) Digitally zoomed images consisting of one z-section from images in panel (C) demonstrate synapsin-1 puncta (green; arrows) that contain pY816 immunoreactivity (red; arrows).** A nearby synapsin-1 puncta (green; arrow with asterisk) does not contain pY816 immunoreactivity (red; arrow with asterisk), the situation for the majority of synapsin-1 puncta assessed. Merged pY816 and synapsin-1 is shown in the rightmost panel. Scale bar = 7 μ m.

from both hippocampi in BDNF^{+/+} (n=14) and BDNF^{-/-} (n=10) animals, and axons measured for the intensity of their immunoreactivity. This axonal quantification of pY816 immunoreactivity revealed an approximately 30% reduction in BDNF^{-/-} compared to BDNF^{+/+} animals which was statistically significant (Fig. 17C; p<0.05, Student's t-test). In order to examine synaptic immunoreactivity, an antibody labeling the synaptic marker synapsin-1 was employed and assessed for colocalization with pY816 (De Camilli et al., 1983; Fletcher et al., 1991; Moore and Bernstein, 1989). As expected, in wild type animals a minority of synapsin-1 puncta contained pY816 immunoreactivity, also punctate in nature (Fig. 16C, D). In order to quantify synaptic immunoreactivity in BDNF^{+/+} (n=9) and BDNF^{-/-} (n=6) mice, synapsin-1 puncta were identified in z-section stacks and scored for pY816 immunoreactivity by a blinded investigator. Such a

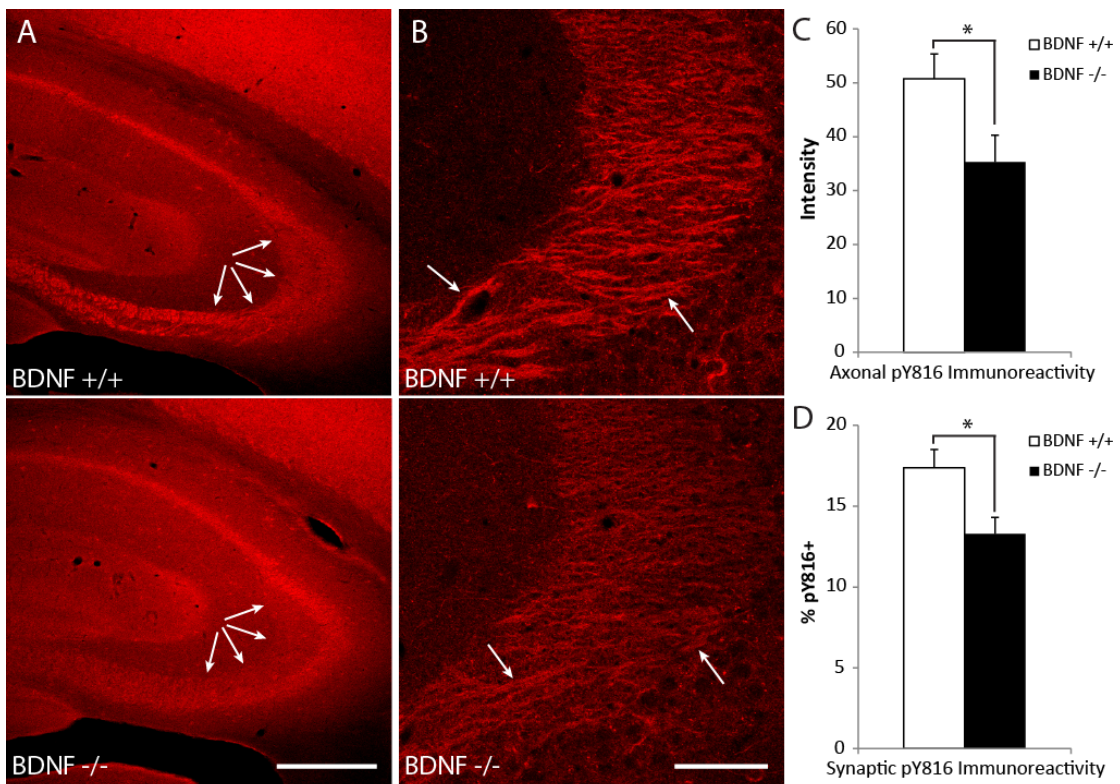


Figure 17: pY816 TrkB immunoreactivity in mossy fiber axons and synapses within SL is decreased in BDNF^{-/-} compared to BDNF^{+/+} mice.

A) Representative low power micrographs taken of hippocampi from BDNF^{+/+} (top) and BDNF^{-/-} (bottom) mice stained with pY816, revealing that immunoreactivity within SL of the BDNF^{-/-} animal (arrows, bottom) is reduced compared to its BDNF^{+/+} littermate (arrows, top). Scale bar = 300 μ m. **B)** Images of SL taken at high power from pY816 stained sections from the same BDNF^{+/+} (top) and BDNF^{-/-} (bottom) mice as in (A) demonstrates that this observed reduction is due to decreased pY816 immunoreactivity within mossy fiber axons of the BDNF^{-/-} mouse (arrows point to pY816 enriched regions shown in Fig. 16 to correspond anatomically to mossy fiber axons; compare top and bottom images). Scale bar = 50 μ m. **C)** Quantification of axonal pY816 immunoreactivity in BDNF^{+/+} ($n=14$) and BDNF^{-/-} ($n=10$) mice demonstrates a significant decrease in immunoreactivity in the BDNF^{-/-} animal compared to BDNF^{+/+} ($p<0.05$, Student's t-test). Quantification is presented as mean pY816 axonal immunoreactivity \pm SEM. **D)** Quantification of percentages of synapsin-1 puncta within SL found to contain pY816 immunoreactivity in BDNF^{+/+} ($n=9$) and BDNF^{-/-} ($n=6$) mice. A 30.8% reduction in synaptic pY816 immunoreactivity was found in BDNF^{-/-} mice compared to their BDNF^{+/+} littermates ($p<0.05$, Student's t-test). A total of 2700 synapsin-1 puncta

were analyzed in BDNF^{+/+} mice, and 1800 in BDNF^{-/-} animals. Quantification is presented as mean % ± SEM. All data were analyzed by Student's t-test; *p<0.05.

structure was scored as pY816+ if it contained a discrete pY816 puncta that filled at least 20% of its area in at least one z-section, and at least 300 synapsin-1 puncta were examined in each animal in order to compute a percentage of synapsin-1 puncta that contained pY816 immunoreactivity for each mouse (4500 synapsin-1 puncta total). In BDNF^{+/+} animals, an average of 17.4 ± 1.1% of synapsin-1 puncta were found to contain pY816 immunoreactivity, whereas only 13.3 ± 1.0% contained pY816 in the BDNF^{-/-} mouse, a statistically significant reduction (Fig. 17D; mean ± SEM, p<0.05 by Student's t-test). The reductions of pY816 immunoreactivity within both axons and boutons of mossy fibers support the conclusion that BDNF contributes to TrkB activation under these conditions.

3.3.2 Enhanced Axonal and Unchanged Synaptic pY816 TrkB Immunoreactivity within Stratum Lucidum of ZnT3^{-/-} Mice

To assess the contribution of vesicular zinc to activation of TrkB within stratum lucidum of hippocampus, pY816 immunoreactivity was examined in hippocampal sections from mice in which the transporter required for concentrating zinc within synaptic vesicles (ZnT3) had been eliminated. Timm's staining labeling vesicular zinc in mossy fibers was abolished in these animals, demonstrating that knocking out ZnT3 eliminated vesicular zinc (Cole et al., 1999). Experimental evidence that zinc can transactivate TrkB (Huang et al., 2008) led us to hypothesize that pY816 immunoreactivity would be reduced in mossy fiber boutons and axons, as observed in

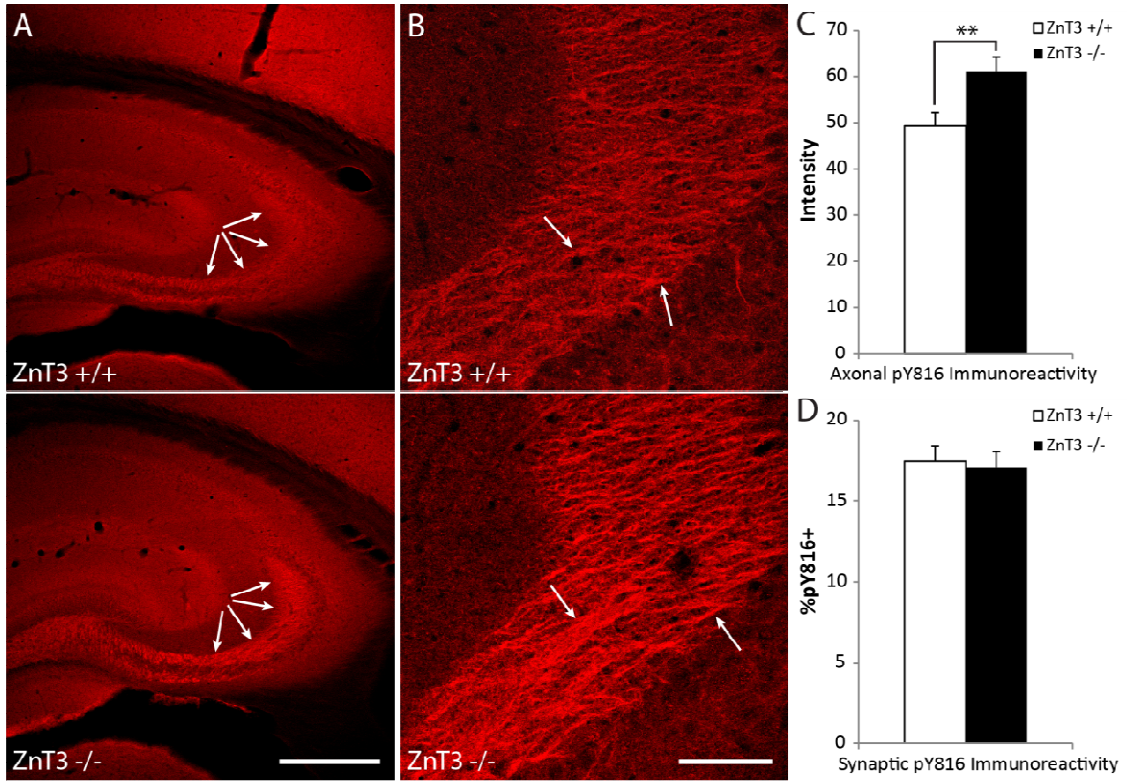


Figure 18: Axonal pY816 TrkB immunoreactivity increases in axons but remains unchanged at synapses within SL in $ZnT3^{-/-}$ compared to $ZnT3^{+/+}$ mice.

A) Representative low power images of hippocampi stained with pY816, taken from $ZnT3^{+/+}$ (top) and $ZnT3^{-/-}$ (bottom) mice showing increased immunoreactivity within SL in the $ZnT3^{-/-}$ mouse (arrows, bottom) compared to its $ZnT3^{+/+}$ littermate (arrows, top). Scale bar = 300 μ m. **B)** High power micrographs of SL taken from pY816 stained sections from the same $ZnT3^{+/+}$ (top) and $ZnT3^{-/-}$ (bottom) animals as in (A), demonstrating that the increased intensity within SL is due to enriched pY816 immunoreactivity within mossy fiber axons (arrows point to pY816 enriched regions shown in Fig. 16 to correspond anatomically to mossy fiber axons; compare top and bottom images). Scale bar = 50 μ m. **C)** Quantification of axonal pY816 immunoreactivity in $ZnT3^{+/+}$ (n=19) and $ZnT3^{-/-}$ (n=19) mice demonstrating an increase in the $ZnT3^{-/-}$ mouse compared to $ZnT3^{+/+}$ ($p < 0.01$, Student's t-test). Quantification is presented as mean pY816 axonal immunoreactivity \pm SEM. **D)** Percentages of synapsin-1 puncta within SL found to be pY816+ in $ZnT3^{+/+}$ (n=19) and $ZnT3^{-/-}$ (n=19) animals. No significant differences in synaptic pY816 immunoreactivity was found in $ZnT3^{-/-}$ compared to $ZnT3^{+/+}$ mice ($p = 0.77$, Student's t-test). A total of 5760 synapsin-1 puncta were analyzed in

ZnT3^{+/+} animals, and 5758 in ZnT3^{-/-} mice. Quantification is presented as mean % ± SEM. All data were analyzed by Student's t-test; **p<0.01.

BDNF^{-/-} mice. Synaptic immunoreactivity was assayed in the same fashion as was performed in the BDNF knockout animals above, with over 11,500 synapsin-1 puncta examined in ZnT3^{+/+} (n=19) and ZnT3^{-/-} (n=19) animals. Contrary to our hypothesis, no significant differences in the percentages of pY816+ synapses were detected between the two genotypes (Fig. 18D; ZnT3^{+/+} = 17.5 ± 0.9%, ZnT3^{-/-} = 17.1 ± 0.9%, mean % ± SEM, p=0.77 by Student's t-test). Unexpectedly, low power inspection of stratum lucidum from ZnT3^{-/-} mice revealed *increased* pY816 immunoreactivity within this region compared to the ZnT3^{+/+} animal (Fig. 18A). High power micrographs demonstrated that, as in the wild type animal, pY816 immunoreactivity in the ZnT3 mutant colocalized with tau and was therefore located within axons of mossy fibers (data not shown).

Quantification of axonal immunoreactivity in ZnT3^{+/+} (n=19) and ZnT3^{-/-} (n=19) animals confirmed this observation, demonstrating that pY816 immunoreactivity was increased by approximately 24% in the ZnT3 knockout mouse compared to wild type (Fig. 18B, C; p<0.01 by Student's t-test). Finding an increase, rather than the hypothesized reduction, of axonal pY816 immunoreactivity raised the possibility of a homeostatic response to the absence of vesicular zinc, perhaps involving either BDNF and/or TrkB expression.

3.3.3 Total TrkB Levels Are Unchanged in the Hippocampi of ZnT3^{-/-} Mice

The increases observed in pY816 immunoreactivity within mossy fiber axons in the *ZnT3* knockout animal could be due to increased numbers of TrkB molecules in ZnT3^{-/-} compared to ZnT3^{+/+} controls, a similar proportion of which are phosphorylated. Such a finding would reflect one potential compensatory response that could be responsible for increased pY816 in the absence of vesicular zinc. Alternatively, the numbers of TrkB molecules could be equivalent in ZnT3^{-/-} compared to ZnT3^{+/+} controls, but a greater proportion could be phosphorylated in the mutant compared to wild type. To begin to assess these possibilities, Western blots were performed on whole hippocampal lysates from ZnT3^{+/+} and ZnT3^{-/-} animals, probing for TrkB receptor (Fig. 19A). Quantification of wild type (n=13) and knockout (n=11) animals revealed no overt differences in TrkB receptor levels between these two genotypes (Fig. 19B; p=0.64 by Student's t-test).

3.3.4 BDNF Levels Increase within Hippocampi of ZnT3^{-/-} Mice

The unexpected increase of axonal pY816 immunoreactivity together with the lack of change in TrkB protein levels raised the possibility of a homeostatic increase in expression of the canonical TrkB ligand, BDNF, in the *ZnT3* mutant mouse. To examine this possibility, BDNF content was measured in hippocampal lysates isolated from ZnT3^{+/+} (n=10) and ZnT3^{-/-} (n=8) animals using an ELISA. This revealed a 51% increase in BDNF content (ZnT3^{+/+} = 81.1 ± 9.1 pg/g, ZnT3^{-/-} = 123.0 ± 10.0 pg/g, mean pg

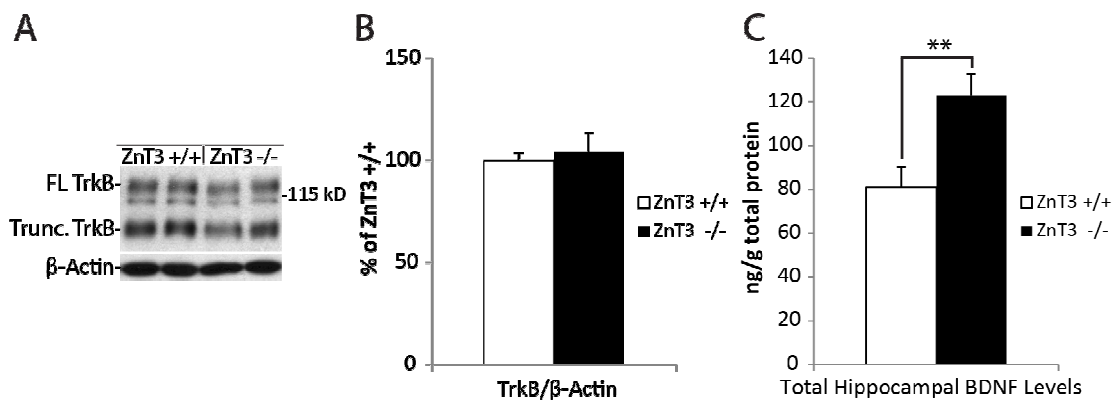


Figure 19: Total TrkB and BDNF levels in whole hippocampal homogenates comparing ZnT3^{-/-} and ZnT3^{+/+} animals.

A) Representative Western blot demonstrating TrkB levels in ZnT3^{+/+} and ZnT3^{-/-} mice assayed in whole hippocampal lysates. FL TrkB = full length TrkB. Trunc. TrkB = truncated TrkB. **B)** Quantification of full-length TrkB levels demonstrates no significant difference between wild type (n=13) and knockout (n=11) animals. Data are represented as mean percent of average TrkB levels found in the ZnT3^{+/+} animal ± SEM, and was normalized to β-actin as a loading control. **C)** Total BDNF levels in whole hippocampal lysates assayed by ELISA demonstrates an approximately 52% increase in the ZnT3^{-/-} (n=10) compared to the ZnT3^{+/+} (n=8) mouse. Data are represented as ng BDNF levels per gram of total protein ± SEM. All data were analyzed by Student's t-test; **p<0.01.

BDNF/g total protein ± SEM, p<0.01 by Student's t-test) in ZnT3^{-/-} compared to ZnT3^{+/+} mice (Fig. 19C). It seems plausible that this homeostatic increase of BDNF content contributes to the similar levels of synaptic pY816 and increased levels of axonal pY816 in ZnT3 mutant compared to wild type mice.

3.3.5 Axonal and Synaptic pY816 TrkB Immunoreactivity within Stratum Lucidum Is Reduced in ZnT3^{-/-} BDNF^{-/-} Compared to ZnT3^{-/-} BDNF^{+/+} Mice

The increased BDNF content in *ZnT3* mutant mice led us to hypothesize that this homeostatic response is required for the increased mossy fiber axonal pY816 detected in these animals. To test this hypothesis, the effects of eliminating BDNF from *ZnT3* mutant mice on pY816 immunoreactivity were examined by breeding *BDNF* mutant mice on to a *ZnT3* null mutant background (see Materials and Methods). Importantly, *ZnT3* and *BDNF* double mutant animals (*ZnT3*^{-/-} *BDNF*^{-/-}) were behaviorally indistinguishable from wild type mice by casual observation, were born in normal Mendelian ratios, and did not show any differences in weight compared to their *ZnT3*^{-/-} single knockout littermates (data not shown).

Consistent with our hypothesis, elimination of BDNF protein reduced pY816 immunoreactivity in mossy fiber axons in *ZnT3*^{-/-} *BDNF*^{-/-} compared to *ZnT3*^{-/-} *BDNF*^{+/+} littermate controls (Fig. 20A, B). Quantification of axonal immunoreactivity revealed a significant 36% reduction in *ZnT3*^{-/-} *BDNF*^{-/-} (n=10) compared to *ZnT3*^{-/-} *BDNF*^{+/+} (n=11) littermate controls (Fig. 20C; p<0.001 by Student's t-test). Similar results were evident with measures of pY816 immunoreactivity in mossy fiber boutons. That is, quantification of over 4800 synapsin-1 puncta revealed significant reductions of pY816 positive synapsin puncta in *ZnT3*^{-/-} *BDNF*^{-/-} (n=8) animals compared to *ZnT3*^{-/-} *BDNF*^{+/+} (n=8) control mice (Fig. 20D; *ZnT3*^{-/-} *BDNF*^{+/+} = 17.5 ± 1.4%, *ZnT3*^{-/-} *BDNF*^{-/-} = 11.8 ± 1.6%, mean % ± SEM, p<0.05 by Student's t-test). In sum, these findings support the

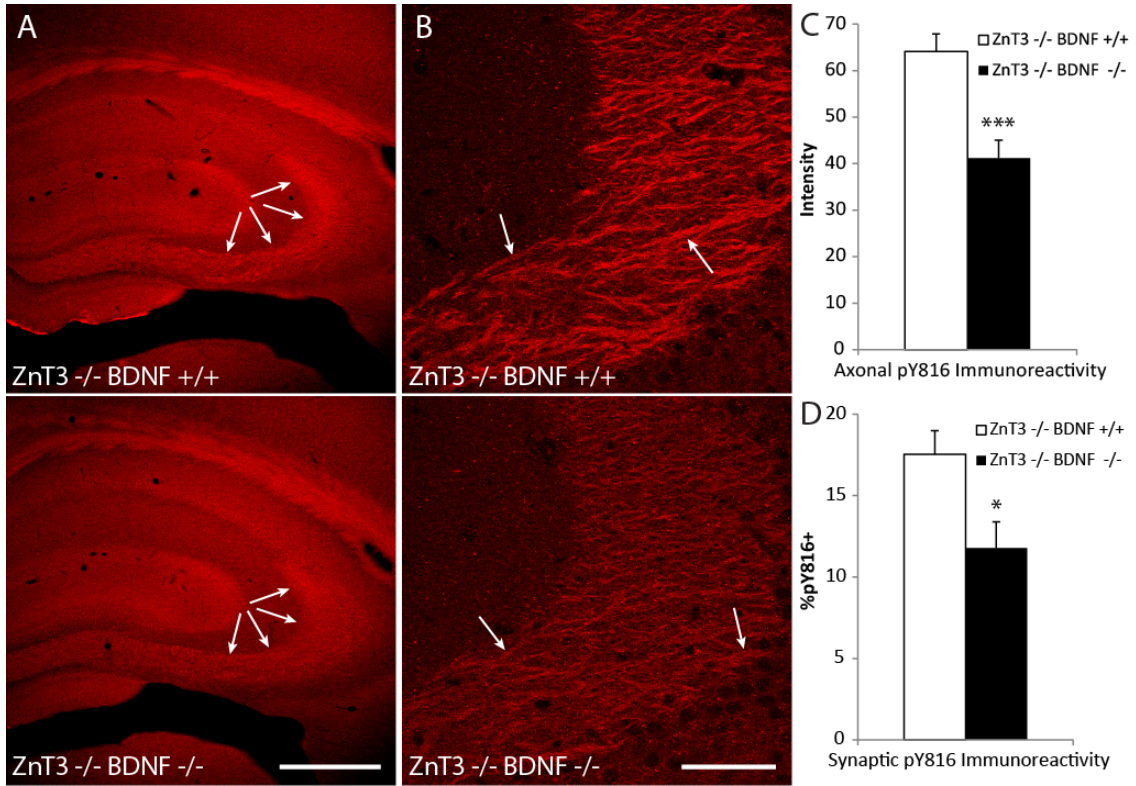


Figure 20: pY816 TrkB immunoreactivity in mossy fiber axons and synapses within SL is decreased in ZnT3^{-/-} BDNF^{-/-} double knockouts compared to ZnT3^{-/-} BDNF^{+/+} single knockout mice.

A) Representative low power micrographs of hippocampal sections from ZnT3^{-/-} BDNF^{+/+} (top) and ZnT3^{-/-} BDNF^{-/-} (bottom) mice stained with pY816, demonstrating that immunoreactivity within SL of the ZnT3^{-/-} BDNF^{-/-} mouse (arrows, bottom) is diminished compared to its ZnT3^{-/-} BDNF^{+/+} littermate (arrows, top). Scale bar = 300 μ m. **B)** Images of SL taken at high power from hippocampal sections stained with pY816 from the same ZnT3^{-/-} BDNF^{+/+} (top) and ZnT3^{-/-} BDNF^{-/-} (bottom) mice as in (A) demonstrates that this observed reduction is due to decreased pY816 immunoreactivity within mossy fiber axons of the ZnT3^{-/-} BDNF^{-/-} double knockout (arrows point to pY816 enriched regions shown in Fig. 16 to correspond anatomically to mossy fiber axons; compare top and bottom images). Scale bar = 50 μ m. **C)** Quantification of axonal pY816 immunoreactivity shows a significant decrease in immunoreactivity in ZnT3^{-/-} BDNF^{-/-} ($n=11$) compared to ZnT3^{-/-} BDNF^{+/+} ($n=10$) mice ($p<0.001$, Student's t-test). Quantification is presented as mean pY816 axonal immunoreactivity \pm SEM. **D)** Quantification of percentages of synapsin-1 puncta within SL found to contain pY816 immunoreactivity in ZnT3^{-/-} BDNF^{+/+} ($n=8$) and ZnT3^{-/-} BDNF^{-/-} ($n=8$) mice demonstrates a 32.6% reduction in

synaptic pY816 immunoreactivity in the double knockout ($p<0.05$, Student's t-test). A total of 2400 synapsin-1 puncta were analyzed in $ZnT3^{-/-}$ $BDNF^{+/+}$ animals and 2401 in $ZnT3^{-/-}$ $BDNF^{-/-}$ mice. Quantification is presented as mean % \pm SEM. All data were analyzed by Student's t-test; * $p<0.001$, * $p<0.05$.**

hypothesis that BDNF contributed to both synaptic and axonal pY816 content in the $ZnT3$ null mutant mice.

3.3.6 Axonal and Synaptic pY816 TrkB Immunoreactivity in Stratum Lucidum Is Not Further Reduced in $ZnT3^{-/-}$ $BDNF^{-/-}$ Compared to $ZnT3^{+/+}$ $BDNF^{-/-}$ Mice

If the homeostatic increase of BDNF is responsible for the increased pY816 immunoreactivity in the $ZnT3$ mutant mice, then eliminating $ZnT3$ from mice mutant for BDNF would not be expected to increase pY816 immunoreactivity. To test this idea, we compared pY816 immunoreactivity within mossy fiber axons and boutons of *BDNF* mutant mice in those wild type ($ZnT3^{+/+}$ $BDNF^{-/-}$ single knockout) and null ($ZnT3^{-/-}$ $BDNF^{-/-}$ double knockout) for $ZnT3$. As predicted, no significant increases of pY816 immunoreactivity within mossy fiber axons were detected in the double compared to single knockout animals (Fig. 21A, B, C; $p=0.25$ by Student's t-test). Likewise, no significant change in the percent of pY816 immunoreactive synapses was detected in the double knockout ($n=8$) compared to *BDNF* single knockout ($n=6$) mice (Fig. 21D; $ZnT3^{+/+}$ $BDNF^{-/-} = 13.3 \pm 1.0\%$, $ZnT3^{-/-}$ $BDNF^{-/-} = 11.8 \pm 1.6\%$, mean % \pm SEM, $p=0.49$ by Student's t-test). In sum, these findings support the idea that BDNF contributes to both synaptic and axonal pY816 immunoreactivity detected in the $ZnT3$ mutant mice.

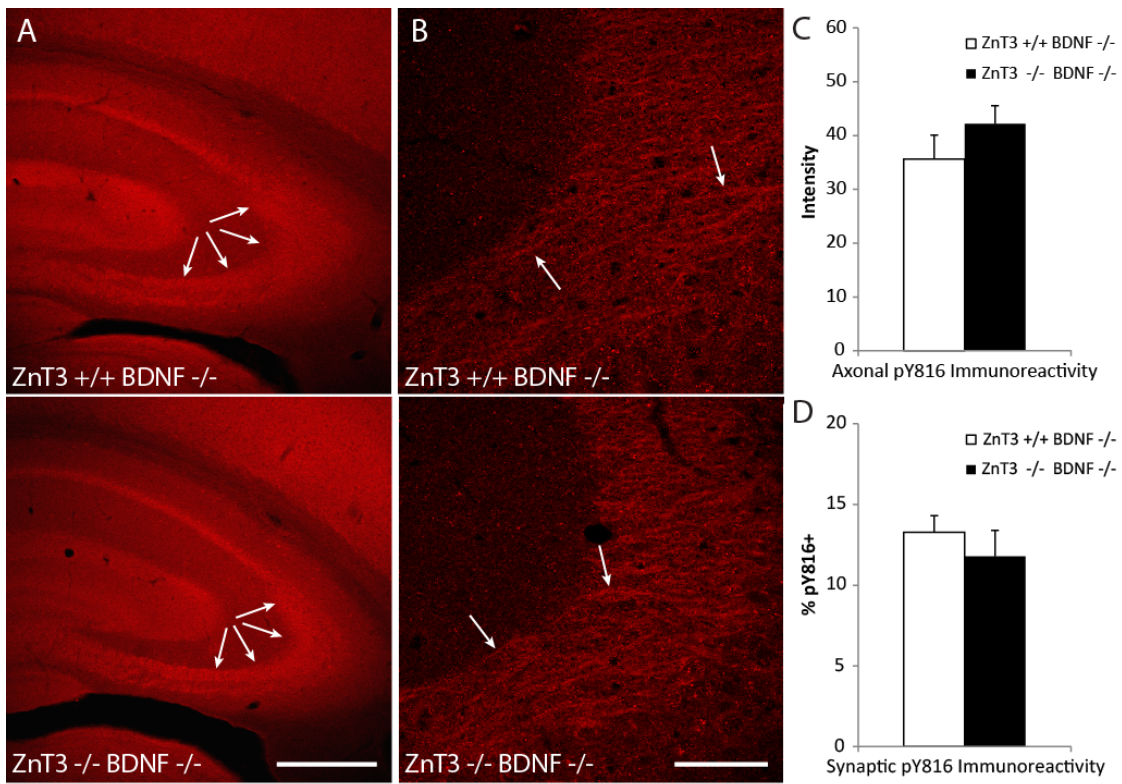


Figure 21: Axonal and synaptic pY816 TrkB immunoreactivity is not further reduced within SL in ZnT3^{-/-} BDNF^{-/-} double knockouts compared to ZnT3^{+/+} BDNF^{-/-} single knockout mice.

A) Representative low power images of hippocampi stained with pY816, taken from ZnT3^{+/+} BDNF^{-/-} (top) and ZnT3^{-/-} BDNF^{-/-} (bottom) mice. Immunoreactivity does not appear further changed in the double knockout (arrows, bottom) compared to the ZnT3^{+/+} BDNF^{-/-} animal (arrows, top). Scale bar = 300 μ m.

B) High power micrographs of SL taken from pY816 stained sections from the same ZnT3^{+/+} BDNF^{-/-} (top) and ZnT3^{-/-} BDNF^{-/-} (bottom) animals as in (A), demonstrating that pY816 immunoreactivity within mossy fiber axons (arrows point to pY816 enriched regions shown in Fig. 16 to correspond anatomically to mossy fiber axons; compare top and bottom images), already weak in the absence of BDNF, is not further changed in the absence of both ZnT3 and BDNF. Scale bar = 50 μ m.

C) Quantification of axonal pY816 immunoreactivity in ZnT3^{+/+} BDNF^{-/-} (n=12) and ZnT3^{-/-} BDNF^{-/-} (n=12) mice reveals no change in the double compared to single knockout ($p=0.25$, Student's t-test). Quantification is presented as mean pY816 axonal immunoreactivity \pm SEM. **D)** Percentages of synapsin-1 puncta within SL found to be pY816+ in ZnT3^{+/+} BDNF^{-/-} (n=6) and ZnT3^{-/-} BDNF^{-/-} (n=8) mice. No

significant difference in synaptic pY816 immunoreactivity was found between the two genotypes ($p=0.48$, Student's t-test). A total of 1800 synapsin-1 puncta were analyzed in $ZnT3^{+/+}$ $BDNF^{-/-}$ mice, and 2401 in $ZnT3^{-/-}$ $BDNF^{-/-}$ animals. Quantification is presented as mean % \pm SEM. All data were analyzed by Student's t-test.

3.4 Discussion

This study tested the hypothesis that synaptic vesicular zinc transactivates TrkB within the axons and presynaptic boutons of hippocampal dentate granule cells of adult mice. We conducted immunohistochemical experiments with high resolution confocal microscopy using an antibody that probes for pY816 of TrkB in sections isolated from genetically modified mice devoid of BDNF and/or synaptic zinc within mossy fiber axons. Four principal findings emerged: (1) pY816 immunoreactivity is reduced in both axons and synaptic boutons of mossy fibers in mice lacking BDNF. (2) Unexpectedly, axonal pY816 immunoreactivity is increased in mice deficient in synaptic vesicular zinc in dentate granule cells, whereas immunoreactivity within presynaptic boutons is unchanged. (3) Marked increases of BDNF content were evident within the hippocampus in mice devoid of synaptic vesicular zinc. (4) In mice null for BDNF, elimination of synaptic vesicular zinc failed to produce significant increases of pY816 in either axons or synaptic boutons. These findings support the conclusion that both BDNF and synaptic vesicular zinc regulate TrkB activation within mossy fiber axons and boutons of adult mice.

The reduction of pY816 immunoreactivity within axons and boutons of mossy fibers in BDNF mutants implicates BDNF in activation of TrkB under physiological

conditions in adult mice. Using antibodies to phosphorylated TrkB as surrogate measures of TrkB activation (Segal et al., 1996), Western blot analyses have revealed altered TrkB activation in adult rodent brains following exposure to cocaine (Crooks et al., 2010) and treatment with antidepressant drugs (Saarelainen et al., 2003). Immunohistochemical studies have confirmed and extended these biochemical results, revealing regulation of TrkB activation with distinct stages of estrous cycle (Spencer-Segal et al., 2011), and with learning paradigms (Chen et al., 2010a; Chen et al., 2010b). While the favored molecular mechanism mediating TrkB activation in these diverse studies has been its canonical ligand, BDNF, few studies have directly tested this idea. The present evidence implicating endogenous BDNF in TrkB activation under physiological conditions in the adult brain is consistent with behavioral observations of impaired learning and memory (Heldt et al., 2007; Linnarsson et al., 1997; Mizuno et al., 2000; Monteggia et al., 2004), as well as impaired synaptic plasticity caused by genetic or pharmacological perturbations of BDNF (Figurov et al., 1996; Korte et al., 1995; Korte et al., 1996; Patterson et al., 1996; Zakharenko et al., 2003). In contrast to the present results, our earlier studies found no reduction of pTrkB immunoreactivity under physiological conditions in adult mice; this discrepancy is likely due to the insensitivity of the pTrkB antibody in the earlier study which precluded resolution at a cellular or subcellular level and assessed immunoreactivity within stratum lucidum averaging cellular and extracellular locales. Assessing pTrkB immunoreactivity specifically within axons in the

present study was critical to establishing significant differences between wild type and *BDNF* knockout mice under physiological conditions (data not shown).

The present findings are consistent with a model in which endogenous BDNF is released from mossy fiber boutons under physiological conditions, binds to the ectodomain of TrkB in the synaptic membrane of the same or nearby terminals, and is subsequently endocytosed. We favor the mossy fiber axons as the cellular source because of the predominant immunohistochemical evidence of high levels of BDNF protein in giant boutons of the mossy fibers (Danzer and McNamara, 2004; Yan et al., 1997), and within these boutons to dense core vesicles in particular (Dieni et al., 2012). By contrast, immunohistochemical studies failed to detect BDNF protein in dendrites of CA3 pyramidal cells (Danzer and McNamara, 2004; Dieni et al., 2012; Yan et al., 1997). It should be noted, however, that a small fraction of dendritic spines of CA3 pyramidal cells within stratum lucidum were found to be immunoreactive for BDNF (Danzer and McNamara, 2004), a localization consistent with putative dendritic translation of BDNF (Baj et al., 2011; Chiaruttini et al., 2009; Tongiorgi et al., 2004). The idea that pTrkB immunoreactivity detected within boutons in this study may be localized to small organelles is consistent with its undergoing endocytosis following its activation at the membrane of the presynaptic terminal. The established model of retrograde transport of NGF-activated TrkA based upon studies of the peripheral nervous system suggests that the pTrkB within mossy fiber axons may be en route from the presynaptic terminals to the granule cell bodies (Bhattacharyya et al., 1997; Niewiadomska et al., 2011; Watson et

al., 1999a). Alternatively, the pTrkB in mossy fiber axons may reflect locally processed TrkB following its activation; the absence of detectable pY816 immunoreactivity in granule cell bodies favors this latter possibility (data not shown). Electrophysiological studies reveal that one biological consequence of BDNF-mediated TrkB activation locally within mossy fiber boutons may be a form of LTP of the mossy fiber-CA3 synapse that is presynaptic in both its induction and expression (Huang et al., 2008; Pan et al., 2011).

The hypothesis that synaptic vesicular zinc contributed to TrkB activation under physiologic conditions in adult mice predicted reductions of synaptic and axonal pTrkB in *ZnT3* knockouts similar to that observed in the *BDNF* knockouts. The absence of a reduction of synaptic pTrkB and the paradoxical increase of axonal pTrkB in the *ZnT3* knockouts suggested the presence of a homeostatic response to the absence of vesicular zinc, leading to discovery of increased BDNF content in the *ZnT3* null mutants. Importantly, reducing BDNF expression in the *ZnT3* null mutants in turn reduced both synaptic and axonal pTrkB, implying that BDNF contributes to residual TrkB activation in the absence of vesicular zinc. The homeostatic increase of BDNF and axonal pTrkB in the *ZnT3* null mutants implicates vesicular zinc in regulation of BDNF and TrkB signaling under physiological conditions in adult mice. One potential trigger of the homeostatic increase of BDNF expression is a reduction of transactivation of TrkB by vesicular zinc under physiological conditions. Whether vesicular zinc contributes to the seizure-induced increases of TrkB activation detected in the same BDNF knockout mice

(He et al., 2004) used in this study, however, remains unclear. Finally, whether disrupted BDNF content and TrkB signaling contributes to the defective hippocampal-dependent memory observed in the ZnT3 null mutant mice is presently uncertain (Adlard et al., 2010; Martel et al., 2011; Sindreu et al., 2011).

In summary, the present study demonstrates that BDNF and synaptic zinc are both important for TrkB activation within stratum lucidum of hippocampus under physiological conditions. BDNF was directly implicated in TrkB activation within both mossy fiber axons and boutons. Though the present study failed to provide direct evidence that synaptic zinc transactivates TrkB at these same locales, the presence of a compensatory increase in BDNF in the absence of vesicular zinc and consequential enhanced TrkB activation within mossy fiber axons shows that this ligand is important for regulating BDNF/TrkB signaling. The precise mechanisms by which the absence of vesicular zinc leads to increased BDNF levels, as well as the contribution of vesicular zinc to transactivation of TrkB under epileptic conditions, may be topics of future study.

4. Concluding Remarks and Future Directions

The objectives of this dissertation were (1) to study the cellular and synaptic locales within hippocampus at which TrkB is activated in hippocampus during epileptogenesis, and (2) to test the relative contributions of BDNF and synaptic vesicular zinc to activation of this receptor within this structure. Understanding the cellular and subcellular locations whereby TrkB signaling occurs during epileptogenesis, given the pinnacle role of this receptor in the development of epilepsy and neuronal excitability, will elucidate specific locales where processes contributing to the pathogenesis of this disease likely occur. Defining such locales will greatly simplify future studies of epileptogenesis as such lines of inquiry can specifically focus on these critical locations in examining potential epileptogenic processes. Furthermore, understanding the specific ligands involved in activating TrkB at these cellular locales may help to elucidate molecules that contribute to neuronal excitability through this receptor. Such molecules can also be the topics of future lines of study into epilepsy, as well as targets of potential therapies.

The first part of this dissertation revealed that TrkB activation was enhanced in a model of epileptogenesis within two important cell populations of hippocampus—dentate granule cells and CA1 pyramidal neurons. Within these cell populations, TrkB was activated within mossy fiber boutons and axons of dentate granule cells which populate stratum lucidum, whereas within CA1 pyramidal neurons it was localized to the spines and shafts of proximal apical dendrites within CA1 stratum radiatum. Both the mf-CA3

and CA3-CA1 synapses have been extensively studied in terms of their ability to undergo LTP (Minichiello, 2009; Nicoll and Schmitz, 2005), synaptic plasticity at these locales has been hypothesized to contribute to learning and memory formation, and it seems likely that their contribution to neuronal excitability within the limbic system also promotes the process of epileptogenesis. Mossy fiber axons and boutons form the presynaptic innervation of the mf-CA3 synapse, whereas spines and dendrites of CA1 pyramidal neurons comprise the postsynaptic component of the CA3-CA1 synapse. Interestingly, TrkB has been implicated in LTP at both of these synapses (Huang et al., 2008; Minichiello et al., 1999), making it likely that TrkB signaling from both of these locales may contribute to the development of neural excitability, likely facilitating the process of epileptogenesis. The second part of this dissertation found that BDNF plays an important role in activation of TrkB within mossy fiber boutons and axons within stratum lucidum of hippocampus. Furthermore, the presence of an increase in BDNF protein and concomitant increased activation of TrkB within mossy fiber axons found in the *ZnT3* mutant animal suggests that synaptic zinc also has a role in regulating TrkB signaling through a mechanism dependent on BDNF.

4.1 Examples of How the Findings of This Dissertation May Guide Epilepsy Research

How might understanding the cellular and synaptic locales of TrkB activation within hippocampus guide future research into epilepsy? The findings of this dissertation demonstrate activated TrkB to be prominent within mossy fibers of dentate granule cells,

an interesting observation given that LTP is induced and expressed at a presynaptic locale at the mf-CA3 synapse (Nicoll and Schmitz, 2005; Pan et al., 2011). Such findings implicate the plasticity of dentate granule cells as likely being integral to the process of epileptogenesis. Such findings would inform future lines of study by suggesting that they specifically examine processes intrinsic to dentate granule cells that could contribute to the development of epilepsy. For example, one may want to test the role of TrkB signaling within dentate granule cells in epileptogenesis by generating a conditional knockout mouse deficient in this receptor only within this cell population, and examining its ability to develop epilepsy. One may also hypothesize that LTP, expressed through increased glutamate release from the mossy fiber itself, is necessary for the process of epileptogenesis. In this case, do mice with genetic or pharmacologic perturbations preventing enhanced glutamate release from the mf-CA3 synapse, impairing LTP, also show impairments in their ability to undergo epileptogenesis? If so, such findings may even suggest that targeting molecules involved in LTP induction and/or expression at this synapse, such as *rim1α*, could be viable ways to interfere with epileptogenesis. Furthermore, given that TrkB signaling within the dentate granule cell is pinnacle to the process of epileptogenesis, understanding the ligands involved in activating it at this locale would further inform studies seeking to block its activation and prevent this process. For example, the results of this dissertation suggest that synaptic vesicular zinc could contribute to TrkB transactivation. If this is the case, could finding a drug that blocks the zinc transporter, ZnT3, be a potential therapy preventing epileptogenesis?

Beginning to answer these questions will require significant further study, but the findings presented within this dissertation lay the groundwork for such further investigations.

4.2 Better Elucidating the Cellular and Synaptic Locales of Activated TrkB within Mouse Hippocampus

A major future direction which is a logical extension from the present work would be to more accurately identify the subcellular and synaptic structures where TrkB is activated within mossy fibers and dendrites of CA1 pyramidal neurons. Ultrastructural analyses of synapses, as well as many subcellular structures, requires a level of resolution that is simply unobtainable using conventional light imaging techniques, including the confocal microscopy methods used in the present study (Dani et al., 2010). Resolution of confocal microscopy is particularly limited in the *z*-plane, which in practice is rarely better than 700 nm, and even in the *x-y*-plane is generally on the order of around 250 nm (Pawley, 1995). For comparison, a synaptic cleft is about 20 nm (Kandel, 2013), and electron microscopy can routinely achieve resolution higher than this (Slayter and Slayter, 1992). To this end, the use of electron microscopy and immunogold labeling, such as what was used in a study which localized pTrkB under physiological conditions within mouse hippocampus (Spencer-Segal et al., 2011), would be an invaluable tool. Questions that could be elucidated using this method include whether activated TrkB within mossy fiber axons resides within a signaling endosome, likely undergoing retrograde axonal transport, or at the plasma membrane. Is activated TrkB in mossy fiber boutons located

at the cell membrane, and if so what is its proximity to the active zone? Alternatively, does it reside within the bouton in association with an organelle, such as endosomes or synaptic vesicles? Similar questions could be asked for activated TrkB within spines and dendrites of CA1 pyramidal neurons. Is activated TrkB located at the plasma membrane of spines, and if so what is its proximity to the postsynaptic density? Alternatively, might it be located intracellularly, possibly in association with signaling endosomes or secretory vesicles? Electron microscopy would be a particularly powerful tool for answering these questions as there is intrinsic contrast of membranes, allowing easy identification of structures such as organelles and the synaptic cleft (Dani et al., 2010).

In addition to electron microscopy, new light microscopy techniques have recently been developed that allow fluorescent localization of cellular and synaptic markers at a resolution that could better answer questions about subcellular locale. One is array tomography, which relies on immunofluorescent markers and confocal imaging, but utilizes numerous sequential, ultrathin sections of around 200 nm each which are assembled digitally into 3D reconstructions following image acquisition (Micheva and Smith, 2007). Instead of digital *z*-sections, this method creates physical *z*-sections, thereby largely circumventing the resolution limitations encountered with confocal microscopy in the *z*-plane. Given the ultrathin nature of the sections, it also eliminates the problem of incomplete antibody penetration. This is of added value given that the sections utilized in our studies were 40 μm in thickness, yet we frequently found penetration to be at best several micrometers. Notably, this method is able to discern pre-

and postsynaptic markers, which normally appear to overlap using confocal imaging techniques. Superresolution fluorescence microscopy, including stochastic optical reconstruction microscopy (STORM), is a recent advance which allows for imaging fluorescent immunohistochemical markers with sub-diffraction limit resolution (Dani et al., 2010). One study reported a resolution of 14 nm in the *x*-*y*-plane and 35 nm in the *z*-plane, far superior to what could ever be achieved with confocal microscopy. This method was able to discern synaptic markers located directly on the membrane of the synaptic cleft from those located intracellularly, thus showing incredible precision in its ability to localize protein markers to subcellular locales (Dani et al., 2010). Use of such techniques could prove invaluable tools for better elucidating the precise subcellular and synaptic locales whereby TrkB is activated, particularly if one wanted to examine the relationship of this receptor to other subcellular proteins, as double labeling is not possible with electron microscopy techniques.

Another interesting potential line of investigation for future studies involves better understanding of the cellular location of different forms of activated TrkB receptor. Interestingly, preliminary work examining the cellular distribution of an entirely different antibody, probing for pY515 of TrkB, demonstrated a very different localization pattern within stratum lucidum than that found with the pY816 antibody. The specificity of this antibody was demonstrated in preliminary studies by showing that increased immunoreactivity within stratum lucidum following SE was blocked in a Y515F mutant mouse. Use of this antibody found pY515 to be highly enriched within mossy fiber

boutons following SE, demonstrated by using both Thy1-GFP expressing mice and a synapsin-1 marker, whereas it was noticeably devoid from mossy fiber axons. This was in striking contrast to the pY816 antibody, which demonstrated enrichment most prominently in mossy fiber axons of stratum lucidum, and labeled only a minority of boutons even after SE.

We speculated that these contrasting cellular distributions were likely to be explained by one of two possibilities: (1) The cellular locales of pY515 and pY816 are largely non-overlapping, implying that individual activated TrkB molecules may only be phosphorylated at one, and not both, tyrosines. This implies that the conventional model of TrkB being activated in a lockstep fashion by a ligand (Barbacid, 1995; Cunningham and Greene, 1998), involving phosphorylation of all of its tyrosine residues at once, may not be entirely correct. Such an idea is supported by work showing that activation of TrkB by zinc versus BDNF may lead to preferential phosphorylation of different signaling residues (Huang and McNamara, 2010), and also raises the possibility that the ligands activating TrkB at these different cellular locales may be different. (2) The different cellular distributions detected by these antibodies may be because each antibody is only recognizing a subset of activated TrkB, though both subsets are equally phosphorylated at both Y515 and Y816 residues. The reason why these antibodies recognize different subsets may have to do with a conformational difference on the receptor which fundamentally alters the epitope that these antibodies recognize, rendering them only capable of detecting a particular conformation of pTrkB that resides at a

particular cellular locale. For example, Trk receptors are glycosylated at a variety of sites, their glycosylation status appears to change as they mature through the secretory pathway, and this may even regulate membrane delivery (Watson et al., 1999b). Such posttranslational modifications could fundamentally alter the ability of an antibody to detect a particular form of activated TrkB if it changes the epitope that the antibody recognizes. It may be possible, therefore, that one antibody is preferentially detecting an intracellular form of TrkB (probably the pY816 antibody), whereas another is preferentially detecting a form that is located on the synaptic membrane (probably the pY515 antibody). Examining the reasons for why these different cellular distributions of pTrkB were detected using these two different antibodies would undoubtedly make an exciting line of future investigation.

4.3 Further Assessing the Contribution of Vesicular Zinc to Transactivation of TrkB in Stratum Lucidum of Mouse Hippocampus

Given the finding of increased BDNF levels in the *ZnT3* knockout, it would be interesting to see if levels of other neurotrophins also increase, such as NT-3 and NT-4. Furthermore, given changes in BDNF levels in the *ZnT3*^{-/-} mouse, it would be interesting to see if levels of ZnT3 protein may change in *BDNF* mutants. Such a finding, particularly if ZnT3 levels were found to increase in a manner that was consistent with a homeostatic response to elimination of BDNF, would further suggest that vesicular zinc is likely to have an important role in contributing to TrkB signaling. Furthermore, the presence of increased BDNF levels in the *ZnT3*^{-/-} animal makes it possible that, if

synaptic vesicular zinc contributes a fundamental role to transactivation of TrkB which could not be directly detected in these studies, other homeostatic compensations also occur in the *ZnT3* mutant. Such compensations would block our ability to detect further decreased TrkB activation in the *ZnT3/BDNF* double knockout compared to the *BDNF* knockout alone, a finding that would directly implicate vesicular zinc in TrkB transactivation under physiological conditions. In this regard, it is notable that *ZnT3*^{-/-} animals are complete knockouts for the *ZnT3* protein (Cole et al., 1999), unlike in the *BDNF* animal which is a conditional knockout (He et al., 2004). Such complete knockouts may be particularly prone to compensatory responses if the gene they lack is important for normal function. For this reason, future work may focus on generation of *ZnT3* conditional knockouts, employing Cre-loxP technology (Gu et al., 1994) in a similar fashion as was utilized for *BDNF* conditional knockouts. Examination of such animals using similar studies as performed in Chapter 3 of this dissertation may more directly reveal a role for synaptic zinc in transactivation of TrkB.

Examination of the contribution of synaptic vesicular zinc to TrkB transactivation during epileptogenesis, as well as the development of epileptogenesis itself, is an important future direction for this work. Due to increased BDNF and the possibility of other homeostatic responses in the *ZnT3* knockout mouse, however, this would have to be done in an animal in which such compensatory mechanisms did not occur, such as could hopefully be achieved with a conditional knockout for *ZnT3*. An alternative would be to compare *BDNF* and *ZnT3/BDNF* knockout animals, as performed in Chapter 3 of this

dissertation, in models of epileptogenesis. This would eliminate changes in BDNF protein levels between genotypes, though one could not exclude other compensatory effects. Such studies could involve examining kindling development in these animals to see if mice lacking ZnT3 protein exhibited impaired kindling, and examination of pTrkB levels in fully kindled animals would reveal the contribution of vesicular zinc to activation of this receptor in the epileptic state. It is possible, given the low probability of release at the mf-CA3 synapse (Nicoll and Schmitz, 2005), that synaptic vesicular zinc plays a much more profound role in TrkB transactivation under conditions of enhanced neuronal activity than under physiological conditions.

In conclusion, the findings presented within this dissertation reveal cellular and synaptic locales within hippocampus where TrkB signaling is likely to be important for the development of neuronal excitability culminating in the development of limbic epilepsy. Furthermore, they suggest the importance of a novel endogenous ligand, synaptic vesicular zinc, in regulation of TrkB signaling within mossy fibers of stratum lucidum. Future studies may use higher resolution microscopy techniques to further define the specific subcellular locales whereby TrkB is activated during epileptogenesis. They may also seek to further elucidate the specific contribution of vesicular zinc to transactivation of TrkB under both physiological conditions and following the development of epilepsy, as well as its contribution to the process of epileptogenesis itself. Altogether, the findings contained within this dissertation contribute new and

important knowledge to the field of neurotrophin signaling, and will hopefully help to inform future lines of inquiry on this topic.

Works Cited

1989. Proposal for revised classification of epilepsies and epileptic syndromes. Commission on Classification and Terminology of the International League Against Epilepsy. *Epilepsia* 30(4):389-399.
- Abramoff MD, Magelhaes, P.J., Ram, S.J. 2004. Image Processing with ImageJ. *Biophotonics International* 11(7):36-42.
- Adlard PA, Parncutt JM, Finkelstein DI, Bush AI. 2010. Cognitive loss in zinc transporter-3 knock-out mice: a phenocopy for the synaptic and memory deficits of Alzheimer's disease? *J Neurosci* 30(5):1631-1636.
- Amaral DG, Dent JA. 1981. Development of the mossy fibers of the dentate gyrus: I. A light and electron microscopic study of the mossy fibers and their expansions. *J Comp Neurol* 195(1):51-86.
- Andersen P, Bliss TV, Skrede KK. 1971. Lamellar organization of hippocampal pathways. *Exp Brain Res* 13(2):222-238.
- Annegers JF, Hauser WA, Elveback LR, Kurland LT. 1979. The risk of epilepsy following febrile convulsions. *Neurology* 29(3):297-303.
- Araki T, Simon RP, Taki W, Lan JQ, Henshall DC. 2002. Characterization of neuronal death induced by focally evoked limbic seizures in the C57BL/6 mouse. *J Neurosci Res* 69(5):614-621.
- Arroyo S, Brodie MJ, Avanzini G, Baumgartner C, Chiron C, Dulac O, French JA, Serratosa JM. 2002. Is refractory epilepsy preventable? *Epilepsia* 43(4):437-444.
- Aslamkhan AG, Aslamkhan A, Ahearn GA. 2002. Preparation of metal ion buffers for biological experimentation: a methods approach with emphasis on iron and zinc. *J Exp Zool* 292(6):507-522.

- Baj G, Leone E, Chao MV, Tongiorgi E. 2011. Spatial segregation of BDNF transcripts enables BDNF to differentially shape distinct dendritic compartments. *Proc Natl Acad Sci U S A* 108(40):16813-16818.
- Barbacid M. 1995. Neurotrophic factors and their receptors. *Curr Opin Cell Biol* 7(2):148-155.
- Barbacid M, Lamballe F, Pulido D, Klein R. 1991. The trk family of tyrosine protein kinase receptors. *Biochim Biophys Acta* 1072(2-3):115-127.
- Barde YA, Edgar D, Thoenen H. 1982. Purification of a new neurotrophic factor from mammalian brain. *Embo J* 1(5):549-553.
- Bartolomei F, Khalil M, Wendling F, Sontheimer A, Regis J, Ranjeva JP, Guye M, Chauvel P. 2005. Entorhinal cortex involvement in human mesial temporal lobe epilepsy: an electrophysiologic and volumetric study. *Epilepsia* 46(5):677-687.
- Berg AT, Berkovic SF, Brodie MJ, Buchhalter J, Cross JH, van Emde Boas W, Engel J, French J, Glauser TA, Mathern GW, Moshe SL, Nordli D, Plouin P, Scheffer IE. 2010. Revised terminology and concepts for organization of seizures and epilepsies: report of the ILAE Commission on Classification and Terminology, 2005-2009. *Epilepsia* 51(4):676-685.
- Berg JM. 1990. Zinc fingers and other metal-binding domains. Elements for interactions between macromolecules. *J Biol Chem* 265(12):6513-6516.
- Bhattacharyya A, Watson FL, Bradlee TA, Pomeroy SL, Stiles CD, Segal RA. 1997. Trk receptors function as rapid retrograde signal carriers in the adult nervous system. *J Neurosci* 17(18):7007-7016.
- Binder DK, Routbort MJ, McNamara JO. 1999a. Immunohistochemical evidence of seizure-induced activation of trk receptors in the mossy fiber pathway of adult rat hippocampus. *J Neurosci* 19(11):4616-4626.

- Binder DK, Routbort MJ, Ryan TE, Yancopoulos GD, McNamara JO. 1999b. Selective inhibition of kindling development by intraventricular administration of TrkB receptor body. *J Neurosci* 19(4):1424-1436.
- Binder LI, Frankfurter A, Rebhun LI. 1985. The distribution of tau in the mammalian central nervous system. *J Cell Biol* 101(4):1371-1378.
- Bortolotto ZA, Lauri S, Isaac JT, Collingridge GL. 2003. Kainate receptors and the induction of mossy fibre long-term potentiation. *Philos Trans R Soc Lond B Biol Sci* 358(1432):657-666.
- Bouchet J. 1826. *Le panegyric du chevallier sans reproche, ou, Mémoires de La Trémoille*. Paris,: Foucault.
- Carpenter G. 1999. Employment of the epidermal growth factor receptor in growth factor-independent signaling pathways. *J Cell Biol* 146(4):697-702.
- Castillo PE, Schoch S, Schmitz F, Sudhof TC, Malenka RC. 2002. RIM1alpha is required for presynaptic long-term potentiation. *Nature* 415(6869):327-330.
- Cavalheiro EA, Leite JP, Bortolotto ZA, Turski WA, Ikonomidou C, Turski L. 1991. Long-term effects of pilocarpine in rats: structural damage of the brain triggers kindling and spontaneous recurrent seizures. *Epilepsia* 32(6):778-782.
- Cavazos JE, Das I, Sutula TP. 1994. Neuronal loss induced in limbic pathways by kindling: evidence for induction of hippocampal sclerosis by repeated brief seizures. *J Neurosci* 14(5 Pt 2):3106-3121.
- Cavazos JE, Golarai G, Sutula TP. 1991. Mossy fiber synaptic reorganization induced by kindling: time course of development, progression, and permanence. *J Neurosci* 11(9):2795-2803.
- Chao MV, Rajagopal R, Lee FS. 2006. Neurotrophin signalling in health and disease. *Clin Sci (Lond)* 110(2):167-173.

Chen LY, Rex CS, Pham DT, Lynch G, Gall CM. 2010a. BDNF signaling during learning is regionally differentiated within hippocampus. *J Neurosci* 30(45):15097-15101.

Chen LY, Rex CS, Sanaiha Y, Lynch G, Gall CM. 2010b. Learning induces neurotrophin signaling at hippocampal synapses. *Proc Natl Acad Sci U S A* 107(15):7030-7035.

Chiaruttini C, Vicario A, Li Z, Baj G, Braiuca P, Wu Y, Lee FS, Gardossi L, Baraban JM, Tongiorgi E. 2009. Dendritic trafficking of BDNF mRNA is mediated by translin and blocked by the G196A (Val66Met) mutation. *Proc Natl Acad Sci U S A* 106(38):16481-16486.

Choi DW, Koh JY. 1998. Zinc and brain injury. *Annual review of neuroscience* 21:347-375.

Clifford DB, Olney JW, Maniotis A, Collins RC, Zorumski CF. 1987. The functional anatomy and pathology of lithium-pilocarpine and high-dose pilocarpine seizures. *Neuroscience* 23(3):953-968.

Cole PA, Shen K, Qiao Y, Wang D. 2003. Protein tyrosine kinases Src and Csk: a tail's tale. *Curr Opin Chem Biol* 7(5):580-585.

Cole TB, Martyanova A, Palmiter RD. 2001. Removing zinc from synaptic vesicles does not impair spatial learning, memory, or sensorimotor functions in the mouse. *Brain Res* 891(1-2):253-265.

Cole TB, Robbins CA, Wenzel HJ, Schwartzkroin PA, Palmiter RD. 2000. Seizures and neuronal damage in mice lacking vesicular zinc. *Epilepsy Res* 39(2):153-169.

Cole TB, Wenzel HJ, Kafer KE, Schwartzkroin PA, Palmiter RD. 1999. Elimination of zinc from synaptic vesicles in the intact mouse brain by disruption of the ZnT3 gene. *Proc Natl Acad Sci U S A* 96(4):1716-1721.

- Conner JM, Lauterborn JC, Yan Q, Gall CM, Varon S. 1997. Distribution of brain-derived neurotrophic factor (BDNF) protein and mRNA in the normal adult rat CNS: evidence for anterograde axonal transport. *J Neurosci* 17(7):2295-2313.
- Cooper JA, Howell B. 1993. The when and how of Src regulation. *Cell* 73(6):1051-1054.
- Copanaki E, Chang S, Vlachos A, Tschape JA, Muller UC, Kogel D, Deller T. 2010. sAPPalpha antagonizes dendritic degeneration and neuron death triggered by proteasomal stress. *Mol Cell Neurosci* 44(4):386-393.
- Coughenour LL, Barr BM. 2001. Use of trifluoroperazine isolates a [(3)H]Ifenprodil binding site in rat brain membranes with the pharmacology of the voltage-independent ifenprodil site on N-methyl-D-aspartate receptors containing NR2B subunits. *J Pharmacol Exp Ther* 296(1):150-159.
- Cowan WM. 2001. Viktor Hamburger and Rita Levi-Montalcini: the path to the discovery of nerve growth factor. *Annual review of neuroscience* 24:551-600.
- Cowan WM, Südhof TC, Stevens CF, Howard Hughes Medical Institute. 2001. *Synapses*. Baltimore: Johns Hopkins University Press. xiii, 767 p. p.
- Croll SD, Suri C, Compton DL, Simmons MV, Yancopoulos GD, Lindsay RM, Wiegand SJ, Rudge JS, Scharfman HE. 1999. Brain-derived neurotrophic factor transgenic mice exhibit passive avoidance deficits, increased seizure severity and in vitro hyperexcitability in the hippocampus and entorhinal cortex. *Neuroscience* 93(4):1491-1506.
- Crooks KR, Kleven DT, Rodriguez RM, Wetsel WC, McNamara JO. 2010. TrkB signaling is required for behavioral sensitization and conditioned place preference induced by a single injection of cocaine. *Neuropharmacology* 58(7):1067-1077.
- Cunningham ME, Greene LA. 1998. A function-structure model for NGF-activated TRK. *Embo J* 17(24):7282-7293.

Curia G, Longo D, Biagini G, Jones RS, Avoli M. 2008. The pilocarpine model of temporal lobe epilepsy. *J Neurosci Methods* 172(2):143-157.

Dani A, Huang B, Bergan J, Dulac C, Zhuang X. 2010. Superresolution imaging of chemical synapses in the brain. *Neuron* 68(5):843-856.

Danzer SC, He X, McNamara JO. 2004. Ontogeny of seizure-induced increases in BDNF immunoreactivity and TrkB receptor activation in rat hippocampus. *Hippocampus* 14(3):345-355.

Danzer SC, Kotloski RJ, Walter C, Hughes M, McNamara JO. 2008. Altered morphology of hippocampal dentate granule cell presynaptic and postsynaptic terminals following conditional deletion of TrkB. *Hippocampus* 18(7):668-678.

Danzer SC, McNamara JO. 2004. Localization of brain-derived neurotrophic factor to distinct terminals of mossy fiber axons implies regulation of both excitation and feedforward inhibition of CA3 pyramidal cells. *J Neurosci* 24(50):11346-11355.

Dasheiff RM, McNamara JO. 1982. Intradentate colchicine retards the development of amygdala kindling. *Ann Neurol* 11(4):347-352.

De Camilli P, Harris SM, Jr., Huttner WB, Greengard P. 1983. Synapsin I (Protein I), a nerve terminal-specific phosphoprotein. II. Its specific association with synaptic vesicles demonstrated by immunocytochemistry in agarose-embedded synaptosomes. *J Cell Biol* 96(5):1355-1373.

Dechant G, Barde YA. 1997. Signalling through the neurotrophin receptor p75NTR. *Curr Opin Neurobiol* 7(3):413-418.

Dieni S, Matsumoto T, Dekkers M, Rauskolb S, Ionescu MS, Deogracias R, Gundelfinger ED, Kojima M, Nestel S, Frotscher M, Barde YA. 2012. BDNF and its pro-peptide are stored in presynaptic dense core vesicles in brain neurons. *J Cell Biol* 196(6):775-788.

Dunleavy M, Shinoda S, Schindler C, Ewart C, Dolan R, Gobbo OL, Kerskens CM, Henshall DC. 2010. Experimental neonatal status epilepticus and the development of temporal lobe epilepsy with unilateral hippocampal sclerosis. *Am J Pathol* 176(1):330-342.

Eide FF, Vining ER, Eide BL, Zang K, Wang XY, Reichardt LF. 1996. Naturally occurring truncated trkB receptors have dominant inhibitory effects on brain-derived neurotrophic factor signaling. *J Neurosci* 16(10):3123-3129.

Engel J, Pedley TA. 2008. *Epilepsy : a comprehensive textbook*. Philadelphia: Wolters Kluwer Health/Lippincott Williams & Wilkins.

Ernfors P, Bengzon J, Kokaia Z, Persson H, Lindvall O. 1991. Increased levels of messenger RNAs for neurotrophic factors in the brain during kindling epileptogenesis. *Neuron* 7(1):165-176.

Feng G, Mellor RH, Bernstein M, Keller-Peck C, Nguyen QT, Wallace M, Nerbonne JM, Lichtman JW, Sanes JR. 2000. Imaging neuronal subsets in transgenic mice expressing multiple spectral variants of GFP. *Neuron* 28(1):41-51.

Figurov A, Pozzo-Miller LD, Olafsson P, Wang T, Lu B. 1996. Regulation of synaptic responses to high-frequency stimulation and LTP by neurotrophins in the hippocampus. *Nature* 381(6584):706-709.

Fletcher TL, Cameron P, De Camilli P, Banker G. 1991. The distribution of synapsin I and synaptophysin in hippocampal neurons developing in culture. *J Neurosci* 11(6):1617-1626.

Forsgren L, Beghi E, Oun A, Sillanpaa M. 2005. The epidemiology of epilepsy in Europe - a systematic review. *Eur J Neurol* 12(4):245-253.

Frederickson CJ, Danscher G. 1990. Zinc-containing neurons in hippocampus and related CNS structures. *Progress in brain research* 83:71-84.

Frederickson CJ, Koh JY, Bush AI. 2005. The neurobiology of zinc in health and disease. *Nature reviews Neuroscience* 6(6):449-462.

Gaitatzis A, Johnson AL, Chadwick DW, Shorvon SD, Sander JW. 2004. Life expectancy in people with newly diagnosed epilepsy. *Brain* 127(Pt 11):2427-2432.

Goddard GV. 1967. Development of epileptic seizures through brain stimulation at low intensity. *Nature* 214(5092):1020-1021.

Goddard GV, McIntyre DC, Leech CK. 1969. A permanent change in brain function resulting from daily electrical stimulation. *Exp Neurol* 25(3):295-330.

Goussakov IV, Fink K, Elger CE, Beck H. 2000. Metaplasticity of mossy fiber synaptic transmission involves altered release probability. *J Neurosci* 20(9):3434-3441.

Gowers WR. 1881. Epilepsy and other chronic convulsive diseases: their causes, symptoms, & treatment. London,: Churchill. xiv, 309 p. p.

Gruart A, Sciarretta C, Valenzuela-Harrington M, Delgado-Garcia JM, Minichiello L. 2007. Mutation at the TrkB PLC γ -docking site affects hippocampal LTP and associative learning in conscious mice. *Learn Mem* 14(1):54-62.

Gu H, Marth JD, Orban PC, Mossman H, Rajewsky K. 1994. Deletion of a DNA polymerase beta gene segment in T cells using cell type-specific gene targeting. *Science* 265(5168):103-106.

Hamilton SE, Loose MD, Qi M, Levey AI, Hille B, McKnight GS, Idzerda RL, Nathanson NM. 1997. Disruption of the m1 receptor gene ablates muscarinic receptor-dependent M current regulation and seizure activity in mice. *Proc Natl Acad Sci U S A* 94(24):13311-13316.

Harvey BD, Sloviter RS. 2005. Hippocampal granule cell activity and c-Fos expression during spontaneous seizures in awake, chronically epileptic, pilocarpine-treated

rats: implications for hippocampal epileptogenesis. *J Comp Neurol* 488(4):442-463.

He XP, Butler L, Liu X, McNamara JO. 2006. The tyrosine receptor kinase B ligand, neurotrophin-4, is not required for either epileptogenesis or tyrosine receptor kinase B activation in the kindling model. *Neuroscience* 141(1):515-520.

He XP, Kotloski R, Nef S, Luikart BW, Parada LF, McNamara JO. 2004. Conditional deletion of TrkB but not BDNF prevents epileptogenesis in the kindling model. *Neuron* 43(1):31-42.

He XP, Minichiello L, Klein R, McNamara JO. 2002. Immunohistochemical evidence of seizure-induced activation of trkB receptors in the mossy fiber pathway of adult mouse hippocampus. *J Neurosci* 22(17):7502-7508.

He XP, Pan E, Sciarretta C, Minichiello L, McNamara JO. 2010. Disruption of TrkB-mediated phospholipase C γ signaling inhibits limbic epileptogenesis. *J Neurosci* 30(18):6188-6196.

Heldt SA, Stanek L, Chhatwal JP, Ressler KJ. 2007. Hippocampus-specific deletion of BDNF in adult mice impairs spatial memory and extinction of aversive memories. *Mol Psychiatry* 12(7):656-670.

Helgager J, Liu G, McNamara JO. 2013. The cellular and synaptic location of activated TrkB in mouse hippocampus during limbic epileptogenesis. *J Comp Neurol* 521(3):499-521.

Hetman M, Xia Z. 2000. Signaling pathways mediating anti-apoptotic action of neurotrophins. *Acta Neurobiol Exp (Wars)* 60(4):531-545.

Howe CL, Mobley WC. 2005. Long-distance retrograde neurotrophic signaling. *Curr Opin Neurobiol* 15(1):40-48.

Huang EJ, Reichardt LF. 2001. Neurotrophins: roles in neuronal development and function. *Annual review of neuroscience* 24:677-736.

Huang EJ, Reichardt LF. 2003. Trk receptors: roles in neuronal signal transduction. *Annu Rev Biochem* 72:609-642.

Huang YZ, McNamara JO. 2010. Mutual regulation of Src family kinases and the neurotrophin receptor TrkB. *J Biol Chem* 285(11):8207-8217.

Huang YZ, Pan E, Xiong ZQ, McNamara JO. 2008. Zinc-mediated transactivation of TrkB potentiates the hippocampal mossy fiber-CA3 pyramid synapse. *Neuron* 57(4):546-558.

Huber G, Matus A. 1984. Differences in the cellular distributions of two microtubule-associated proteins, MAP1 and MAP2, in rat brain. *J Neurosci* 4(1):151-160.

Isackson PJ, Huntsman MM, Murray KD, Gall CM. 1991. BDNF mRNA expression is increased in adult rat forebrain after limbic seizures: temporal patterns of induction distinct from NGF. *Neuron* 6(6):937-948.

Ishizuka N, Weber J, Amaral DG. 1990. Organization of intrahippocampal projections originating from CA3 pyramidal cells in the rat. *J Comp Neurol* 295(4):580-623.

Kandel ER. 2013. Principles of neural science. New York: McGraw-Hill Medical. 1, 1709 p. p.

Kaplan DR, Hempstead BL, Martin-Zanca D, Chao MV, Parada LF. 1991. The trk proto-oncogene product: a signal transducing receptor for nerve growth factor. *Science* 252(5005):554-558.

Kasugai M, Akaike K, Imamura S, Matsukubo H, Tojo H, Nakamura M, Tanaka S, Sano A. 2007. Differences in two mice strains on kainic acid-induced amygdalar seizures. *Biochem Biophys Res Commun* 357(4):1078-1083.

Klein R, Jing SQ, Nanduri V, O'Rourke E, Barbacid M. 1991. The trk proto-oncogene encodes a receptor for nerve growth factor. *Cell* 65(1):189-197.

- Koh JY, Suh SW, Gwag BJ, He YY, Hsu CY, Choi DW. 1996. The role of zinc in selective neuronal death after transient global cerebral ischemia. *Science* 272(5264):1013-1016.
- Kokaia M, Ernfors P, Kokaia Z, Elmer E, Jaenisch R, Lindvall O. 1995. Suppressed epileptogenesis in BDNF mutant mice. *Exp Neurol* 133(2):215-224.
- Korte M, Carroll P, Wolf E, Brem G, Thoenen H, Bonhoeffer T. 1995. Hippocampal long-term potentiation is impaired in mice lacking brain-derived neurotrophic factor. *Proc Natl Acad Sci U S A* 92(19):8856-8860.
- Korte M, Griesbeck O, Gravel C, Carroll P, Staiger V, Thoenen H, Bonhoeffer T. 1996. Virus-mediated gene transfer into hippocampal CA1 region restores long-term potentiation in brain-derived neurotrophic factor mutant mice. *Proc Natl Acad Sci U S A* 93(22):12547-12552.
- Korte M, Kang H, Bonhoeffer T, Schuman E. 1998. A role for BDNF in the late-phase of hippocampal long-term potentiation. *Neuropharmacology* 37(4-5):553-559.
- Korte M, Minichiello L, Klein R, Bonhoeffer T. 2000. Shc-binding site in the TrkB receptor is not required for hippocampal long-term potentiation. *Neuropharmacology* 39(5):717-724.
- Kwan P, Sander JW. 2004. The natural history of epilepsy: an epidemiological view. *J Neurol Neurosurg Psychiatry* 75(10):1376-1381.
- Lee FS, Rajagopal R, Chao MV. 2002a. Distinctive features of Trk neurotrophin receptor transactivation by G protein-coupled receptors. *Cytokine Growth Factor Rev* 13(1):11-17.
- Lee FS, Rajagopal R, Kim AH, Chang PC, Chao MV. 2002b. Activation of Trk neurotrophin receptor signaling by pituitary adenylate cyclase-activating polypeptides. *J Biol Chem* 277(11):9096-9102.

- Lehnart SE, Mongillo M, Bellinger A, Lindegger N, Chen BX, Hsueh W, Reiken S, Wronska A, Drew LJ, Ward CW, Lederer WJ, Kass RS, Morley G, Marks AR. 2008. Leaky Ca₂₊ release channel/ryanodine receptor 2 causes seizures and sudden cardiac death in mice. *J Clin Invest* 118(6):2230-2245.
- Leite JP, Garcia-Cairasco N, Cavalheiro EA. 2002. New insights from the use of pilocarpine and kainate models. *Epilepsy Res* 50(1-2):93-103.
- Lessmann V, Brigadski T. 2009. Mechanisms, locations, and kinetics of synaptic BDNF secretion: an update. *Neurosci Res* 65(1):11-22.
- Lhatoo SD, Johnson AL, Goodridge DM, MacDonald BK, Sander JW, Shorvon SD. 2001. Mortality in epilepsy in the first 11 to 14 years after diagnosis: multivariate analysis of a long-term, prospective, population-based cohort. *Ann Neurol* 49(3):336-344.
- Li T, Ren G, Lusardi T, Wilz A, Lan JQ, Iwasato T, Itohara S, Simon RP, Boison D. 2008. Adenosine kinase is a target for the prediction and prevention of epileptogenesis in mice. *J Clin Invest* 118(2):571-582.
- Li Y, Hough CJ, Suh SW, Sarvey JM, Frederickson CJ. 2001. Rapid translocation of Zn(2+) from presynaptic terminals into postsynaptic hippocampal neurons after physiological stimulation. *J Neurophysiol* 86(5):2597-2604.
- Lindsay RM. 1996. Role of neurotrophins and trk receptors in the development and maintenance of sensory neurons: an overview. *Philos Trans R Soc Lond B Biol Sci* 351(1338):365-373.
- Linnarsson S, Björklund A, Ernfors P. 1997. Learning deficit in BDNF mutant mice. *Eur J Neurosci* 9(12):2581-2587.
- Lopantsev V, Wenzel HJ, Cole TB, Palmiter RD, Schwartzkroin PA. 2003. Lack of vesicular zinc in mossy fibers does not affect synaptic excitability of CA3 pyramidal cells in zinc transporter 3 knockout mice. *Neuroscience* 116(1):237-248.

Loscher W. 2002. Animal models of epilepsy for the development of antiepileptogenic and disease-modifying drugs. A comparison of the pharmacology of kindling and post-status epilepticus models of temporal lobe epilepsy. *Epilepsy Res* 50(1-2):105-123.

Low CM, Zheng F, Lyuboslavsky P, Traynelis SF. 2000. Molecular determinants of coordinated proton and zinc inhibition of N-methyl-D-aspartate NR1/NR2A receptors. *Proc Natl Acad Sci U S A* 97(20):11062-11067.

Lu B. 2003. BDNF and activity-dependent synaptic modulation. *Learn Mem* 10(2):86-98.

Lu Y, Christian K, Lu B. 2008. BDNF: a key regulator for protein synthesis-dependent LTP and long-term memory? *Neurobiol Learn Mem* 89(3):312-323.

Lu Y, Ji Y, Ganesan S, Schloesser R, Martinowich K, Sun M, Mei F, Chao MV, Lu B. 2011. TrkB as a potential synaptic and behavioral tag. *J Neurosci* 31(33):11762-11771.

Malmgren K, Thom M. 2012. Hippocampal sclerosis--origins and imaging. *Epilepsia* 53 Suppl 4:19-33.

Martel G, Hevi C, Friebely O, Baybutt T, Shumyatsky GP. 2010. Zinc transporter 3 is involved in learned fear and extinction, but not in innate fear. *Learn Mem* 17(11):582-590.

Martel G, Hevi C, Kane-Goldsmith N, Shumyatsky GP. 2011. Zinc transporter ZnT3 is involved in memory dependent on the hippocampus and perirhinal cortex. *Behav Brain Res* 223(1):233-238.

Martin D, Ault B, Nadler JV. 1992. NMDA receptor-mediated depolarizing action of proline on CA1 pyramidal cells. *Eur J Pharmacol* 219(1):59-66.

Maske H. 1955. [A new method for demonstrating A and B cells in the islands of Langerhans]. *Klin Wochenschr* 33(43-44):1058.

Mathern GW, Adelson PD, Cahan LD, Leite JP. 2002. Hippocampal neuron damage in human epilepsy: Meyer's hypothesis revisited. Progress in brain research 135:237-251.

Mathern GW, Babb TL, Armstrong DL. 1997. Hippocampal Sclerosis. In: Engel J, Pedley TA, editors. Epilepsy : a comprehensive textbook. Philadelphia: Lippincott-Raven. p 133-155.

McAllister AK, Katz LC, Lo DC. 1999. Neurotrophins and synaptic plasticity. Annual review of neuroscience 22:295-318.

McNamara JO, Huang YZ, Leonard AS. 2006. Molecular signaling mechanisms underlying epileptogenesis. Sci STKE 2006(356):re12.

Micheva KD, Smith SJ. 2007. Array tomography: a new tool for imaging the molecular architecture and ultrastructure of neural circuits. Neuron 55(1):25-36.

Minichiello L. 2009. TrkB signalling pathways in LTP and learning. Nature reviews Neuroscience 10(12):850-860.

Minichiello L, Calella AM, Medina DL, Bonhoeffer T, Klein R, Korte M. 2002. Mechanism of TrkB-mediated hippocampal long-term potentiation. Neuron 36(1):121-137.

Minichiello L, Korte M, Wolfer D, Kuhn R, Unsicker K, Cestari V, Rossi-Arnaud C, Lipp HP, Bonhoeffer T, Klein R. 1999. Essential role for TrkB receptors in hippocampus-mediated learning. Neuron 24(2):401-414.

Mizuno M, Yamada K, Olariu A, Nawa H, Nabeshima T. 2000. Involvement of brain-derived neurotrophic factor in spatial memory formation and maintenance in a radial arm maze test in rats. J Neurosci 20(18):7116-7121.

Monteggia LM, Barrot M, Powell CM, Berton O, Galanis V, Gemelli T, Meuth S, Nagy A, Greene RW, Nestler EJ. 2004. Essential role of brain-derived neurotrophic

factor in adult hippocampal function. Proc Natl Acad Sci U S A 101(29):10827-10832.

Moore RY, Bernstein ME. 1989. Synaptogenesis in the rat suprachiasmatic nucleus demonstrated by electron microscopy and synapsin I immunoreactivity. J Neurosci 9(6):2151-2162.

Mouri G, Jimenez-Mateos E, Engel T, Dunleavy M, Hatazaki S, Paucard A, Matsushima S, Taki W, Henshall DC. 2008. Unilateral hippocampal CA3-predominant damage and short latency epileptogenesis after intra-amygdala microinjection of kainic acid in mice. Brain Res 1213:140-151.

Nadler JV, Perry BW, Cotman CW. 1978. Intraventricular kainic acid preferentially destroys hippocampal pyramidal cells. Nature 271(5646):676-677.

Nadler JV, Perry BW, Cotman CW. 1980. Selective reinnervation of hippocampal area CA1 and the fascia dentata after destruction of CA3-CA4 afferents with kainic acid. Brain Res 182(1):1-9.

Nair PP, Kalita J, Misra UK. 2011. Status epilepticus: why, what, and how. J Postgrad Med 57(3):242-252.

Nicoll RA, Schmitz D. 2005. Synaptic plasticity at hippocampal mossy fibre synapses. Nature reviews Neuroscience 6(11):863-876.

Niewiadomska G, Mietelska-Porowska A, Mazurkiewicz M. 2011. The cholinergic system, nerve growth factor and the cytoskeleton. Behav Brain Res 221(2):515-526.

Nozaki C, Vergnano AM, Filliol D, Ouagazzal AM, Le Goff A, Carvalho S, Reiss D, Gaveriaux-Ruff C, Neyton J, Paoletti P, Kieffer BL. 2011. Zinc alleviates pain through high-affinity binding to the NMDA receptor NR2A subunit. Nat Neurosci 14(8):1017-1022.

- Okragly AJ, Haak-Frendscho M. 1997. An acid-treatment method for the enhanced detection of GDNF in biological samples. *Exp Neurol* 145(2 Pt 1):592-596.
- Palko ME, Coppola V, Tessarollo L. 1999. Evidence for a role of truncated trkC receptor isoforms in mouse development. *J Neurosci* 19(2):775-782.
- Palmiter RD, Huang L. 2004. Efflux and compartmentalization of zinc by members of the SLC30 family of solute carriers. *Pflugers Archiv : European journal of physiology* 447(5):744-751.
- Pan E, Zhang XA, Huang Z, Krezel A, Zhao M, Tinberg CE, Lippard SJ, McNamara JO. 2011. Vesicular zinc promotes presynaptic and inhibits postsynaptic long-term potentiation of mossy fiber-CA3 synapse. *Neuron* 71(6):1116-1126.
- Paoletti P, Ascher P, Neyton J. 1997. High-affinity zinc inhibition of NMDA NR1-NR2A receptors. *J Neurosci* 17(15):5711-5725.
- Papp E, Leinekugel X, Henze DA, Lee J, Buzsaki G. 2001. The apical shaft of CA1 pyramidal cells is under GABAergic interneuronal control. *Neuroscience* 102(4):715-721.
- Patterson SL, Abel T, Deuel TA, Martin KC, Rose JC, Kandel ER. 1996. Recombinant BDNF rescues deficits in basal synaptic transmission and hippocampal LTP in BDNF knockout mice. *Neuron* 16(6):1137-1145.
- Pawley JB. 1995. *Handbook of biological confocal microscopy*. New York: Plenum Press. xxiii, 632 p., 634 p. of plates p.
- Perucca P, Gilliam FG. 2012. Adverse effects of antiepileptic drugs. *Lancet Neurol* 11(9):792-802.
- Peters S, Koh J, Choi DW. 1987. Zinc selectively blocks the action of N-methyl-D-aspartate on cortical neurons. *Science* 236(4801):589-593.

- Pikkarainen M, Ronkko S, Savander V, Insausti R, Pitkanen A. 1999. Projections from the lateral, basal, and accessory basal nuclei of the amygdala to the hippocampal formation in rat. *J Comp Neurol* 403(2):229-260.
- Poo MM. 2001. Neurotrophins as synaptic modulators. *Nature reviews Neuroscience* 2(1):24-32.
- Pozzo-Miller LD, Gottschalk W, Zhang L, McDermott K, Du J, Gopalakrishnan R, Oho C, Sheng ZH, Lu B. 1999. Impairments in high-frequency transmission, synaptic vesicle docking, and synaptic protein distribution in the hippocampus of BDNF knockout mice. *J Neurosci* 19(12):4972-4983.
- Qian J, Noebels JL. 2005. Visualization of transmitter release with zinc fluorescence detection at the mouse hippocampal mossy fibre synapse. *J Physiol* 566(Pt 3):747-758.
- Racine RJ. 1972a. Modification of seizure activity by electrical stimulation. I. After-discharge threshold. *Electroencephalogr Clin Neurophysiol* 32(3):269-279.
- Racine RJ. 1972b. Modification of seizure activity by electrical stimulation. II. Motor seizure. *Electroencephalogr Clin Neurophysiol* 32(3):281-294.
- Rajagopal R, Chen ZY, Lee FS, Chao MV. 2004. Transactivation of Trk neurotrophin receptors by G-protein-coupled receptor ligands occurs on intracellular membranes. *J Neurosci* 24(30):6650-6658.
- Ramón y Cajal S. 1911. *Histologie du système nerveux de l'homme & des vertébrés*. Paris,: Maloine.
- Rao YH, Brooks-Kayal AR. 2012. Experimental models of seizures and epilepsies. *Prog Mol Biol Transl Sci* 105:57-82.
- Saarelainen T, Hendolin P, Lucas G, Koponen E, Sairanen M, MacDonald E, Agerman K, Haapasalo A, Nawa H, Aloyz R, Ernfors P, Castren E. 2003. Activation of the

- TrkB neurotrophin receptor is induced by antidepressant drugs and is required for antidepressant-induced behavioral effects. *J Neurosci* 23(1):349-357.
- Sander JW. 2003. The epidemiology of epilepsy revisited. *Curr Opin Neurol* 16(2):165-170.
- Sandstead HH. 2000. Causes of iron and zinc deficiencies and their effects on brain. *J Nutr* 130(2S Suppl):347S-349S.
- Savage DD, Rigsbee LC, McNamara JO. 1985. Knife cuts of entorhinal cortex: effects on development of amygdaloid kindling and seizure-induced decrease of muscarinic cholinergic receptors. *J Neurosci* 5(2):408-413.
- Sayin U, Osting S, Hagen J, Rutecki P, Sutula T. 2003. Spontaneous seizures and loss of axo-axonic and axo-somatic inhibition induced by repeated brief seizures in kindled rats. *J Neurosci* 23(7):2759-2768.
- Schauwecker PE, Steward O. 1997. Genetic determinants of susceptibility to excitotoxic cell death: implications for gene targeting approaches. *Proc Natl Acad Sci U S A* 94(8):4103-4108.
- Segal RA, Bhattacharyya A, Rua LA, Alberta JA, Stephens RM, Kaplan DR, Stiles CD. 1996. Differential utilization of Trk autophosphorylation sites. *J Biol Chem* 271(33):20175-20181.
- Sensi SL, Paoletti P, Bush AI, Sekler I. 2009. Zinc in the physiology and pathology of the CNS. *Nature reviews Neuroscience* 10(11):780-791.
- Shepherd GM. 2004. The synaptic organization of the brain. Oxford ; New York: Oxford University Press. xiv, 719 p. p.
- Shimizu H, Fukaya M, Yamasaki M, Watanabe M, Manabe T, Kamiya H. 2008. Use-dependent amplification of presynaptic Ca²⁺ signaling by axonal ryanodine receptors at the hippocampal mossy fiber synapse. *Proc Natl Acad Sci U S A* 105(33):11998-12003.

Shorvon SD. 1996. The epidemiology and treatment of chronic and refractory epilepsy. *Epilepsia* 37 Suppl 2:S1-S3.

Shukla G, Prasad AN. 2012. Natural history of temporal lobe epilepsy: antecedents and progression. *Epilepsy Res Treat* 2012:195073.

Sindreu C, Palmiter RD, Storm DR. 2011. Zinc transporter ZnT-3 regulates presynaptic Erk1/2 signaling and hippocampus-dependent memory. *Proc Natl Acad Sci U S A* 108(8):3366-3370.

Sindreu CB, Varoqui H, Erickson JD, Perez-Claussell J. 2003. Boutons containing vesicular zinc define a subpopulation of synapses with low AMPAR content in rat hippocampus. *Cereb Cortex* 13(8):823-829.

Slayter EM, Slayter HS. 1992. Light and electron microscopy. Cambridge England ; New York: Cambridge University Press.

Spencer-Segal JL, Waters EM, Bath KG, Chao MV, McEwen BS, Milner TA. 2011. Distribution of phosphorylated TrkB receptor in the mouse hippocampal formation depends on sex and estrous cycle stage. *J Neurosci* 31(18):6780-6790.

Sun G, Budde RJ. 1999. Mutations in the N-terminal regulatory region reduce the catalytic activity of Csk, but do not affect its recognition of Src. *Arch Biochem Biophys* 367(2):167-172.

Sutula T, Steward O. 1987. Facilitation of kindling by prior induction of long-term potentiation in the perforant path. *Brain Res* 420(1):109-117.

Tauck DL, Nadler JV. 1985. Evidence of functional mossy fiber sprouting in hippocampal formation of kainic acid-treated rats. *J Neurosci* 5(4):1016-1022.

Thompson RB, Whetsell WO, Jr., Maliwal BP, Fierke CA, Frederickson CJ. 2000. Fluorescence microscopy of stimulated Zn(II) release from organotypic cultures of mammalian hippocampus using a carbonic anhydrase-based biosensor system. *J Neurosci Methods* 96(1):35-45.

- Tongiorgi E, Armellin M, Julianini PG, Bregola G, Zucchini S, Paradiso B, Steward O, Cattaneo A, Simonato M. 2004. Brain-derived neurotrophic factor mRNA and protein are targeted to discrete dendritic laminas by events that trigger epileptogenesis. *J Neurosci* 24(30):6842-6852.
- Trinka E, Hofler J, Zerbs A. 2012. Causes of status epilepticus. *Epilepsia* 53 Suppl 4:127-138.
- Tsai MH, Chuang YC, Chang HW, Chang WN, Lai SL, Huang CR, Tsai NW, Wang HC, Lin YJ, Lu CH. 2009. Factors predictive of outcome in patients with de novo status epilepticus. *Qjm* 102(1):57-62.
- Turski WA, Cavalheiro EA, Schwarz M, Czuczwar SJ, Kleinrok Z, Turski L. 1983a. Limbic seizures produced by pilocarpine in rats: behavioural, electroencephalographic and neuropathological study. *Behav Brain Res* 9(3):315-335.
- Turski WA, Czuczwar SJ, Kleinrok Z, Turski L. 1983b. Cholinomimetics produce seizures and brain damage in rats. *Experientia* 39(12):1408-1411.
- Ueno S, Tsukamoto M, Hirano T, Kikuchi K, Yamada MK, Nishiyama N, Nagano T, Matsuki N, Ikegaya Y. 2002. Mossy fiber Zn²⁺ spillover modulates heterosynaptic N-methyl-D-aspartate receptor activity in hippocampal CA3 circuits. *J Cell Biol* 158(2):215-220.
- VanLandingham KE, Heinz ER, Cavazos JE, Lewis DV. 1998. Magnetic resonance imaging evidence of hippocampal injury after prolonged focal febrile convulsions. *Ann Neurol* 43(4):413-426.
- Verkhratsky A. 2005. Physiology and pathophysiology of the calcium store in the endoplasmic reticulum of neurons. *Physiol Rev* 85(1):201-279.
- Vogt K, Mellor J, Tong G, Nicoll R. 2000. The actions of synaptically released zinc at hippocampal mossy fiber synapses. *Neuron* 26(1):187-196.

- Walter C, Murphy BL, Pun RY, Spieles-Engemann AL, Danzer SC. 2007. Pilocarpine-induced seizures cause selective time-dependent changes to adult-generated hippocampal dentate granule cells. *J Neurosci* 27(28):7541-7552.
- Watson FL, Heerssen HM, Moheban DB, Lin MZ, Sauvageot CM, Bhattacharyya A, Pomeroy SL, Segal RA. 1999a. Rapid nuclear responses to target-derived neurotrophins require retrograde transport of ligand-receptor complex. *J Neurosci* 19(18):7889-7900.
- Watson FL, Porcionatto MA, Bhattacharyya A, Stiles CD, Segal RA. 1999b. TrkA glycosylation regulates receptor localization and activity. *J Neurobiol* 39(2):323-336.
- Wiese S, Jablonka S, Holtmann B, Orel N, Rajagopal R, Chao MV, Sendtner M. 2007. Adenosine receptor A2A-R contributes to motoneuron survival by transactivating the tyrosine kinase receptor TrkB. *Proc Natl Acad Sci U S A* 104(43):17210-17215.
- Williams PA, White AM, Clark S, Ferraro DJ, Swiercz W, Staley KJ, Dudek FE. 2009. Development of spontaneous recurrent seizures after kainate-induced status epilepticus. *J Neurosci* 29(7):2103-2112.
- Wu W, Graves LM, Gill GN, Parsons SJ, Samet JM. 2002. Src-dependent phosphorylation of the epidermal growth factor receptor on tyrosine 845 is required for zinc-induced Ras activation. *J Biol Chem* 277(27):24252-24257.
- Xu B, Gottschalk W, Chow A, Wilson RI, Schnell E, Zang K, Wang D, Nicoll RA, Lu B, Reichardt LF. 2000. The role of brain-derived neurotrophic factor receptors in the mature hippocampus: modulation of long-term potentiation through a presynaptic mechanism involving TrkB. *J Neurosci* 20(18):6888-6897.
- Xu B, Michalski B, Racine RJ, Fahnstock M. 2004. The effects of brain-derived neurotrophic factor (BDNF) administration on kindling induction, Trk expression and seizure-related morphological changes. *Neuroscience* 126(3):521-531.

Yan Q, Rosenfeld RD, Matheson CR, Hawkins N, Lopez OT, Bennett L, Welcher AA.
1997. Expression of brain-derived neurotrophic factor protein in the adult rat
central nervous system. *Neuroscience* 78(2):431-448.

Yeckel MF, Kapur A, Johnston D. 1999. Multiple forms of LTP in hippocampal CA3
neurons use a common postsynaptic mechanism. *Nat Neurosci* 2(7):625-633.

Zakharenko SS, Patterson SL, Dragatsis I, Zeitlin SO, Siegelbaum SA, Kandel ER,
Morozov A. 2003. Presynaptic BDNF required for a presynaptic but not
postsynaptic component of LTP at hippocampal CA1-CA3 synapses. *Neuron*
39(6):975-990.

Zhu Y, Romero MI, Ghosh P, Ye Z, Charnay P, Rushing EJ, Marth JD, Parada LF. 2001.
Ablation of NF1 function in neurons induces abnormal development of cerebral
cortex and reactive gliosis in the brain. *Genes Dev* 15(7):859-876.

Biography

Jeffrey Helgager was born in San Diego, California, on October 23, 1980. He attended The University of California at Berkeley, graduating with honors in 2003 with a degree in Molecular and Cell Biology. He then attended Duke University School of Medicine, where he found his medical school courses in Neurobiology and Neurology to be of particular interest. After completing a research fellowship at the National Institutes of Health (NIH) known as the Clinical Research Training Program (CRTP), he decided to further pursue research in basic science. In 2007, he joined the Medical Scientist Training Program (MSTP) at Duke University through the Wakeman Award Fellowship in order to pursue a PhD in Neurobiology. He is a current member of the Society for Neuroscience. While enrolled at Duke, Helgager has published two first author publications, and coauthored another:

Helgager J, Liu G, McNamara JO. 2013. The cellular and synaptic location of activated TrkB in mouse hippocampus during limbic epileptogenesis. *J Comp Neurol* 521(3):499-521.

Helgager J, Li J, Lubensky IA, Lonser R, Zhuang Z. 2010. Troglitazone reduces glyoxalase I protein expression in glioma and potentiates the effects of chemotherapeutic agents. *J Oncol* 2010:373491.

Soren Leonard A, Puranam RS, Helgager J, Liu G, McNamara JO. 2012. Conditional deletion of TrkC does not modify limbic epileptogenesis. *Epilepsy Res* 102(1-2):126-130.